

UNITED KINGDOM • CHINA • MALAYSIA
DIVISION OF MOLECULAR THERAPEUTICS AND FORMULATION

POLYMER COATED IRON OXIDE NANOPARTICLES FOR INTRACELLULAR TRACKING AND DIAGNOSTIC APPLICATIONS

Ibteisam Elhuni

Thesis submitted to the University of Nottingham for the degree of Doctor of Philosophy

DECEMBER 17, 2018

Abstract

Engineering iron oxide nanoparticles (IONPs) is essential to enhance their efficiency and specificity for biomedical applications such as MRI contrast enhancement, cellular therapy such as cell labelling and cell targeting. IONPs were prepared by a co-precipitation method and coated with various polymers poly(Glycerol Adipate) (PGA 40%C_{18}), Poly(Ethylene Glycol) - poly(Glycerol Adipate)-Succinic Acid (PEG-PGA-SA) and Poly(Ethylene Glycol) - poly(Glycerol Adipate) 40%C_{18} (PEGylated PGA 40%C_{18}). From the three different coated IONP preparations, only PEGylated PGA 40%C_{18} demonstrated the ability to produce small-coated particle sizes. The size, shape and surface charge of uncoated and coated IONPs were characterised using dynamic light scattering (DLS), transmission electron microscopy (TEM) and zeta-potential. The sizes of IONPs after coating were 22, 50, 80 nm respectively, and the results of zeta potential measurement indicated that the surface charge of uncoated nanoparticles changed from positive to negative after coating with polymer. PEGylated PGA 40%C_{18} coated iron oxide nanoparticles showed high stability against aggregation under physiological conditions. Rhodamine B isothiocyanate was incorporated into the polymer layer and used as a fluorescent marker.

The effect of PEGylated PGA 40%C_{18} coated IONP of various sizes on the uptake by a respiratory epithelial cell line (Calu-3) was investigated. The internalisation mechanism and intracellular localisation was determined using a range of advanced imaging techniques including confocal microscopy and transmission electron microscopy (TEM). The

results suggested that for PEGylated PGA 40%C_{18} coated IONPs there was a clear correlation between particle size and cellular uptake. Uptake was particularly high for nanoparticles with size 22 nm. Quantitative determination of cellular iron uptake performed by colorimetric ferrozine assay was in agreement with confocal microscopy results. The permeability coefficient (P_{app}) was used to determine the permeability of 22 nm coated IONP, but the larger particles showed a negligible permeability. Mechanism of nanoparticle cellular uptake was mainly by direct diffusion through the cell membrane for all IONP sizes. However, some particle uptake for the larger IONP (50 and 80 nm) was by the expected vesicular route, and this was probably seen due to the slower diffusion of these IONP through the membranes.

The MRI contrast of IONPs coated with a thin layer of PEGylated PGA 40%C_{18} was evaluated with1.5T Philips Achieva MRI scanner through measurement of their relaxivities. Polymer coated IONPs of size 50 nm have a good r2 relaxivity value but the other sizes were inferior. The MRI results highlight an opportunity for further optimisation of the core/shell ratio of IONPs, which could enhance relaxivity effects for their medical applications as contrast agents in the near future.

Acknowledgements

I would like to thank my supervisor Dr Martin Garnett for the guidance and for his continuous scientific advice and insights. I am very grateful for his support during these 4 years of my PhD and for broadening my horizon and making me learn various aspects. Also, wish to express my gratitude to Dr Snow Stolnik-Trenkic for her guidance and advice.

I would also thank Dr Richard Argent for cell culture training and for his kind guidance and advice in biology part of this project. Particular thanks to Dr Luca Marciani in GI MRI, Faculty of Medicine & Health Sciences for providing his support and guidance for MRI measurements. Many thanks to Dr Hilary Collins for help with confocal microscopy.

I would like to acknowledge Vincenzo Taresco for providing polymers for my research and for his guidance and advice. I would like to extend my thanks to Denise Christie and Rhys Lodge for their competent assistance with TEM and taking beautiful TEM images. The whole of the technical staff in the molecular therapeutics and formulation division in pharmacy especially Paul Cooling, Tom Booth, Tammy Lydamore and Colin Rowe for their help.

I would like to express my gratitude to my friends in the University of Nottingam: Rehab Elfakhri and Rashidat Animasawun. The time spent with you was wonderful. Thanks also to all the people working in our school for their help.

My deepest gratitude goes to the best woman ever in my life, my mother, who is always with me and prays for me.

Last but not least, I would like to express my sincere gratitude to my wonderful husband, Khaled and my kids: Anas, Arwa and Ayham for the understanding during these years. Thank you for always being considerate in my good and bad times. I would not have made it without you.

I would like to dedicate this thesis to my dad who passed away on the 6th of June 2016, but would have been proud of me for completing my PhD.

Table of Contents

ABSTRACT I
ACKNOWLEDGEMENTS III
TABLE OF CONTENTS V
LIST OF FIGURES X
LIST OF ABBREVIATIONS XV
1 INTRODUCTION 1
1.1 General Application of IONPs 6
1.1.1 Drug Delivery 6
1.2 Specific Applications of IONPs 8
1.2.1 Magnetic Resonance Imaging (MRI) 8
1.2.2 Hyperthermia 10
1.2.3 Cell Labelling and IONPs Tracking 10
1.3 Synthesis of IONPs 12
1.3.1 Co-Precipitation Method 13
1.3.2 Hydrothermal Method 14
1.3.3 Microemulsion Method 15
1.3.4 Sonochemical Method 15
1.4 Surface Modification of IONPs 16
1.5 Biocompatibility and Toxicology of IONPs 21
1.6 The Internalisation Strategy of IONPs for Crossing Biological Barriers 22
1.6.1 Endocytosis of Nanoparticles 24
1.6.2 Exocytosis of Nanoparticles 27
1.6.3 Paracellular Transport of Nanoparticles 28
1.6.4 Transcytosis of Nanoparticles 29
1.7 Factors Affecting Particle Uptake and Transport 30
1.7.1 Size 30
1.7.2 Surface Properties 32
1.7.3 Shape 34
1.7.4 Cell Type 34
1.8 Epithelia Cells (Calu-3) for IONPs Uptake Studies 35

1.9 IONPs FOR UPTAKE STUDY 37
1.10 AIMS OF THE PROJECT 37
2 MATERIALS AND METHODS 41
2.1 MATERIALS 41
2.1.1 General chemicals 41
2.1.2 Cell culture reagents 41
2.1.3 Polymers Used in This Study 42
2.2 METHODS 44
2.2.1 Synthesis Processes 44
2.2.1.1 Synthesis of IONPs 44
2.2.1.2 Surface Coating of IONPs 45
2.2.1.3 Formation of RBITC-Labelled Coated IONPs 46
2.2.2 Analytical Instrumentation 46
2.2.2.1 Dynamic Light Scattering 47
2.2.2.2 Transmission Electron Microscopy 48
2.2.2.3 Zeta Potential Analysis 49
2.2.2.4 Colloidal Stability of Uncoated and Coated IONPs 50
2.2.2.5 Determination the Amount of RBITC Bound to Coated IONPs 50
2.2.2.6 Ferrozine Assay for Measuring IONPs 51
2.2.3 Preparation of IONPs for Biological Study 51
2.2.4 Routine Cell Culture 52
2.2.4.1 Calu-3 Cell Culture 52
2.2.4.2 Cell Maintenance and Splitting 52
2.2.4.3 Cells Seeding onto a 6-Well Plate 53
2.2.4.4 Cells Seeding onto Transwell® Permeable Supports 53
2.2.4.5 TEER Measurements 53
2.2.5 Cytotoxicity Studies 54
2.2.5.1 Metabolic Activity (MTT) Assay 54
2.2.5.2 Trypan Blue Exclusion Assay 55
2.2.6 Cellular Uptake of IONPs 56
2.2.7 Microscopy Studies 57

2.2.7.1 Confocal Laser Scanning Microscopy 57

2.2.7.1.1 Fixed Imaging Method 58

2.2.7.1.2 Live Imaging Method 59

2.2.7.2 Electron microscopy 60

2.2.7.2.1 Evaluation of time dependent uptake of IONPs by calu-3 cells growing in monolayer culture using TEM 60

2.2.7.2.2 Dehydration and Embedding of Cells 60

2.2.8 In Vitro Transcytosis Study 61

2.2.9 Relaxivity Measurement 62

2.2.10 Statistical Analysis 63

3 PHYSICOCHEMICAL CHARACTERISTICS OF IRON OXIDE NANOPARTICLES 65

3.1 INTRODUCTION 65

3.2 AIMS OF THE CHAPTER 68

3.3 RESULTS 69

3.3.1 Synthesis of IONPs 69

3.3.1.1 The Effect of pH Variation on the Size of IONPs 69

3.3.1.2 Particle Sizes Distribution of Uncoated IONPs 70

3.3.1.3 Zeta Potential 72

3.3.1.4 Dispersion and Stability of Uncoated IONPs 72

3.3.2 Particle Size of Coated IONPs with Different Polymers 72

3.3.2.1 PGA 40%C_{18} Coated IONPs 73

3.3.2.2 PEG–PGA-SA Coated IONPs 75

3.3.2.3 PEGylated PGA 40% C_{18} Coated IONPs 76

3.3.3 TEM Images 83

3.3.4 Surface Charge of IONPs 85

3.3.5 Colloidal Stability of PEGylated PGA 40%C_{18} Coated IONPs 88

3.3.6 Quantification of Uncoated and PEGylated PGA 40%C_{18} Coated IONPs 91

3.4 DISCUSSION 92

3.4.1 IONPs Preparation and Characterisation 92

3.4.2 Optimised Conditions for Synthesis IONPs with Controlled Sizes 95

3.4.2.1 Effect of pH Variation on Particle Sizes 95

3.4.3 Surface Charge of IONPs 96

3.4.4 Stability of IONPs 96

3.4.5 Size Distribution of Polymer Coated IONPs 97

3.4.6 Surface Charges of coated IONPs 102

3.4.7 Colloidal Stability of PEGylated PGA 40% C_{18} IONPs 103

3.5 CONCLUSION 105

4 EVALUATION OF ENDOCYTOSIS AND TRANSCYTOSIS OF RHODAMINE B ISOTHIOCYANATE LABELLED POLYMER COATED IRON OXIDE NANOPARTICLES 106

4.1 INTRODUCTION 106

4.2 AIM 110

4.3 RESULTS 111

4.3.1 Physicochemical Properties of RBITC Dye Labelled IONPs 111

4.3.2 Amount of RBITC Incorporated to the Coated IONPs 112

4.3.3 Cell viability study of different coated IONPs size 113

4.3.3.1 Metabolic Activity (MTT) Assay 113

4.3.3.2 Trypan Blue Exclusion Method 115

4.3.4 Interactions of Polymer Coated IONPs with Calu-3 cells 116

4.3.4.1 Effect of IONP Amounts on Calu-3 Cellular Interaction 117

4.3.4.2 Effect of Incubation Time on Calu-3 Cellular Interactions 118

4.3.5 Quantitative Determination of Unbound IONPs in Cell Culture Medium . 120

4.3.6 Microscopy Studies 121

4.3.6.1 Dose dependent and intracellular distribution of RBITC labelled polymer coated IONPs in Calu-3 cells using confocal laser scanning microscopy 122

4.3.6.2 Intracellular Localisation of RBITC Labelled Polymer Coated IONPs in Calu-3 Cells 129

4.3.6.3 Time Dependent Intracellular Localisation of Polymer Coated IONPs Using Transmission Electron Microscopy (TEM) 132

4.3.7 In Vitro Assessment of Polymer Coated IONPs Permeability across Calu-3 Epithelial Line 139

4.4 DISCUSSION 142

4.4.1 Cytotoxicity of Polymer Coated IONPs 142

4.4.2 Polymer Coated IONPs Uptake in Cultured Cells 143

4.4.3 Transcytosis of Polymer Coated IONPs 159

4.5 CONCLUSION: 161
5 POLYMER COATED IRON OXIDE NANOPARTICLES AS MRI CONTRAST AGENTS 162
5.1 INTRODUCTION 162
5.2 AIM 167
5.3 RESULTS 168
5.3.1 Size Dependent MRI Relaxivity 168
5.4 DISCUSSION 171
5.5 CONCLUSION 173
6 CONCLUSION AND FUTURE PROGRESS 175
6.1 CONCLUSION 175
6.2 LIMITATIONS OF CURRENT WORK 180
6.3 FUTURE WORK 180
REFERENCES 184
APPENDIX 216

List of Figures

Figure 1-1: Particle stabilisation by (a) an electrostatic layer, (b) steric repulsion. Source:[78]. 18

Figure 1-2: Cellular internalisation of nanoparticles by endocytosis, phagocytosis, micropinocytosis, clathrin dependant endocytosis and receptor mediated endocytosis pathways. Source: [143]..... 27

Figure 1-3: Transport mechanisms through epithelial cells held together by tight junctions sitting on a basal lamina with mucus cover layer. The main different transport pathways are shown in the numbered cells. Modified from Garnett et al [152]. 29

Figure 2-1: Structure of poly(Glycerol Adipate) 40%C_{18}. 42

Figure 2-2: Structure of Poly(Ethylene Glycol) poly(Glycerol Adipate) 40%C_{18}. 43

Figure 2-3: Structure of PEG-PGA-SA which has Pendant PEG chains from reaction with pendant succinic acid side chains on succinylated PGA... 43

Figure 2-4: A 1.5T Philips Achieva MRI scanner image of sample suspensions of different polymer coated IONPs sizes (22, 50 80 nm). 63

Figure 3-1: Variation in IONP hydrodynamic radii as a function of pH during the synthesis process. Different sized nanoparticles were obtained simply by varying the sodium hydroxide amount and with variation in the pH of precipitates. The particle size of the nanoparticles was determined by DLS. IONPs produced over the pH range 0.5-4 were of smaller size, as compared to those formed over the pH range 6 and 12, as IONPs were larger. The Rh of each sample is expressed as the mean particle hydrodynamic radius ± standard deviation of 5 readings. 70

Figure 3-2: The hydrodynamic radii (Rh) intensity of uncoated IONPs by DLS. NPs were prepared by the co-precipitation method at different pH where (A) at pH 0.5, (B) at pH 3 and (C) at pH 4. NP suspension was diluted with ultrapure water to an appropriate concentration to give 300-600 kcps. The Rh of each sample is expressed as the mean particle hydrodynamic radius ± standard deviation of 10 readings. 71

Figure 3-3: Hydrodynamic radii of PGA 40%C_{18} coated IONPs: NPs of radius 10 nm were coated with different amounts of polymer using the interfacial deposition method. NP suspension was diluted with ultrapure water to an appropriate concentration to give 300-600 kcps. Particle size was the mean hydrodynamic radius and measured by Dynamic light scattering instrument. The Rh of each sample is expressed as the mean particle hydrodynamic radius ± standard deviation of 10 readings. 74

Figure 3-4: Hydrodynamic radii distribution of PEG-PGA-SA coated IONPs: NPs of radius 10 nm were coated with different amounts of polymer using the interfacial deposition method. NP suspension was diluted with ultrapure water to an appropriate concentration to give 300-600 kcps. Particle size was the mean hydrodynamic radius and measured by Dynamic light scattering instrument. The particle size of each sample is

expressed as the mean particle hydrodynamic radius ± standard deviation of 10 readings. 75

Figure 3-5: Hydrodynamic radius distribution of PEG-PGA 40%C_{18} coated IONPs: NP of radius 10 nm were coated with different amounts of polymer using the interfacial deposition method. NP suspension was diluted with ultrapure water to an appropriate concentration to give 300-600 kcps. Particle size was the mean hydrodynamic radius and measured by Dynamic light scattering instrument. The particle size of each sample is expressed as the mean particle hydrodynamic radius ± standard deviation of 10 readings 76

Figure 3-6: The hydrodynamic radii (Rh) intensity of PEGylated PGA 40% C_{18} coated IONPs by DLS. NP of radius 10 nm were coated with different amounts of polymer using the interfacial deposition method where (A) 0.1 mg (B) 0.2 mg and (C) 0.3 mg PEGylated PGA 40% C_{18}. NP suspension was diluted with ultrapure water to an appropriate concentration to give 300-600 kcps. The Rh of each sample is expressed as the mean particle hydrodynamic radius ± standard deviation of 10 readings. 78

Figure 3-7: The hydrodynamic radii (Rh) intensity of PEGylated PGA 40%C_{18} coated IONPs by DLS. NP of radius 18 nm were coated with different amounts of polymer using the interfacial deposition method where (A) 0.05 mg (B) 0.1 mg and (C) 0.2 mg PEGylated PGA 40% C_{18}. NP suspension was diluted with ultrapure water to an appropriate concentration to give 300-600 kcps. The Rh of each sample is expressed as the mean particle hydrodynamic radius ± standard deviation of 10 readings. 80

Figure 3-8: The hydrodynamic radii (Rh) intensity of PEGylated PGA 40% C18 coated IONPs by DLS. NP of radius 25 nm were coated with different amounts of polymer using the interfacial deposition method where (A) 0.05 mg (B) 0.1 mg and (C) 0.2 mg PEGylated PGA 40% C18. NP suspension was diluted with ultrapure water to an appropriate concentration to give 300-600 kcps. The Rh of each sample is expressed as the mean particle hydrodynamic radius ± standard deviation of 10 readings. 82

Figure 3-9: TEM images (A, D, G) and particle size distribution graphs (C, F and I) of different batches of PEGylated PGA 40% C_{18} coated IONPs where (A and C) 0.3 mg, (D and F) 0.2 mg and (G and I)) 0.1 mg PEGylated PGA 40% C_{18} coated IONPs. Particle size and standard deviation values are inset (N = 100). Higher magnification of each formulation of PEGylated PGA 40% C_{18} coated IONPs, shows visible lattice planes of individual IONPs (darker structured area) embedded in a polymer matrix (lighter more granular appearance) (B, E and H). Scale bars are (A) 20 nm, (B) 2 nm (D and G) 50 nm and (E and H) 10 nm. 84

Figure 3-10: Surface charge of uncoated and PEGylated PGA 40% C_{18} coated IONPs where, (A) zeta potential of Rh 10 nm, (B) zeta potential of Rh 18 nm and (C) zeta potential of the biggest Rh (25 nm) of uncoated and coated with PEGylated PGA 40%C_{18} of different amounts. The zeta potential of all formulations was evaluated by one way ANOVA with a Sidak's multiple comparisons ($p > 0.05$). The zeta potential of all formulations was not significantly decreased when the amount of PEGylated PGA 40% C18 is increased. Zeta potential measurements were performed in PBS (15 mM) at pH 7.4 using Zeta sizer (Malvern

Instruments,Malvern,UK). Results are expressed as the mean ± standard deviation of 5 readings. 87

Figure 3-11: Stabilities of different formulations of uncoated and coated IONPs with different amount of PEGylated PGA 40% C_{18} (0.05, 0.1, 0.2 and 0.3 mg), where (A, B and C) stability of PEGylated PGA 40% C_{18} IONPs resulting from coating IONPs of hydrodynamic sizes 10, 18 and 25 nm respectively. Coated and uncoated IONPs (25 µg/ml) were mixed with different concentrations of NaCl. The absorbance was measured at 562 nm using a TECAN plate reader. For the IONPs absorbance at 562 nm, a significant difference was found between the uncoated and PEGylated PGA 40%C_{18} of different sizes ($P < 0.0038$), however according to a Tukey's multiple comparisons (2 way ANOVA), there were no significant differences between 0.05, 0.1, 0.2 and 0.3 mg PEG-PGA coated IONPs ($P>0.05$). 90

Figure 3-12: Iron calibration curve in water. The calibration curve was created using standard amount of iron ranging from 7.81 to 0.06 mg and reacted with ferrozine reagent. The absorbance was measured using a TECAN Spark plate reader. All samples are taken triplicate and averages calculate. 92

Figure 4-1: Calibration curve for RBITC in HEPES. The calibration curve was created by preparing a dilution series of a RBITC stock solution ranging from 0.002 to 0.125 mg. The fluorescence intensity was measured using a Dynal MFX Fluorimeter, at Ex 554 nm and Em 575 nm..... 113

Figure 4-2: Viability of Calu-3 cells incubated with increased dose of PEGylated PGA 40%C_{18} IONPs of different sizes (22, 50 and 80 nm) for 24 hours as determined by the MTT assay. Results presented as % viability and shown as the mean ± S.E.M (N=3). A Tukey's multiple comparison test (2 way ANOVA) was used for statistical analysis. ** indicated that the viability of Calu-3 cells is significantly lower than the control with $p<0.01$. 114

Figure 4-3: Viability of Calu-3 cells incubated with different concentrations of PEGylated PGA 40%C_{18} IONPs (10, 50 and 100 µg/ml) for 24 hours as determined by haemocytometer. Results are presented as % viability relative to control cells and shown as the mean ± SD (n=3). A Tukey's multiple comparison test (2 way ANOVA) was used for statistical analysis. The results showed that the viability of Calu-3 cells was not significantly lower than the control with $p>0.05$..... 116

Figure 4-4: Schematic showing the effect of polymer coated IONP amount on accumulation of nanoparticles in Calu-3 cells. Calu-3 cells were incubated with different sizes of PEGylated PGA 40%C_{18} IONPs (22, 50 and 80 nm). The intracellular uptake was evaluated after 2 hours of incubation with different NP amounts (10, 25, 50 and 75 µg). Intracellular iron content was calculated by creating a standard curve of known NP concentration using the ferrozine assay. According to a Tukey's multiple comparison test (2 way ANOVA), there were significant differences between the accumulated amount of particles of size 22, 50 and 80 nm in Calu-3 cells with $P <0.0001$, however cells incubated with 50 µg of particle with sizes 22 and 50nm showed insignificant differences of cellular accumulation with ($P=0.1906$). Error bars represent mean ± S.E.M (N=3). 118

Figure 4-5: Effect of incubation time on polymer coated IONPs accumulation in Calu-3 cells. Calu-3 cells were incubated with different sizes of PEGylated PGA 40%C_{18} IONPs (22, 50 and 80 nm). The intracellular accumulation was evaluated after 30 minutes, 2, 4 and 24 hours of incubation with 50 µg NPs. Intracellular iron content was calculated by creating a standard curve of known concentration NPs using the ferrozine assay. According to a Tukey's multiple comparison test (2 way ANOVA), the amount of particles of size 22 nm that accumulated in Calu-3 cells within 24 hours was significantly higher than particles of size 50 and 80 nm with P <0.0001 within 24 hours. Error bars represent mean ± S.E.M (N=3). 119

Figure 4-6: Analysis of different sizes polymer coated IONP contents in EMEM medium. Calu-3 cells were incubated with 50 µg PEG-PGA 40%C_{18} coated IONPs (22, 50 and 80 nm) for different times (2 and 4 hours). The unbound polymer coated IONPs content that were present in EMEM were analysed by ferrozine assay using a standard curve of known concentrations of NPs. According to a Tukey's multiple comparison test (2 way ANOVA), the amount of particles of size 22 nm in EMEM medium was extremely significant decreased after 4 hours, however the particles of size 50 and 80 nm was extremely significant increased (P <0.0001). Error bar represent mean ± standard deviation (n=3)..... 121

Figure 4-7: Confocal microscopy images of RBITC-labelled polymer coated IONPs incubated with Calu-3 cells for 2 hours, where, (A and B) are untreated cells and cells incubated with free RBITC. (C, D and E) cells incubated with (5, 25 and 50 µg/ml) NPs of size 22 nm, (J, H and I) cells incubated with (5, 25 and 50 µg/ml) NPs of size 50 nm and (K, L and M) cell incubated with (5, 25 and 50 µg/ml) NPs of size 80 nm (Scale bar 20 µm). A slice of 1 µm thickness was imaged from the middle of the sample by an individual confocal optical section..... 124

Figure 4-8: Confocal microscopy images of RBITC-labelled polymer coated IONPs incubated with Calu-3 cells for 4 hours, where (A and B) cells incubated with (25 and 50 µg/ml) NPs of size 22 nm, (C and D) cells incubated with (25 and 50 µg/ml) NPs of size 50 nm and (E and F) cell incubated with (25 and 50 µg/ml) NPs of size 80 nm (Scale bar 20 µm). A slice of 1 µm thickness was imaged from the middle of the sample by an individual confocal optical section. 126

Figure 4-9: Serial confocal images was obtained by multiple optical sectioning of 1 µm thickness of each section (12 slices) showing an in vitro model of Calu-3 cells after 2 h incubation with RBITC-polymer coated IONPs (25 µg/ml, red). (A, B and C) showing Gallery series of images (slices), of polymer coated IONPs of sizes (22, 50 and 80 nm), starting from the top of the cell layers. (A~, B~ and C~) Orthogonal slice view. Cell nuclei (blue) were labelled with Draq-5..... 128

Figure 4-10: Confocal microscopy images demonstrating the intracellular distribution of 22 nm RBITC labelled polymer coated IONPs (50 µg) incubated with Calu-3 cells for 2 hours. (A) Bright field showing the outline of the cells. (B) Cells stained with LysoTracker Green (C) Draq 5 (nuclear stain), (D) Uptake of red fluorescent labelled polymer coated IONPs (E) Overlay of (B) and (D) showing location of nanoparticles compared to lysosomes. Scale bar 10 µm. 130

Figure 4-11: Confocal microscopy images demonstrating the intracellular distribution of 50 nm RBITC labelled polymer coated IONPs (50 µg) incubated with Calu-3 cells for 2 hours. (A) Bright field showing the outline of the cells. (B) Cells stained with LysoTracker Green (C) Draq 5 (nuclear stain), (D) Uptake of red fluorescent polymer coated IONPs (E) Overlay of (B) and (D) showing the relative localisation of nanoparticles and lysosomes. Scale bar 10 µm. 131

Figure 4-12: Confocal microscopy images demonstrating the intracellular distribution of 80 nm RBITC labelled polymer coated IONPs (50 µg) incubated with Calu-3 cells for 2hours. (A) Bright field showing the outline of the cells. (B) Cells stained with LysoTracker Green (C) Draq 5 (nuclear stain), (D) Uptake of red fluorescent labelled polymer coated IONPs (E) Overlay of (B) and (D) showing the relative localisation of nanoparticles and lysosomes. Scale bar 10 µm. 132

Figure 4-13: TEM image of Calu-3 cells grown on transwells incubated with polymer coated IONPs of size 22 nm (50 µg/ml) for different time where (A1 &2) 10 minutes, (B1&2) 2 hours, (C1&2) 4 hours and (D1&2) untreated cell control. Images shows nucleus (N), nuclear envelope (NE), nucleolus (Nu), mitochondria (M), vesicles (V) and apical side (A)..... 134

Figure 4-14: TEM image of Calu-3 cells grown on transwells incubated with polymer coated IONPs of size 50 nm (50 µg/ml) for different time where (A1 &2)) 10 minutes, (B1 &2) 2 hours and (C1 &2) 4 hours. Images shows cell membrane (CM), nucleus (N), vesicles (V), lipid (L) and vesicular boundary (VB)..... 136

Figure 4-15: TEM image of Calu-3 cells grown on transwells incubated with polymer coated IONPs of size 80 nm (50 µg/ml) for different time where (A1 &2) 10 minutes, (B1 &2) 2 hours and (C1 &2) 4 hours. Images shows nucleus (N), nuclear envelope (NE), nucleolus (Nu), mitochondria (M), vesicles (V), cell membrane (CM), apical side (A) and endoplasmic reticulum (ER). 138

Figure 4-16: Cumulative amount for three sizes of polymer coated IONPs (22, 50 and 80 nm) that cross epithelial cell models of Calu-3 cultured on 12 well Transwell® inserts. The amount of NPs were tested at 50 µg in all groups in 3 hours cultures. NP cumulative amount was measured by applying the samples on the apical chamber and sampling the basolateral solution every 30 minutes for 3 hours and quantification of samples by ferrozine assay (through calibration curves) in all cases. Data are means ±SD of three different cell monolayer. One-way analysis of variance (ANOVA) was used for statistical analysis (A Sidak's multiple comparison test). **** indicates significant differences in the accumulation amount with ($p < 0.0001$) of NPs of size 22 nm with those of the 50 or 80 nm. 141

Figure 5-1: Plot of the proton relaxation rates (1/T1) and (1/T2) of water suspensions of polymer coated IONPs at various Iron concentrations versus the corresponding concentrations for samples A (22 nm), B (50 nm), and C (80 nm). 169

List of Abbreviations

ATCC	American Type Culture Collection
CLSM	Confocal Laser Scanning Microscopy
DAPI	4',6-Diamidino-2-Phenylindole
DLS	Dynamic Light Scattering
DMSO	Dimethylsulphoxide
EMEM	Eagle's Minimum Essential Medium
FBS	Foetal Bovine Serum
FDA	Food and drug administration
FB-DMEM	FluoroBrite Dulbecco's Modified Eagle Medium
HEPES	N-(2-hydroxyethyl) piperazine-N- (2-ethanesulphonic acid)
IDP	Interfacial Deposition Method
IONPs	Iron Oxide Nanoparticles
MRI	Magnetic Resonance Imaging
MTT	3-(4,5-dimethylthiazol-2-yl)-2,5-diphenyltetrazolium bromide
MWCO	Molecular Weight Cut off
NEAA	Non-Essential Amino Acid
NPs	Nanoparticles
P_{app}	Apparent Permeability
PBS	Phosphate –Buffer Saline
PLA	P(Lactic Acid)
PEG	Poly(Ethylene Glycol)
PFA	Paraformaldehyde
PGA	Poly(Glycerol Adipate)
PGA 40%C_{18}	Acylation of PGA by 80%
PLGA	Poly(Lactic-co-Glycolic Acid)

PVA	Poly (Vinyl Alcohol)
R	Proton Relaxation Rate
RBITC	Rhodamine B Isothiocyanate
RES	Reticuloendothelial system
SA	Succinic Anhydride
SD	Standard Deviation
SPION	Suprparamagnetic Iron Oxide Nanoparticle
T1	Longitudinal Relaxation Times
T2	Transverse Relaxation Time
TEER	Transepithelial electric resistance
TEM	Transmission Electron Microscope

1 Introduction

Nanoparticles generally refer to synthetically engineered materials which vary in size from 1 to 1000 nm in diameter, are either inorganic or organic [1, 2], and their physical and chemical properties are specific to their applications. They have potential for use in medicine, electronics, tissue engineering, and the pharmaceutical industry. They offer many advantages for site-specific delivery of diagnostic and therapeutic agents [3-5]. In addition, nanoparticles are of great interest for researchers particularly for their potential in cancer therapy due to the enhanced permeability and retention effect that lead to optimisation of the dose and a decrease in systemic side effects [6] by increasing penetration of some therapeutics from the blood stream into the cancer cells which result in increasing selectivity and specificity of the therapy [7, 8].

Iron oxide nanoparticles (IONPs) are an exciting advancement in the field of nanotechnology. They have been extensively investigated as magnetic particles and they attract a great interest in biomedical applications because they allow quantitative determination of their biodistribution by MRI, which may enable early detection, and facilitate targeting tumour cells by nanoparticles for more efficient treatment.

Other magnetic materials such as gadolinium (Gd), cobalt (Co), nickel (Ni), and Manganese (Mn) have been studied due to their higher contrast enhancement in MRI and high magnetic saturation. However, IONPs are more favourable because of their biocompatibility, non-toxicity,

availability of a wide variety of sizes [9-13] and the possibility to exploit their outstanding magnetic properties which allow efficient targeting to the tumour area through external magnetic fields [14]. These excellent properties have enabled IONPs to be employed as contrast agents in MRI, cell labelling as well as drug delivery systems, and hyperthermia therapy [8, 11, 15].

The co-precipitation technique is usually the simplest and most efficient chemical method to obtain IONPs (either (magnetite) Fe_3O_4, or (maghemite) γ-Fe_2O_3), which are of interest for applications in vivo and in vitro, as they become saturated at a low applied magnetic field and they have a high saturation magnetic moment. IONPs administered to humans can be incorporated into natural iron metabolism pathways and biological process such as haemoglobin synthesis. These particles tend to be either superparamagnetic or paramagnetic according to their size as they exhibit superparamagnetic properties generally at a diameter of <20 nm [8, 12, 16]. Superparamagnetic iron oxide nanoparticles (SPION) do not retain any magnetism after the removal of the magnetic field and they no longer exhibit any magnetic interaction. This results in particles, which are unlikely to aggregate, and hence the possible embolization of the capillary vessels can be avoided. However, during exposure to a magnetic field, paramagnetic materials tend to aggregate [9, 12, 17-19].

In biomedical applications, IONPs are exposed to different conditions such as different pH and ionic strength. For example, the pH of cancer cells is about 6.8, while cellular compartments such as endosomes and

lysosomes have a more acidic environment of range 4-5 [20, 21]. Consequently, it is important that IONPs are stable against aggregation in these varying different conditions to ensure reproducibility as well as to maximise the amount of cellular loading. The stability of IONPs can be achieved either by electrostatic or steric repulsion forces. Electrostatic stability is affected by nanoparticle surface charges and ionic strength of the surrounding environment, however steric stability depends on parameters like type and molecular weight of the coating materials [21, 22].

Many polymers have been used to coat IONPs, such as dextran poly(ethylene glycol) (PEG), poly(lactide-co-glycolide) (PLGA), poly(glycerol adipate) (PGA) and poly (vinylalchohol) (PVA) [23-25]. The correct choice of coating materials and their subsequent arrangement on nanoparticle is not only determine the overall size, but also the colloidal stability and biodistribution of the particles in biological medium [26, 27]. It is important to not only choose the correct coating, but also to use the correct amount of the coating substances. According to a study by Pelaz et al. (2013), the inorganic nanoparticle core under physiological condition may undergo corrosion resulting in the release of toxic ions, which may attributed to insufficient coating layer or due to detaching of coating materials from the nanoparticle's surface. These can impede the potential biomedical application of certain nanoparticles [28]. Therefore, sufficient thickness of polymer must cover the entire surface of particles in order to overcome this problem.

Intracellular delivery of nanoparticles is currently gaining attention for use in tumour therapy. IONPs have been used as tracer materials for labelling cells and tracking their distribution with MRI [29-31]. Biologically, MRI requires a high rate of capture of the IONPs by cells [18]. A principle challenge toward developing IONPs is obtaining sufficient permeability across the epithelial barrier. Penetration of IONPs may occur through different endocytic pathways and no general rules have been identified so far on size and the chemical nature of the coating influencing particle uptake, biodistribution and pharmacokinetics [32-37]. In particular, size of the particles is an important parameter that may lead to different endocytic cellular uptake [38, 39]. Many studies have shown that the final localisation of IONPs was mainly within the endosomal-lysosomal compartment [40]. Understanding more about the relationship between physicochemical properties of nanoparticles and the process of uptake could provide a greater degree of understanding and may help in experimental and formulation design development, resulting in production of more efficient targeting systems.

IONPs are advantageous for attacking carcinoma cells, which mainly originate from epithelial cells as they offer the unique possibility to overcome cellular barriers in order to improve the interaction of nanoparticles and target cells for many applications, including diagnostics, imaging, therapy, and drug delivery. The interplay between nanoparticles and cells is mainly governed by the design of nanoparticles. Nowadays many studies have been undertaken to design nanoparticles with regard to their size, shape and surface properties,

however, the fundamental interaction of nanoparticles with target cells in biological environment, which is expected to depend on their surface physicochemical properties, and other properties such as size remains incompletely understood.

The size of the nanoparticles determine the properties and biological fate of these particles [41]. It has a strong influence on their adhesion and interaction with biological cells, as well as the efficiency of cellular uptake and the number of internalised particles. For example, under physiological conditions, IONPs with a diameter less than 200 nm tend to aggregate very readily, and this leads to the formation of large particles that are engulfed by the mononuclear phagocytic system (MPS). This accumulation of particles within the MPS, such as in the liver and spleen, leads to severe systemic toxicity. In contrast, very small particles with a diameter of less than 10 nm are quickly removed through extravasation and renal clearance [9, 17, 42]. Particles in the range of 10-100 nm are a suitable size to escape both reticuloendothelial system as well as to penetrate the very small capillaries inside the body tissues and, thus may offer the most effective distribution in certain organs, tissues and even cells [43]. However, it is often unclear by which intracellular route nanoparticles of different size will enter cells.

The surface charge of nanoparticles is also important for enhancing the efficiency of the cellular internalisation of nanoparticles and reaching intracellular targets. It has been stated that positively charged particles demonstrate a higher rate of cellular uptake than neutral or negatively

charged particles, which tend to be excluded by cells. These results may be attributed to a net negative charge on the surface of most mammalian cells, which interacts electrostatically with the positive surface of a nanoparticle, resulting in the enhanced cellular uptake of nanoparticles [44, 45].

Shape of nanoparticles could be important too as, spherically shaped nanoparticles have been demonstrated to enter the cell more efficiently than non-spherical particles which may be related to the particles surface area that is exposed to cells [46].

1.1 General Application of IONPs

Nanoparticles are being rapidly developed in terms of their application in medicine and biology due to their unique size. A summary of the application of nanoparticles as a drug carrier is provided below.

1.1.1 Drug Delivery

Currently, cancer research is focusing on the development of nanoparticles with higher selectivity for the disease site without engaging with healthy cells [11, 18]. Advantages of using IONPs in drug delivery are the ability to target them to specific sites, even to tiny areas inside the body, to provide more efficient drug distribution and to enhance the aqueous solubility of poorly soluble drugs [9, 17, 47, 48].

The surface properties of nanoparticles and their interaction with cells play an important role in determining the targeting and delivery pathways.

Passive targeting can be achieved through the high permeability of tumour tissue compared to healthy tissue, which allows nanoparticles of the appropriate size and possessing specific surface properties to extravasate from the capillaries and penetrate through the tissue, providing a high delivery rate [7, 35].

The targeting capabilities of IONPs can be increased by the conjugation of target species, such as low molecular weight ligands, hormones and antibodies, to the surface of nanoparticles without altering the physical and chemical properties of the particles. This type of attachment provides active targeting, which can also enhance uptake by different carcinoma cells. For example, the attachment of epidermal growth factor to a magnetic nanoparticle surface can be useful in the treatment of breast and colorectal cancers [9, 17].

Using nanoparticles for the encapsulation of targeted drugs is important for the improvement of drug bioavailability, minimisation of side effects and toxicity in healthy tissues, and increasing the duration of action and therapeutic efficiency [11]. Nanoparticles are preferred over larger particles in intravenous delivery because the diameter of any particles entering the blood stream should be less than 5 μm in order to avoid the formation of an embolism within the capillaries, which could result from the aggregation of particles [9, 47]. Another useful property of nanoparticles is their ability to deliver drugs across different biological barriers, such as the blood brain barrier, through the attachment of appropriate ligands [17, 49].

1.2 Specific Applications of IONPs

IONPs provide advantages of being traceable within the body, using magnetic resonance imaging (MRI), as well as being targetable to selected tissues with application of magnetic fields. These properties of IONPs are of particular interest to overcome obstacles such as non-specific toxicity due to general systematic distribution as well as poor therapeutic effects due to sub-therapeutic concentrations at target site.

1.2.1 Magnetic Resonance Imaging (MRI)

Over the past decade, MRI has been observed as a highly advanced imaging technique that can provide images of anatomy and pathology with excellent contrast and spatial resolution in addition to imaging physiological processes. IONPs have been used as imaging contrast agents due to their core structure, which is superparamagnetic and allows them to be visualised using MRI. They play an important role in MRI when differentiating between healthy and diseased tissues [9]. The development of MRI has greatly improved the visualisation of various tissues, as well as highlighting specific regions, such as tumour or other pathogenic cells at an early stage [50, 51]. IONPs have saturation magnetisation properties at a high spatial resolution (100 μm) allowing the rapid acquisition of images [52]. The clinical use of MRI is based on the properties of protons present particularly in molecules of water within the human body in different environments. The characteristics measured in MRI is the proton relaxation rate or its inverse and the proton relaxation time. In the case of the application of an external magnetic field, the protons of water molecules will be organized in the direction of the

magnetic field. This is because the hydrogen nuclei are charged and spin about themselves, which makes them behave like tiny magnets. It is the ability of the particles to absorb the radiation that excites the nuclei, and when the radiation is switched off the nuclei emit the energy that was absorbed. However, when the magnetic field is absent or changes, the protons align in the opposite direction to the field. The slight differences in the energy of aligned and anti-aligned spin make it possible to obtain an image from the body [53]. In this procedure, there are two different types of proton relaxation times; the longitudinal relaxation time, T_1 (spin-lattice relaxation) and the transverse relaxation time, T_2 (spin-spin relaxation). Therefore, contrast agents are divided to two types which are positive agents, acting on T_1 providing a positive enhancement of the signal and appearing bright on the MRI scan or a negative enhancement which reduces the signal and appears as dark spots in the scan [54]. Thus, the MRI is a powerful tool to obtain high-resolution soft tissue visualization and is non-invasive (compared to with roentgen CT). Gadolinium diethylenetriaminopentaacetic acid (Gd-DTPA), was extensively used as a positive agent [55, 56], nevertheless it has risks of inducing nephrogenic systemic fibrosis (NSF) with patients having impaired kidney function [57]. Other metals such as Mn and Co have shown accumulative toxicity which limit their clinical application [58, 59]. For this reason, IONPs are the most promising contrast agents for clinical use especially due to their natural appearance in the human body which make them preferable over other metals [60, 61].

1.2.2 Hyperthermia

The desired goal in cancer therapy for many years has been the killing of cancerous cells without damage to normal cells; however, most procedures used to date, including radiotherapy, chemotherapy and surgery, fall short of this aim. Currently, through development in the synthesis of inorganic nanoparticles, an advanced type of nanoparticles can accumulate in tumour cells cause variations to the surrounding environment of cells [62]. For example, IONPs with superparamagnetic properties have a greater ability to absorb energy from a magnetic field and convert it into heat than larger particles. Consequently, a heating of small nanoparticles that are concentrated in specific area causes a necrosis of tumour cells, which are more sensitive to high temperatures in excess of 41°C, than normal cells [9, 18, 19, 63, 64]. The heat generated depends on the properties of the nanoparticles, strength of the magnetic field, concentration of IONPs within the tissue, and biological factors.

1.2.3 Cell Labelling and IONPs Tracking

Cell labelling has been important in biomedical applications for many years. It has been used in assessing cell function, cell proliferation, tracking of stem cells and considering the interaction of nanoparticles with cells. For example, the viability of a cell can be assessed by incubation of the cells with particles to determine their properties, such as cell membrane integrity and apoptosis. A number of factors are important when considering the use of nanoparticles in stem cell labelling which include stem cell differentiation impact, cell function and toxicity

from nanoparticles or breakdown products [65]. Replacement of damaged cells by newly derived tissues requires a safe way to track the movement of the implant cells inside the body to ensure they reach their target tissues. Recent studies have investigated the imaging of stem cells using different cell labelling techniques for the treatment of debilitating diseases such as skeletal dysplasia, spinal cord injury, myocardial infarction [8] and cancer [66-68]. The higher resolution imaging used in the stem cells tracking is MRI, which exhibits no invasive properties and is able to produce three dimensional images in addition to accurate image analysis [69]. IONPs have been used for cell labelling, which can be achieved either by attachment of IONPs to the surface of cells or by internalisation of the particles into cells via different endocytic pathways. The labelled cells can then be detected and quantified by MRI in vitro and in vivo. IONPs are preferably to be used for studying intracellular trafficking by MRI or transmission electron microscopy (TEM) due to their electron density. The efficiency of cell labelling depends on the type and properties of the nanoparticles, particularly on the size, surface functionalisation which are essential for cellular uptake specificity and internalisation of labelled nanoparticles [70, 71]. A study showed a significant decrease in the cell proliferation rate after incubation with Gadolinium for 24 hours [72]. Therefore, IONPs appear currently to be the preferred particles for cell labelling and tracking. A study showed that a higher percentage of labelled cells with a higher amount of intracellular iron uptake and lower amount of extracellular iron aggregate were obtained upon using Feridex protamine complexes, however Resovist

without incorporation of facilitator showed lower cellular uptake and labelling properties [73].

A study was done by Jasmin et al. [74] who used Ferumoxide with poly-L-lysine (FePLL) or protamine (FeProt) labelled mesenchymal stem cells (MSCs) in vivo and imaged after one and seven days post exposure. There was no sign of reduced cell viability or proliferation after 24 hours exposure to FeProt, however FePLL complexes affected cell proliferation after 24 hours exposure. Another study was reported by Chapon et al. [75] who used dextran coated IONPs to track bone marrow-derived mesenchymal stem cells to determine their effect in host cardiac tissue after a myocardial infarction. It was reported that the stem cells labelled with dextran coated IONPs could be tracked even after six weeks of injection using MRI. In addition, it was shown by this study that there was a large uptake of stem cells in infarcted tissue. Thus, the future of using IONPs in stem cell tacking and widespread use in clinical cellular therapies is promising. Results of using IONPs for cell tracking could lead to optimising dosage, specialised timing of stem cell injections and allowing for the tailoring of treatments to individual patients [28].

1.3 Synthesis of IONPs

The main challenge to produce IONPs with a narrow size distribution is selecting a reproducible process without any complex purification procedures. A number of approaches have been used to produce IONPs. These include co-precipitation, hydrothermal synthesis, microemulsion methods, and sonochemical and thermal decomposition.

1.3.1 Co-Precipitation Method

IONPs in the form of either magnetite (Fe_3O_4) or maghemite (γ-Fe_2O_3) are commonly prepared by this method, which is considered as the simplest and is inexpensive in comparison to other methods [8, 76, 77]. Other advantages of the co-precipitation method are reproducibility and the ability to produce large amounts of nanoparticles in laboratory. In addition, due to the use of water in this process, no toxic hazards have been observed previously. However, in this synthesis method, particle size distribution is poorly controlled due to the effect of the growth of crystals and nucleation, which results from supersaturation at a specific concentration. The production of nanoparticles with a narrow size distribution can be achieved by avoiding nucleation during the period of growth or by reducing the nucleation time, since particle size is determined by the end of nucleation and does not alter during particle growth [78].

The size and shape of IONPs can be controlled by the adjustment of the reaction conditions, pH value, temperature, stirring rate, dropping speed of each solution, and ionic strength of the reaction [19, 79].

The co-precipitation method was performed for the first time by Massart [80] many years ago and it gained variety of modifications, however the main chemistry did not change. The chemical reaction of magnetite precipitation from ferric and ferrous salts should be expected to occur at a pH between 8 and 12 according to the equation 1-1 below [79]:

$$2Fe^{3+} + Fe^{2+} + 8OH^{-} \rightarrow Fe_3O_4 + 4H_2O$$

Equation 1-1: Precipitation of magnetite from iron salts

However, due to the instability of magnetite, it is oxidised to ferric hydroxide in the presence of oxygen; therefore, the production process must be performed under anaerobic conditions.

The oxidation of magnetite to maghemite is not only due to oxygen, as the pH of the suspension also has an effect on the determination of the surface characteristics of the superparamagnetic IONPs produced. Iron ions present on the surface of magnetic iron oxide can coordinate with acidic or basic groups to form ionic coordinate bonds. This is the reason for the dispersion of IONPs in water, where iron atoms coordinate with water molecules on further dissociation to give a hydroxyl functionalised surface. On the basis of the above theory, IONPs in a specified medium with a desirable pH range should act as an alkali, whereby Fe_3O_4 gives away Fe^{3+} ions which dissolve in a hydroxide form in an acidic medium as in equation 1-2 [78]:

$$Fe_3O_4 + 2H^{+} \rightarrow \gamma\text{-}Fe_2O_3 + Fe^{2+} + H_2O$$

Equation 1-2: Conversion of magnetite to maghemite

1.3.2 Hydrothermal Method

The disadvantage of the hydrothermal method requires chemicals to be placed in a sealed container and exposed to a high pressure of approximately 2000 psi and a temperature greater than 200˚C [2, 78].

The particles produced by this method are crystalline. The time of reaction, temperature and type of solvent all affect the size of the magnetite particles produced. As the time of the reaction increases, the size of the particles increases due to the precipitation of larger particles.

1.3.3 Microemulsion Method

A water in oil microemulsion can be utilised to synthesise IONPs with a uniform and narrow size distribution. The addition of ferric and ferrous salts (molar ratio 2:1) to the aqueous core of the microemulsion system has been found to produce small size particles with a diameter of less than 15 nm, which exhibit supermagnetic properties with a high magnetisation rate [9]. However, the stability of a microemulsion is influenced by the properties of the oil, water and surfactant, in addition to the pH and temperature. These factors can affect the formation of a microemulsion because any small deviation in the preparation may cause the dispersal of the microemulsion and formation of an unstable macroemulsion [8, 81, 82] . Furthermore, the use of a large amount of surfactant for stabilising the nanoparticles can have a toxic effect in pharmaceutical applications.

1.3.4 Sonochemical Method

This method can be also used to produce IONPs with unusual properties by using ferric and ferrous salts with the aid of ultrasonic irradiation for one hour. The temperature, time of sonication, and power of ultrasonication have a significant effect on the size and form of the resulting particles. The preparation of IONPs by this method requires a very high temperature (5000 K) and a pressure of 1800 atm. The higher

temperature vaporises water and results in the formation of various types of oxidising species, including H^+ and OH^- ions, due to the absorption of the ultrasound energy [83]. In addition, they induce a sonochemical reaction, which occurs in two regions; inside the collapsing bubble and at the interface between the bubble and the liquid. These extreme conditions are important in the formation of nanoparticles with good dispersity; however, the size and morphology of the resulting IONPs is very complicated in comparison to the co-precipitation method. The sonochemical method is still poorly understood [8, 83-86].

1.4 Surface Modification of IONPs

IONPs of small size have a hydrophobic surface with a high surface area-to-volume ratio; consequently, these particles will interact, causing them to aggregate and form large clusters, resulting in increased particle sizes. In addition, due to the high chemical activity of IONPs, they also show a tendency to oxidise, especially magnetite particles, which leads to a loss of dispersibility and magnetism [9, 78, 87, 88]. The stability and dispersability of IONPs are important during investigations in biological culture medium and during the storage for biomedical applications since the stability is dependent on whether the nanoparticles remain dispersed or become aggregated. Cell toxicity may arise from the aggregation of nanoparticles, whereas well dispersed particles may have no toxic effect when correctly dispersed [3, 89].

For in vivo use, IONP's surface may also be exposed to plasma protein adsorption or opsonisation resulting in their rapid clearance by RES [18].

Massart (1981), first prepared aqueous dispersions of IONPs that were stabilised by electrical double layers [80]. However, the stability of IONPs resulting from surface charge repulsion is insufficient to prevent aggregation in biological medium, due to the presence of salts or other electrolytes that can neutralise the charges.

In order to overcome the concern of aggregation and improve the colloidal stability and dispersability of nanoparticles for either in vivo or in vitro application, a thin layer of appropriate coating material is added to surround each particle core for the complete and permanent protection with little or no impact on the their properties. The strategy for maintaining the stability of IONPs is achieved either by electrostatic or steric repulsion forces, as shown in Figure **1-1**. Electrostatic repulsion forces between the particles result in charge stabilisation if they are stronger than the attractive forces causing the stabilisation of the nanoparticles. Charge stabilisation maintains the stability of the colloidal system by providing a layer of charged ions, which surround the colloidal particles and result in mutual repulsion. However, steric stabilisation is achieved by adsorption of polymers with mobile chains onto the surface of dispersed particles. The steric repulsion force depends on the graft density and molecular weight of the coating material, while the electrostatic repulsion force is affected by the surface charge of a particle and the pH of the solution [78, 84, 90].

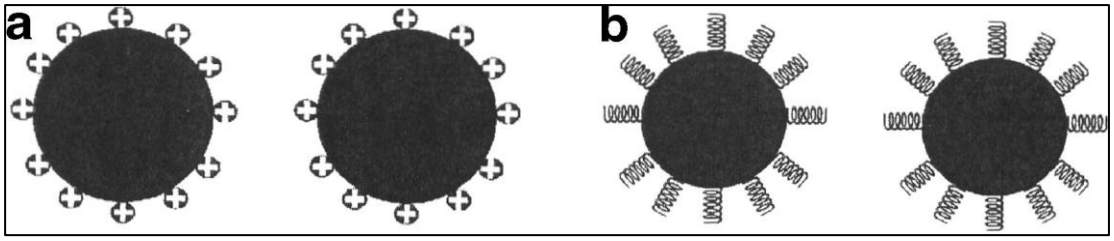


Figure 1-1: Particle stabilisation by (a) an electrostatic layer, (b) steric repulsion. Source:[78].

Various polymers have been used in tissue engineering to increase the stability and biocompatibility of nanoparticles, by providing a layer around the particle core. The type of surface coating materials is very important in the pharmacokinetics and biodistribution of nanoparticles in the body [91, 92]. Polymers can be natural, such as the proteins gelatin, chitosan and albumin, or synthetic, such as [poly (D,L-lactide-co-glycolide)] (PLGA), polylactic acid (PLA), PGA and PEG, with active sites for biological functions [9, 78, 93]. The properties of polymers must be considered for both in vivo and in vitro applications. For example, they should be biocompatible, non-immunogenic or antigenic, prevent the particles from aggregating and should bind or adsorb effectively to the iron oxide surface [84, 94]. They also should prevent opsonisation by plasma proteins.

Polymers may contain specific functional group properties, such as carboxylate, phosphate, hydroxyl or sulphate groups, which are pendant groups that have great affinity for the surface of IONPs. The COOH group has the affinity to form a coordination bond with IONPs, which leads to an increase in particle stability. However, COOH-IONPs bonds are very

weak and can be broken at high temperatures and during ion exchange [49, 95]. Suitable surface functionalisation is therefore very important for achieving a sufficient repulsion force to prevent aggregation and obtain a stable colloidal solution.

Dextran is a polysaccharide polymer, which has been used widely for coating IONPs because of its biocompatibility. However, the resulting high coating thickness contributes significantly to the hydrodynamic size, resulting in a reduction in the labelling efficiency of the particles [96, 97]. Furthermore, because the dextran is not strongly attached to the IONP core, the polymer undergoes detachment [98, 99].

PLGA and PLA are widely termed as biocompatible, biodegradable polymers and have both been used as coating materials for nanoparticles. However, the main disadvantage of these polymers is that they usually lead to formation of large particles sizes resulting in significant loss (about 40 to 50%) in magnetisation of the iron oxide core [10, 100].

Based on the publication of Kallinteri et al (2005) [101], the effect of different coatings on both the nanoparticle size and their stability was investigated. A biodegradable polymer, PGA has been developed from non-toxic monomers which is useful for nanoparticle drug delivery due to their compatibility with the human body; it has the capability to self–assemble into small particles. This polymer, which is obtained as a copolymer of the polycondensation reaction of glycerol, and adipic acid (1:1) that is catalysed by a lipase. It has an advantage over PLA and

PLGA due to the possibility of modifying the pendant hydroxyl groups on the polymer backbone, and the facile introduction of chemically different functional groups in varying proportions, resulting in changes in the physicochemical properties of the polymer. Furthermore, there may be a physical connection of the polymer with IONPs due to the hydrogen bonds between the polymer hydroxyl groups and the particle surface oxide and hydroxyl groups [18, 93, 102-104].

PEG is a biodegradable, hydrophilic and non-toxic polymer which can be conjugated with hydrophobic polymers, such as PGA, which increases aqueous solubility and inhibits particle aggregation in vivo as well as in vitro [10, 15]. This polymer (PEG) provides steric stabilisation of particles by forming a layer around the surface which results in a neutral charge and a barrier that prevents the particles from aggregating [103]. PEG could also be used to prevent unwanted adsorption of serum proteins, as this polymer has the ability to reduce the binding of proteins to the particle surface by the shielding of the surface charges and increase the surface hydrophilicity [105]. The degree of coverage and the density of polymers on the surface of nanoparticles has an effect on cellular uptake, as a complete coverage of each particle with higher density polymer leads to inhibition of the adsorption of proteins in the biological media onto the surface of nanoparticles. In general, this leads to a reduction in non-specific binding to unwanted sites, but also in some cases where serum proteins are recognised by certain cells, adding a serum protein ligand to PEGylated particles results in increased targeting uptake [51, 106-109]. Consequently, for biological application, serum protein should be taken

into account when investigating the interaction of IONPs with an epithelial cell layer.

The coating process can be carried out during the synthesis process, however the pH and temperature have an effect on the surface bond between polymer and particle core [110]. The interfacial deposition method (IFD) has been used previously by our team and showed good results in producing a small nanoparticle size.

1.5 Biocompatibility and Toxicology of IONPs

Many studies have examined the cytotoxicity of IONPs with and without coating materials, and have generally found that IONPs are biocompatible, demonstrate little or no cell toxicity, and maintain cell viability for a long time because iron is stored and transported routinely in the core of an iron storage protein called ferritin [9]. IONPs have not shown any detectable toxicity at a dose of 0.56 mg/kg which was more than the dose permitted for human use by the U.S. Food and Drug Administration [12, 111]. Therefore, IONPs are used in biomedical applications due to their lack of toxicity and are deemed the safest particles for use in humans. In comparison, the acceptable limit for Manganese (Mn) and Zinc (Zn) is much lower than Iron, so a surface control is required [11]. In addition, other elements such as Ni and Co, which are used in hyperthermia applications, are very toxic and require an appropriate coating when they are used in vitro or in vivo [11]. However, other studies reported that IONPs may cause toxicity due to

various factors, such as the type of surface coating or their metabolic products and oxidation states because of the production of reactive oxygen species, such as free oxygen radicals, hydroxyl radicals, and the non-radical hydrogen peroxide, which can potentially directly damage DNA [12, 112]. IONPs coated with PEG have been shown not to exhibit any toxic effects on cells, are often recognised as biocompatible and relatively safe, and do not accumulate in the body [12, 23]. However, one study investigated the effect of dextran-coated IONPs on cells and found that dextran-coated IONPs prevented cell proliferation, resulting in cell death due to the aggregation of IONPs, which was a consequence of the destruction of the dextran shell [6, 112].

1.6 The Internalisation Strategy of IONPs for Crossing Biological Barriers

It has been repeatedly demonstrated that different types of nanoparticles will enter cells by different pathways, however it is unpredictable by which route internalisation will occur. The airway epithelium is approximately 25 to 40 µm thick and plays an important role in the regulation of transport processes as well as controls the movement of particles into and out of a cell. This polarised layer has an apical surface on the luminal side, which is specialised for interactions with biological molecules and macromolecules while the basolateral membrane has a different surface, which attaches to the basal lamina. Epithelial apical membranes consist of a bilayer of phospholipids containing embedded proteins, which vary

between different cell types and therefore influence the properties of a membrane [17, 44, 113].

The entry of substances into cells and their translocation across biological barriers are important and can be through passive or active processes. Small and polar molecules pass freely between adjacent cells through (paracellular uptake), whereas nonpolar substances diffuse through the bilayer (transcellular uptake). Bigger sized nanomaterials require specific energy dependent internalisation mechanisms including clathrin mediated endocytosis, caveolae mediated endocytosis, micropinocytosis and phagocytosis [113, 114]. The cellular uptake pathway and distribution of nanoparticles has been shown dependent on the cell type [115], size [116] as well as surface chemistry of nanoparticles [117]. The process of nanoparticle uptake is important because it can affect their subsequent intracellular trafficking and final destination within cells [118]. Although, various studies have shown IONPs are taken up by cells using endocytic pathway and preferentially localised within endosomal compartments [40, 119-121], there have been few reports that proposed nanoparticles could be taken up into cells via a non-endocytic route [122-124], thus IONPs internalisation pathway need to be fully understood. Biologically, the specificity and efficiency of IONPs targeting to specific cells require strong cell interactions with cell surfaces in order to be delivered inside cells. Therefore, considering the route of cellular uptake, intracellular localisation and distribution of IONPs inside cells are critical in biomedical applications such as intracellular imaging [125].

1.6.1 Endocytosis of Nanoparticles

Endocytosis is an energy-dependant process through which cells internalise macromolecules and nanoparticles [44, 126]. The process of endocytosis consists of macropinocytosis, pinocytosis, phagocytosis and the important receptor-mediated endocytosis pathways (clathrin/ caveolae-mediated endocytosis), as shown in Figure 1-2. The endocytic pathways differ with regard to the size of the endocytic vesicles and cargo properties. Fluids and particles with less than 0.5 µm in diameter are taken up through pinocytosis (cell drinking), which absorbs biological fluids from the external environment of the cells. Pinocytosis occurs in all cells including macrophages and cancer cells to obtain nutrients and biological mediators.

Macropinocytosis covers a broad range of particle sizes from 1 to 5 µm [127, 128]. It is a relatively nonspecific pathway and thus has the potential to transport different types of particles into cells especially those located near the cell membrane resulting in encapsulation by the membrane and formation of macropinosomes which result in uptake of material into cells with a large volume of extracellular fluid [127, 129]. Large particles (more than 0.5 µm) are cleared mainly by phagocytic processes [126, 130, 131]. Pathogens and viruses are also taken up by phagocytosis to protect the host from infection by them. The process of phagocytosis is disadvantageous in general for exhibition of an efficient pharmacological influence of nanoparticle formulation because the uptake of particles by macrophages reduces the extracellular concentration of nanoparticles [128]. When specialised phagocytic cells

such as macrophages, neutrophils or monocytes are exposed to nanoparticles covered with protein (opsonins) in the blood stream, then particles will be engulfed by phagocytic cells [132, 133].

Clathrin mediated endocytosis is the most studied internalisation route used to bring material into cells via membrane proteins that are embedded inside phospholipid bilayer to form a basket like structure [134]. This is then enclosed inside the cell membrane and internalised within specialised vesicles with a diameter of about 150 nm forming clathrin coated vesicles [135, 136]. Most types of clathrin mediated endocytosis progress via a series of steps leading to the endolysosomal route for degradation or recycling [133, 134, 137]. The clathrin coated vesicles have been demonstrated to internalise several different particle types of such as silica and PLGA [137, 138].

Caveolae mediated endocytosis is another major endocytic pathway, which involves the formation of, flask shaped structures in the plasma membrane. Compared to clathrin dependent endocytosis, this pathway can internalise particles of about 50 nm in diameter and has been found at the basolateral membrane of cells [139, 140]. This pathway could avoid lysosomes for certain types of uptake. A number of different cargoes have been shown to be internalised by caveolae mediated endocytosis such as cholera toxin B and glycosylphosphatidylinositol (GPI) linked proteins which can interact with the receptors on the plasma membrane and induce formation of vesicles that pinch off from the membrane and traffic within the cell [133, 141, 142].

Endocytosis is designed to take nanoscale materials, including nanoparticles and viruses, which are normally present in extracellular fluid, into a cell. The particles are encapsulated within a vesicle, which separates the particles from the cytoplasm by the vesicle membrane. Depending on the mode of internalisation, they may either be recycled or exocytosed out of the cells or be trafficked to other intracellular locations, including lysosomes, mitochondria and golgi [108, 143]. In some cases such as lysosomal storage disorders, nanoparticles taken up into the endolysosomal compartment provides immediate accessibility to their targets [144]. However, the entrapment of nanoparticles within vesicles for many applications is undesirable because they undergo degradation at acidic pH by enzymes. For this reason, several strategies have been developed for endosomal escape through protecting nanoparticle surface by selecting suitable coating materials. Once nanoparticle escapes from endosomal network, they must travel freely through the cytoplasm to their specific target cells or subcellular compartments for therapeutic effects without binding to intracellular components such as proteins, small molecules and nutrients [145].

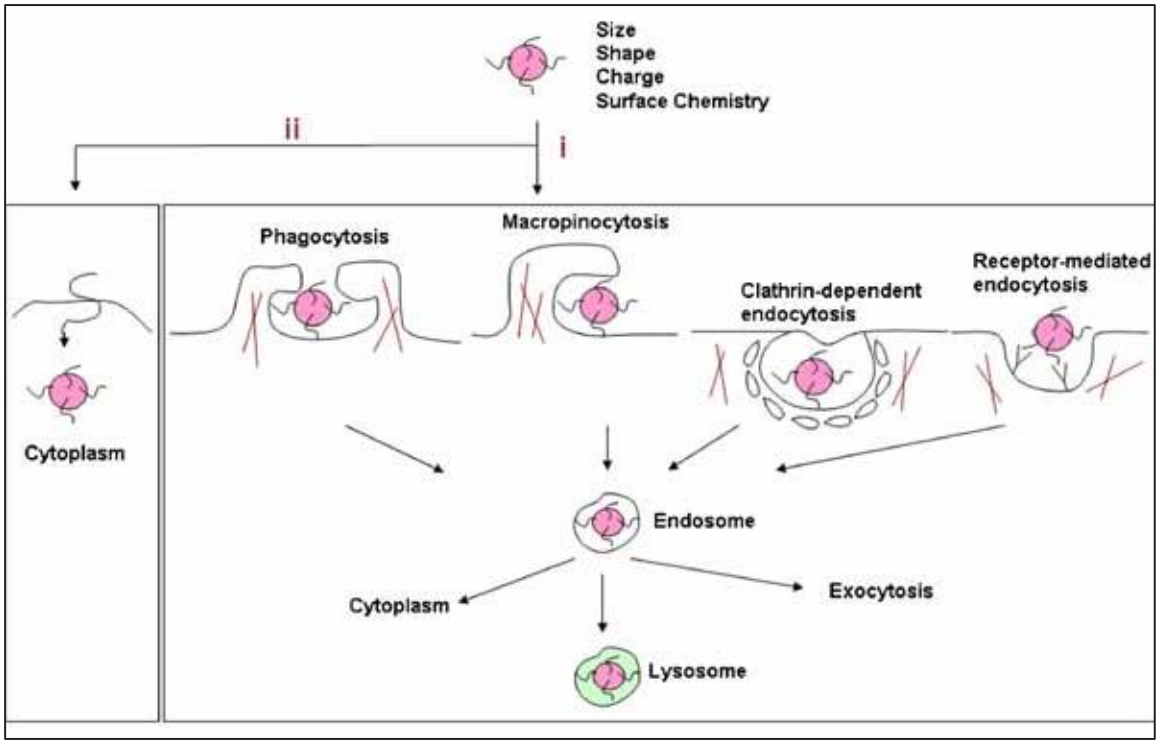


Figure 1-2: Cellular internalisation of nanoparticles by endocytosis, phagocytosis, micropinocytosis, clathrin dependant endocytosis and receptor mediated endocytosis pathways. Source: [143].

1.6.2 Exocytosis of Nanoparticles

Exocytosis processes are important due to the relationship between chronic toxicity and nanoparticle retention times. Exploiting exocytotic properties may allow improvements to be made to drug delivery nanosystems to enhance clearance after delivery. Nanoparticles exposed to the blood stream tend to interact with opsonins especially if their surfaces are not fully protected. When opsonins attach to the nanoparticle surface, they allow the cells of the MPS to easily recognise the nanoparticles resulting in the nanoparticles accumulating in the organs of the MPS such as liver and spleen. Therefore, the targeting efficiency are decreased and severe systemic toxicity may happen. In

the exocytosis process, non-dissolved particles are expelled from the cell cytoplasm by enclosing them inside vesicles that fuse with the cell membrane and then release their contents outside of the cellular environment [146]. Many studies have investigated the effect of the size and shape of nanoparticles on the exocytosis process, and it has been found that small and rod shaped nanoparticles are released at a faster rate from a cell than larger and spherical nanoparticles [108].

1.6.3 Paracellular Transport of Nanoparticles

This is a passive permeation pathway, which allows very small sized particles, ions and water to diffuse in the spaces between epithelial cells Figure 1-3 Polarised epithelial cells have a tight junction that is located at the apical membrane, between adjacent cells, with a pore diameter of 2-4 nm. The tight junction is a selective permeable barrier, which allows the passage of small, hydrophilic molecules while preventing the movement of large molecules [49, 63, 147]. The permeability of tight junctions can be assessed by transepithelial electrical resistance (TEER) which varies greatly among epithelial cells, ranging from 5 to 5000 Ω cm^2 [148]. Movements of ions through the tight junction are largely dependent on the concentration gradients of permeant ions [149]. Tight junctions can also determine the integrity and polarity of an epithelial monolayer in addition to the electrical resistance properties of an epithelial barrier [49, 150]. They also maintain the polarity of the apical and basolateral domains. Although, several proteins have been identified within the structure of a tight junction, the claudin family of proteins are the most important for function and structure, as they create a charge

sensitive channel between adjacent cells. The expression of claudins seems to contribute to a high TEER reading. It was established that some types of molecules could also affect the permeability among different tissues, for examples small peptides less than 40 KDa can passively diffuse through the junction, however larger proteins (> 40 KDa) can only cross the barrier by the transcellular route [147, 151].

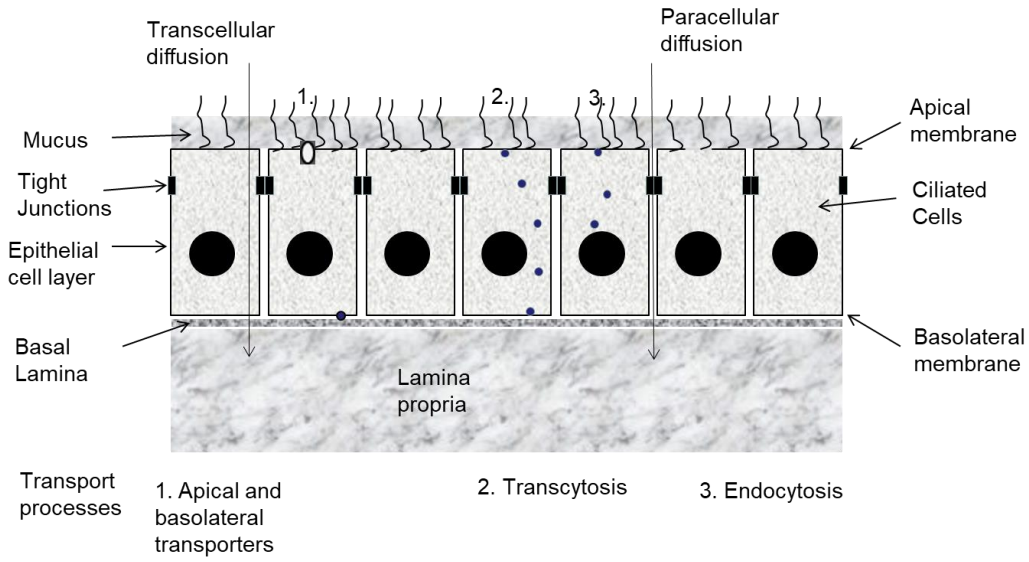


Figure 1-3: Transport mechanisms through epithelial cells held together by tight junctions sitting on a basal lamina with mucus cover layer. The main different transport pathways are shown in the numbered cells. Modified from Garnett et al [152].

1.6.4 Transcytosis of Nanoparticles

In this mechanism, nanoparticles enter cells by crossing the cell membranes without using any of the uptake pathways mentioned above, it also known as transcellular transport (Figure 1-3) [49]. Transcytosis is an active transport pathway that guides molecules by vesicular transport

through the cells without entering the degradation pathway. For example, uptake of nanoparticles from the airspace into the bronchial epithelium requires partitioning through the apical mucus layer. Well-formed nanoparticles can enter the specific organ or cells if they can travel across the epithelial cells and get into blood vessels and after that get to tissue sites by crossing the capillary endothelial cells. Transcytosis plays a critical role in this process, in which particles diffuse into vesicles present on the apical surface of the polarized epithelial cells lining organs and are then transferred across cells in vesicles and exit from the cell at the basolateral membrane [49]. The main function of vesicles when considering nanoparticles, is to increase the uptake of particles through enhancing their transport across the epithelial layer [147]. This kind of transport has been observed for antimicrobial peptides that can form pores in the membrane of bacteria leading to their translocation across the membrane [153].

1.7 Factors Affecting Particle Uptake and Transport

Physicochemical characteristics of nanoparticles such as size, shape, surface charge and chemistry are important aspects in determining whether nanoparticles will be taken up by endocytic or transcytosis route.

1.7.1 Size

The size and type of particles decide the properties and biological fate of these particles [154, 155]. It is important in determining the uptake, targeting, duration of action, and clearance of nanoparticles. The

efficiency of particle uptake is different according to the cell type and the size of the particles. For example, studies showed that the number of gold nanoparticles taken up by cervical cancer cells reaches a maximum at a diameter of 50 nm. Other studies have quantified the uptake of fluorescent polystyrene nanoparticles by measuring in vitro release of fluorescence and they have reported that polystyrene nanoparticles with a diameter of 100 nm being more efficiently taken up by adenocarcinoma cell lines than when the particle diameter is 50 nm [35, 108, 156]. These studies suggest that although size plays an important role in the efficiency of cellular uptake, cell type is another factor that could affect the cellular uptake as size dependent uptake that is observed in one cell type may not be repeated in another. Other examples include particles with a diameter of 15 nm being more readily internalised by cells than larger nanoparticles with a diameter of 45 nm [17, 29]. Previous studies demonstrated that small hydrophobic particles with a diameter of 2 nm have been shown to be located inside the hydrophobic membrane, whereas larger hydrophobic particles tend to disrupt lipid vesicles [17, 157].

Nanoparticle size can also influence the route of cellular uptake. Large particles (>0.5 μm) are shown to be internalised into cells through phagocytosis or micropinocytosis in specialised cells. However, smaller particles may be internalized by clathrin or caveolae mediated endocytosis.

The size of nanoparticles has also been shown to influence their final location within cells. For instance, small nanoparticles with a diameter less than 100 nm can escape blood vessels and this is of particular interest when considering targeting tumours since blood vessels in tumours are often more permeable which in turn leads to accumulation of nanoparticles within tumours. In contrast, particles on the micron scale undergo phagocytosis after entering phagocytic cells such as macrophages, which reduce their effectiveness by reducing the cellular targeting uptake [108, 158, 159]. Therefore, size is an important factor, which should be considered when designing nanoparticles for use as a targeting and diagnostic agent.

1.7.2 Surface Properties

Most mammalian cells, including macrophages, carry a negative charge on their surface, consequently the surface charge of nanoparticles has an effect on the uptake and transport pathways [17, 45]. The charge on the surface of nanoparticles can be controlled by choosing a suitable coating material. Positively charged nanoparticles exhibit a higher cellular uptake than negatively and neutral charged particles, and consequently higher levels of internalisation [17]. Internalisation of positively charged nanoparticles into cells is possibly due to contact with the negatively charged cell surface via electrostatic interactions [109]. Other studies have considered the internalisation of negatively charged particles, and demonstrated a high level of internalisation following binding to the plasma membrane and subsequent endocytosis [158]. When considering the effect of charge, the functional groups that

impart the charge to the nanoparticles should also be taken into consideration as these groups affect other nanoparticle properties such as solubility and interaction with surrounding medium because any change in charge can influence cellular internalisation [109, 160].

A study showed that nanoparticle charge rather than size is an important determinant of the interaction with intestinal epithelial cell model. It was found that the transepithelial movement of both positively and negatively charged nanoparticles did not notably differ between 50 and 100 nm nanoparticles, however, negatively charged nanoparticles were more efficiently transported cross a human colon carcinoma (Caco-2) monolayer compared to positively charged nanoparticles [161]

Hydrophobicity/hydrophilicity surface properties of nanoparticles can also affect their cellular uptake. Colloidal particles with a hydrophobic surface generally adsorb various proteins that present in plasma after I.V. administration which lead to them being specifically recognised by macrophages (opsonisation process) [18, 84]. In order to avoid opsonisation, alteration of nanoparticle hydrophobicity/hydrophilicity is important to reduce uptake by macrophage cells [102, 103]. Studies found that, reducing hydrophobicity of the particle surface leads quantitatively to block the opsonisation process [102]. Nanoparticles without PEGylated layer accumulated in the MPS organs very quickly and usually concentrated in the liver and spleen, however for PEGylated nanoparticles, the speed of clearance and final biodistribution was dependent on many factors such as the size [103, 106, 162].

The surface properties of nanoparticles are very important for their stability in vitro and in targeting many diseases. In the in vitro environment, serum proteins can adsorb to nanoparticle surfaces resulting in aggregation of particles, thus to prevent aggregation and so also to stabilise nanoparticles, a hydrophilic surface is required for a good dispersibility in serum in order to prevent aggregation that results from adsorption of protein in culture medium to the nanoparticle surface. [8, 163]. However, Abo-zeid et al. [164] investigated that nanoparticles could be incubated in serum to prevent aggregation in physiological media.

1.7.3 Shape

The shape of particles can have an effect on the cellular penetration rate, as non-spherical particles with different thicknesses have a lower uptake rate than spherical nanoparticles [4, 17]. Spherical particles can move more easily across epithelial or endothelial cells. As reported in previous studies that the uptake of spherical particles by cervical cancer cells is greater than for triangular, cylindrical or cuboid nanoparticles [156] however, rod-shaped nanoparticles are taken up more efficiently by macrophages than spherical particles [108]. Consequently, spherical particles are preferable over all other shaped particles.

1.7.4 Cell Type

Because each cell type has, a unique phenotype, growing conditions such as cell density, can cause nanoparticles to be internalised by cells via different pathways. Similarly, there is a difference in targeting between normal and tumour cells, with tumour cells exhibiting increased permeability for nanoparticles compared to normal cells [9, 137]. A

previous study by Meng et al. showed that the uptake of Rhodamine B Isothiocyanate Poly (glycerol-adipate) nanoparticles was lower in normal mixed foetal brain cells, than the DAOY cell line (a human medulloblastoma) showing that tumour cells take up nanoparticles more effectively than normal cells in 3-D cell culture [165]. Thus, understanding cell biology and the relationship between cells and nanomaterials is crucial for advancement within nanomedicine.

A study by Fowler et al. [166] considered the uptake of B_{12}-conjugated nanoparticles by the airway epithelium (Calu-3). They found structural cell components are responsible for the process of endocytosis or transcytosis. Long term fate of nanoparticles in the epithelium is either accumulation in late endosomes or rapid transcytosis to the basal side of the cell.

1.8 Epithelia Cells (Calu-3) for IONPs Uptake Studies

In vitro approaches have been utilised by researchers and the pharmaceutical industry to mimic the target tissue, also for drug screening. They can more reliably identify potential drug candidates, and using primary cells reduces the costs associated with downstream animal testing and human clinical trials [167]. In addition, they were used to evaluate the cellular uptake and permeability characteristics of the epithelial cell barrier and to consider the properties of nanoparticles in normal and diseased cells.

In the present study, a bronchial adenocarcinoma of a sub-mucosal gland in a 25-year old Caucasian (Calu-3 cells) was used. They are able to form a monolayer when cultured [168]. The airway epithelium is a mucosal surface composed of ciliated and undifferentiated basal cells that forms the interface separating the external environment from the sub-epithelial tissue [169]. These cells are able to form functional tight junctions and they have been become the principal cell line extensively utilised by researchers as a model of airway barrier for epithelial permeability. In addition, Calu-3 cells are finding increasing application in delivery systems and toxicology. In addition, these cells exhibit in vivo like barrier properties especially when grown by using air-interface culture [170-172].

Calu-3 cells have various morphological and functional characteristics and are the best available cell line for this purpose. When grown as a monolayer on a semipermeable filter, these cells possess a polarised morphology with cilia present on the apical surface and tight junctions between adjacent cells. One disadvantage of these cells is that their characteristics could alter as the number of passages increases. Successful use of Calu-3 cell culture as a model could be an important to determine the pathway of nanoparticle uptake by epithelial layer [173]. Considering the endocytosis and transcytosis of IONPs through airway cell line are important in development of particles, thus detailed study of nanoparticles uptake by epithelial cells in vitro needs to be characterised for maximum uptake.

A potential limitation of nanoparticle delivery across the airway epithelium is the presence of a layer that lines the epithelium and acts as a barrier to transmucosal movement of IONPs. For this reason, this layer should be considered when designing nanoparticles for systemic delivery through the airways. The surface properties is an important factor for the particle movement in mucus, whereby anionic nanoparticles diffuse more efficiently than cationic particles [174]. The presence of PEGylated layer could also enhance nanoparticle movement in mucus [175].

1.9 IONPs for Uptake Study

The present work follows on from a previous study within our group that was done by Abushrida (2012) [176]. Abushrida synthesized PEGylated PGA 40%C_{18} by coupling of PEG MWt 2000 to the core of PGA 40%C_{18}.The study showed that IONPs of approximately 13 nm diameter could be coated with a thin PEGylated PGA 40%C_{18} layer resulting in a much more hydrophilic surface, with a very high particle uptake into C6 medulloblastoma cells.

1.10 Aims of the Project

The enormous diversity of nanoparticles that can be produced makes it difficult to definitively link between a certain parameter and cellular uptake because it is likely to vary between cell line and environment.. IONPs are ideal for cellular tracking because they are electron dense particles, which allow a high-resolution visualization of cell biodistribution

under TEM. IONPs have a number of applications in the medical area, such as a diagnostic agent, tracer material and drug delivery agents. Consequently, there is an increasing need to develop general design for IONPs in order to improve nanoparticle specificity, efficacy and intracellular targeting.

The cellular uptake of IONPs coated with PEGylated PGA 40%C_{18} was studied previously by Abushrida using C6 medulloblastoma and he showed very high uptake into C6 cells, but with an unusual subcellular distribution. The even subcellular distribution of IONPs was in all compartments throughout the cell, which may indicate that the normal endocytic mechanisms were not the main uptake route. However, the study suffered from a variety of limitations. First, the nanoparticles possessed a wide distribution of size with uncontrolled coating thickness which may affect the predictability of nanoparticle behaviour within cells as different sizes of the same batch might affect the outcome and interpretation of results. Second, the study focused on the effect of nanoparticles of size 13 nm, however there may be an optimal size for an efficient uptake. Third, C6 cell aggregates was used rather than epithelial layer, for this reason it was not possible to investigate the nanoparticle translocation. Thus, there is still a need to modify some parameters such as coating thickness and size distribution for the production of a narrow particle distribution with thin coating layers. In addition, there is still more need to confirm the location of the nanoparticles and their non-endocytic route and how this relates to properties of the NPs such as size. Due to the ability of Calu-3 to form

an epithelial layer acting as a barrier, it becomes possible to investigate and evaluate the endocytosis and transcytosis of fluorescently labelled IONPs. Therefore, the use of this lung epithelial cell line will allow examination of the in vitro permeability of IONPs as well as their cellular uptake pathway and intracellular accumulation within cellular compartments of the lung epithelium. The data will indicate whether IONPs offer promise for both imaging and delivery platform that could be used to deliver drug cargo either into peripheral location or across the deep lung respiratory epithelium for biomedical applications. Additionally, a non-endocytic route may provide an alternative uptake route which may be useful to deliver therapeutic agents directly to the cytoplasm especially for those that can be trapped in the endosomal compartment or inactivated by acid hydrolases.

The first aim of this work is to produce IONPs of different sizes and show in detail the effect of amount of different polymer types on the size of IONPs. The objective is to synthesis IONPs coated with biodegradable polymer using a simple method that resulting in formation small coated IONPs. Physico-chemical characteristics of the coated IONPs will be determined. In addition, the stability of these particles will be assessed for using in physiological conditions.

The second aim of this study is to understand the effects of IONPs with different particle sizes on cellular uptake and internalisation using bronchial epithelial cell line. Additionally, the study will explore the cellular localisation of the labelled IONPs existing in the in vitro bronchial

epithelium models. The effects of internalisation of these particles on the cells will be investigated through an examination of cell morphology, viability and proliferation.

The final chapter assesses the potential usefulness of these particles coated with a thin layer of copolymer as MRI contrast agent, as there is an interest in the use of IONPs in this manner to improve the sensitivity when imaging tissues.

2 Materials and Methods

2.1 Materials

2.1.1 General chemicals

Ferric chloride hexahydrate ($FeCl_3.6H_2O$) granules were purchased from RS components (Northants, U.K), ferrous chloride tetrahydrate ($FeCl_2.4H_2O$) powder was obtained from MP Biomedical (Cambridge, UK), acetone was obtained from Fischer (Loughborough, UK), and sodium hydroxide pellets, concentrated hydrochloric acid, and phosphate buffered saline (PBS) tablets were purchased from Sigma Aldrich (Poole, U.K). Deionised water was obtained from an ELGA purification system (ELGA, High Wycombe, UK), which provided water with a resistivity of more than 15 MΩcm. HEPES (0.01M buffer N-(2-hydroxyethyl) piperazine-N'-(2-ethanesulphonic acid) was adjusted to pH 7.4.

2.1.2 Cell culture reagents

Calu-3 epithelial cells (from ATCC) were stored in liquid nitrogen and maintained in Eagle's Minimum Essential Medium (EMEM, ATCC) supplemented with 1% v/v penicillin/streptomycin antibiotic solution, 1% nonessential amino acids (NEAA) and Foetal Bovine Serum (FBS, 10% v/v, Sigma Aldrich, UK), which were sterilised prior to use by filtration through a 0.22 µm Whatman sterile filter. PBS was prepared by dissolving the PBS tablets in 200ml in purified water. FluoroBrite DMEM (made in 50ml aliquots: 49ml FB-DMEM + 0.5ml NEAA + 0.5ml L-glutamine, and sterilised prior to use by filtration through a 0.22 µm

Whatman sterile filter). Formaldehyde (4% w/v solution) was purchased from Genta Medical (York). Rhodamine B Isothiocyanate (RBITC) was purchased from Sigma (Poole, UK) and Prolong® Diamond Antifade Mountant with DAPI were obtained from Thermo-Fisher Scientific (Loughborough). LysoTracker® Green DND-26 (Molecular Probes, U.S.A) provided as 1mM stock solution, was prepared by diluting the probe stock solution to concentration at 50nM with HEPES buffer (0.01M, pH 7.4). Draq-5 (5 mM, 1 µl in 5 ml of FB-DMEM) was purchased from Biostatus Limited (Leicestershire,U.K.). Reagents used in TEM were from Agar Scientific Ltd. (Essex, UK) and all other reagents were purchased from Sigma-Aldrich (Poole).

Clear or black 96 well plates, clear 24 and 6 well plates and 75 cm^2 flasks, Polycarbonate Transwells® 0.4 µm pore size, 12 wells (1.12 cm^2) were obtained from Corning Costar (Nottingham, Nottinghamshire, UK). Corning cell culture plastics were also obtained from Sigma Aldrich.

2.1.3 Polymers Used in This Study

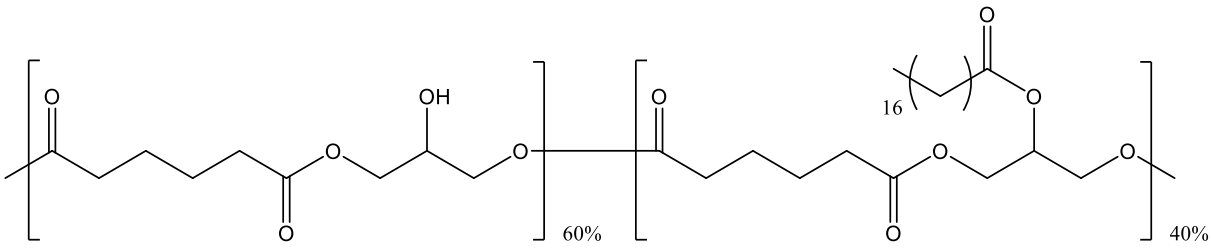
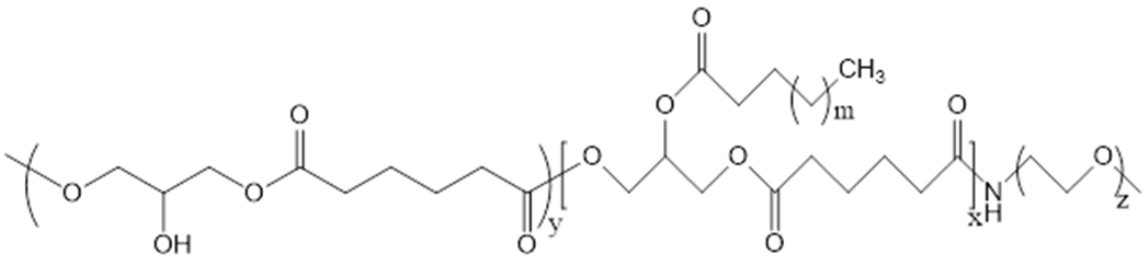


Figure 2-1: Structure of poly(Glycerol Adipate) 40%C_{18}.



m=14 for stearoyl chloride
x=40%
y=60%
z=44%

Figure 2-2: Structure of Poly(Ethylene Glycol) poly(Glycerol Adipate) 40%C_{18}.

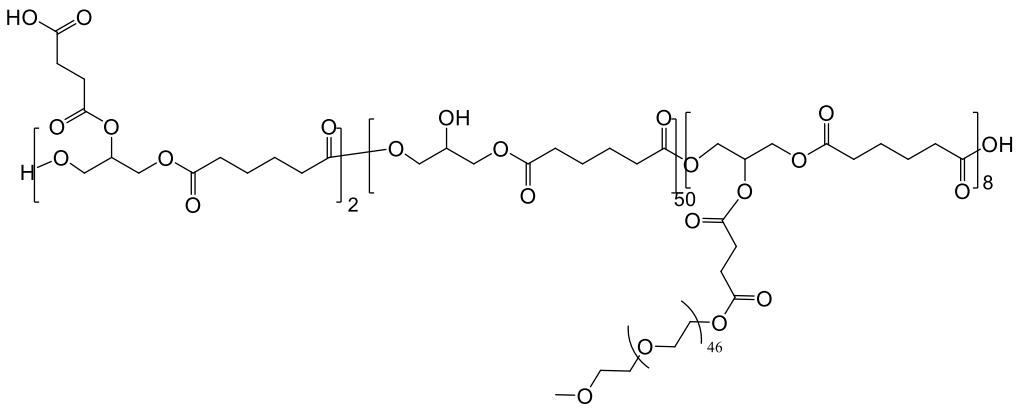


Figure 2-3: Structure of PEG-PGA-SA which has Pendant PEG chains from reaction with pendant succinic acid side chains on succinylated PGA

Poly(Ethylene Glycol) - poly(Glycerol Adipate) 40%C_{18} (PEGylated PGA 40%C_{18}) used in present studies was synthesised by Ahmed Abushrida, at the University of Nottingham [176]. The PEGylated PGA 40%C_{18} was produced using carbonyldiimidazole to activate the carboxyl group of the PGA substituted with 40%C_{18} for coupling with the amine group on PEG amine to produce the PEGylated copolymer at 1:1 molar ratio.

PEG-Poly(Glycerol Adipate)-succinic acid (PEG-PGA-SA) was synthesised by Vincenzo Taresco at the University of Nottingham. Starting PGA (5% of branching) with an estimated 60 repeat units along the main backbone, succinylation was performed in THF using 10% mol/mol of Succinic anhydride compared to PGA units. The reaction was almost quantitative. Subsequently, PGA was added drop-wise to a DCM/THF solution of mPEG, DCC and DMAP equimolar with the succinyl groups. The crosslinked precipitate was removed by filtration and the soluble polymer precipitated in cold Hexane. PEGylation was around 80% in yield, giving an estimate of a small excess of succinic acid pendant groups.

2.2 Methods

2.2.1 Synthesis Processes

2.2.1.1 Synthesis of IONPs

IONPs were prepared by a modified co-precipitation method [176, 177]. FeCl3.6H2O (14 g) was dissolved in water (50 ml), and a flask containing $FeCl_2$.4H2O salt (0.98 g, 1.232 M) was mixed with 4 ml 1.036M $FeCl_3$.6H2O (ferric-to-ferrous 0.84:1 molar ratio). Next, 10 ml of deionised water was added with constant and rapid stirring for at least 30 minutes. In order to avoid oxidation of the ferrous ions, the reaction was carried out under reflux conditions in a nitrogen atmosphere. The temperature of the whole mixture was kept at 80°C for 1 hour, and then allowed to cool to room temperature. Subsequently, 6 M NaOH was

added to precipitate the magnetite formed. To achieve different sizes of IONPs, the amount of NaOH (6 M) was varied and the final pH of the mixture was controlled by the addition of 4 M HCl. The temperature was then elevated to 100°C for 1 hour followed by cooling. The product was purified by dialysis using a MWCO 1000 dialysis membrane (Spectrapor) against deionized (DI) water over 24 hours. Finally, the dispersed particles were filtered through a 0.2 µm filter and stored at 4°C (without further treatment after dialysis) for further investigation.

2.2.1.2 Surface Coating of IONPs

Following synthesis, the IONPs were coated with different polymers using the interfacial deposition method, which involves the slow addition of an organic phase containing the polymer to the aqueous phase containing the IONP with constant stirring. Three polymers, PGA 40%C_{18}, PEG-PGA-SA and PEGylated PGA 40%C_{18} were used for coating the IONPs. The required amounts of the polymers were weighed accurately in order to make stock solutions in acetone (20 mg in 2 ml). Varying amounts of polymers (equivalent to 0.05 mg, 0.1 mg, 0.2 mg and 0.3 mg) were taken from these stock solutions and diluted to make them up to 2 ml with acetone.

The IONP solution (2 ml nanoparticles and 3 ml of DI water) and polymer solution (2 ml) were mixed using two pumps and a mixer (Pharmacia LKB, Pump p-1, Amersham Biosciences), with both solutions being pumped at different rates through a mixing chamber in proportion to the volumes of each component. The flow rates were chosen in order to give

complete mixing of the reagents over 1–2 minutes. Following mixing, the particle suspension was left on a stirrer overnight in a fume hood in order to completely evaporate the acetone. The coated nanoparticles were collected the next day and further characterised. This modified method was based on that of Fessi et al. (1989) for polymer nanoparticle production [178].

2.2.1.3 Formation of RBITC-Labelled Coated IONPs

Rhodamine B Isothiocyanate (RBITC) in acetone (2 mg/ml, 150 µl) was added dropwise into the coated IONPs in HEPES buffer (0.01 M, pH 7.4, 7 ml) with vigorous stirring overnight in fume hood in order to evaporate the acetone. The IONP suspension was dialysed against PBS using a MWCO 10,000 dialysis membrane to remove unbound fluorescent dye. The conditions of experiment was carried out in dark using an aluminium foil cover.

2.2.2 Analytical Instrumentation

The most important part of experiments is characterization, which gives an opportunity to analyse results of synthesis experiments and to choose the next step to achieve expected results. Different parameters need different characterization procedures. Prepared samples were routinely analysed for particle size and surface charge.

2.2.2.1 Dynamic Light Scattering

A Malvern Instruments Viscotek 802 DLS (Malvern, UK) was used for hydrodynamic radius particle size measurement and to provide information about polydispersity. The principle of size determination depends on the random movement of particles through a suspension (diffusion coefficient). When a laser beam is passed through a suspension of different size particles, the light is scattered according to their size and velocity; smaller and faster moving particles cause more intensity fluctuations than larger ones. There are many advantages of using this technique, including the ability to provide an accurate particle size analysis in one to two minutes. It is a very simple technique, requires a low sample volume, and can measure particles with a diameter of less than 1 nm. Measurements of the samples were performed using a scattering angle of 90° to the incident beam at 25°C ± 0.1°C. The analysis mode was CONTIN and 10 readings were taken for each sample. The concentration of coated and uncoated IONPs was set at 50 µg/ml for all measurements in order to reach a count of below 300–600 KCps while measuring the samples. The solution was diluted to the desired concentration in DI water and filtered with a 0.2 µm filter and vortexed for 1 minute to remove any aggregates before each measurement. DLS scattering data were collected at room temperature and processed using Omnisize 3 software. The experiments were repeated three times, and the results of value ± standard deviation were averaged.

2.2.2.2 Transmission Electron Microscopy

TEM is a powerful instrument for determining the shape, size distribution and mean size of particles. The nanoparticles produced were investigated using TEM (JEOL Ltd, Japan) using an electron beam as the light source, and due to their much lower wavelength, it is possible to obtain a resolution a thousand times higher than when using a light microscope. Small objects of the order of a few Angstroms (10^{-10} m) can be seen and small details in different materials down to near atomic levels can be studied. The possibility of high magnification has made TEM a valuable tool for studying the nanostructure of materials in many fields, such as in biological, medical, and chemical research.

Principle

A beam of electrons strikes the sample surface and shows some scattering behaviour from the surface of the sample particles which carries information regarding the image of the specimen structure, giving thousand-fold magnifications. The electron microscope uses electromagnetic lenses that collect the electrons into a very thin beam. A high voltage electron beam of about 100 kV is transmitted through a very thin sample. Depending on the density of the specimen, some of the electrons are scattered and other scattered electrons pass to the bottom of the microscope to hit a fluorescent screen, where they produce different dark parts according to their density, and then an enlarged image is made by the operator with a camera. By using this method, a particle size of less than 1 nm can be measured with high accuracy.

Samples are dispersed on a copper grid which is placed in a holder at the bottom under a vacuum environment because air affects the transmission of electrons.

The samples were diluted to 10 µg/ml with deionised water and mixed with vortex for one minute to disperse any aggregates. A drop of diluted IONPs was placed on a carbon (Formvar) coated sample grid and then mixed with one drop of 3% (w/v) phosphotungstic acid for 1 minute. Excess sample was wicked away using Whatman filter paper and the sample was viewed under the various magnification powers of the electron microscope. In order to determine the diameter distribution of particles, the major length of non-spherical particles was measured using Gatan Digital Micrograph software (N = 100). The image measures the longest (major) rather than the shortest (minor) axis of each particles and the size is obtained from the average of the major axis.

2.2.2.3 Zeta Potential Analysis

Zeta potential (ζ) is the description of the charge of particles in suspension. Determination the surface charges were collected in order to study the colloidal stability of the nanoparticles. The principle of the zeta potential instrument (Malvern Instrument Ltd, UK) depends on the electrostatic repulsion/attraction forces between particles. The formation of charges around each particle surface affects the distribution of ions in the medium, which lead to an increase in the concentration of the opposite ions to the surface particle charge. Consequently, an electrical double layer exists around each particle, and if particles move due to gravity, then this surrounding layer moves as part of the particle. The

zeta potential is the potential at the point in this layer where it moves past the bulk solution and is usually called the slipping plane. The charge at this plane is very sensitive to concentration and the type of ions in solution. The nanoparticle suspension (200 µl) was diluted with filtered PBS diluted 1 in 10 (0.5 ml, 15 mM, pH 7.4), and the results were expressed as the mean ± standard deviation for six readings and data plotted in GraphPad Prism. All measurements were carried out at 20˚C.

2.2.2.4 Colloidal Stability of Uncoated and Coated IONPs

The colloidal stability of coated IONPs in different environments is very important, therefore the stability of uncoated and coated IONPs was investigated by turbidity measurements using a TECAN Spark 10M plate reader. To the diluted dispersion of IONPs (50 µl), various concentrations of sodium chloride (from 1 to 600 mM) was added (200 µl). Then, vortexing for 5 seconds, and optical density determined immediately at 562 nm. The experiment was repeated three times to verify the reproducibility, and the average of optical density was calculated.

2.2.2.5 Determination the Amount of RBITC Bound to Coated IONPs

RBITC labelling efficiency was determined by a direct method: Freeze-drying. This method relies upon the release of RBITC by dissolving freeze-dried RBITC-labelled IONPs in an acetone/methanol (0.5 ml/1 ml) mixture. A serial dilution of RBITC in HEPES buffer was performed and 200 µl of each dilution was added to the black 96-well plate. The fluorescence intensity was measured at Ex 554 nm and Em 575 nm using a Dynal MFX Fluorimeter. A calibration curve could then be constructed

for the determination of dye loading and entrapment efficiency using RBITC of known amounts. The experiment was repeated with RBITC at amounts ranging from 0.002 to 0.125 mg.

2.2.2.6 Ferrozine Assay for Measuring IONPs

Quantitative determination of IONP content in suspension, cell and culture media samples was performed using the ferrozine assay as this assay is an absorbance based assay to determine soluble iron [179]. IONPs in the suspension, cell lysate and media samples were first solubilizing by addition of 12 M HCl (500 µl). This mixture was incubated at room temperature for one hour with gentle mixing and then neutralised with 12 M NaOH (500 µl). Ammonium acetate solution (50 µl, 10 M) and 10 mM ferrozine (300 µl) were added to each sample. At the end of the reaction, 200 µl of each sample was placed into the 96-well plate. Absorbance was measured at 562 nm using Multifunction Plate Reader, TECAN Spark 10M. Determination the amount of IONPs was based on a standard curve prepared using known concentration IONPs in a way similar to that of the sample.

2.2.3 Preparation of IONPs for Biological Study

In the present study, the effect of the cellular uptake of different sized IONPs are based on the exposure to the same concentration of particles measured in mass of iron per unit volume. Prior to all biological experiments, fluorescently labelled IONP dispersion were passed through a syringe filter (0.2 µm, Vivascience, Gemany) to sterilize the IONP suspension. A stock particle suspension was diluted to the required concentration in a normal cell culture medium.

2.2.4 Routine Cell Culture

2.2.4.1 Calu-3 Cell Culture

The bronchial epithelial cell line, Calu-3 was used at passage (30-34) for all experiments. Cells were cultured in EMEM containing 10% (v/v) foetal bovine serum (FBS), 1% penicillin-streptomycin antibiotic solution, 2mM L-glutamine and 1% v/v non-essential amino acids at 37˚C in a 5% CO_2 air-humidified atmosphere. Cells were passaged when 90% confluent using a 1:3 split ratio as will be described in the next section.

2.2.4.2 Cell Maintenance and Splitting

Calu-3 cells were cultured in 75 cm^2 flasks in EMEM containing 10% (v/v) FBS at 37°C in a 5% CO_2 air-humidified atmosphere until they reached 90% confluence. Cells then were detached from the flask by washing the adherent cells with approximately 4 ml of warmed PBS to remove any dead cells, followed by the addition of approximately 3 ml of trypsin-EDTA solution (2.5 mg/ml trypsin, 0.2 mg/ml EDTA). Cells were incubated with trypsin for 15 min until the cells detached from the flask surface. Next, culture medium (8 ml) was added to the suspension of cells in order to inhibit the damaging effect of trypsin, and the cell suspension was harvested by centrifugation at 500x*g* for 5 min. The supernatant was discarded and the pellet re-suspended in fresh culture medium to produce a homogeneous cell suspension. Approximately 1/3 of the cell suspension was transferred to a new flask containing 12 ml warmed fresh culture medium. The culture medium (EMEM) was regularly replaced every 2-3 days.

2.2.4.3 Cells Seeding onto a 6-Well Plate

Calu-3 cells were detached from the flasks and seeded onto 6-well plates at 2×10^5 cells/well. Culture medium (EMEM, 2 ml) was added to each well and the plates were incubated at 37°C in a 5% CO_2 air-humidified atmosphere for 2 days before experiments were conducted.

2.2.4.4 Cells Seeding onto Transwell® Permeable Supports

Cells were detached from the flasks and seeded at a density of 2×10^5 cells/cm^2 and cultured on filter inserts (Transwells®). Cells were maintained at 5% CO_2, 37°C in EMEM supplemented with FBS (10%). Cells were seeded to the apical compartments in 0.5 ml cell suspension and fresh medium (1.5 ml) was added to the basolateral chamber. Air-liquid interface was created after two days of culturing, in which the medium was added only to the basolateral compartment and replaced every other day. Calu-3 cells were typically cultured on permeable supports for 21 days before their use as polarized cell layers. Cell layer integrity was routinely screened by measuring the transepithelial electrical resistance (TEER); only those samples displaying TEER ≥ 800 Ω.cm^2 were deemed appropriate for the permeability experiments.

2.2.4.5 TEER Measurements

The transepithelial resistance (TEER) was measured before changing the culture medium to determine the integrity of the cellular monolayer in vitro. TEER measurement has been applied for assessing the permeability of tight junction [180]. An epithelial volt-ohm meter (EVOM; World Precision Instruments) has become the most widely used and convenient instrument to measure the TEER of epithelial cells in 12 and

24 well Transwells® respectively. The EVOM qualitatively measures cell resistance which indicate the monolayer health and cell confluence. For electrical resistance measurement, two electrodes were first sterilised in 70% IMS followed by placing one electrode in the apical compartment and the other in the basolateral compartment to measure the blank resistance of the semipermeable membrane only (without cells) and measuring the resistance across the cellular monolayer on the semipermeable membrane in units of $\Omega.cm^2$. The confluence of the cellular monolayer is readily determined by a sharp increase in TEER.

2.2.5 Cytotoxicity Studies

2.2.5.1 Metabolic Activity (MTT) Assay

The MTT assay is a colourimetric assay for assessing cell metabolic activity and can measure cytotoxicity of nanoparticles. NAD(P)-dependent cellular oxidoreductase enzymes reflect the number of live cells present and this enzyme is capable of reducing tetrazolium dye MTT 3-(4,5-dimethylthiazol-2-yl)-2,5-diphenyltetrazolium bromide to its insoluble formazan, which has a purple colour. MTT assays are usually done in the dark because it is sensitive to the light.

Into a 96-well plate, 15000 cells/well of Calu-3 were seeded and incubated in fully supplemented EMEM medium (100ul) until sub confluent. Then cells were treated with IONPs of different sizes at defined concentration (10, 25, 50, 100, 200 µg/ml) and incubated for 24 hours. After that, the metabolic activity of cells was determined by direct addition of MTT reagent (25µl, 5mg/ml in PBS) to cell culture medium and

incubated for 3 hours. The medium was discarded, then Cells were solubilized in 150 µl dimethylsulfoxide (DMSO), and the formazan product resulting from mitochondrial metabolism in viable cells was measured by absorbance at 570 nm using a SpectraFluor spectrophotometer (Tecan Group Ltd Männedorf, Switzerland). Cells treated with EMEM medium and Triton 0.2 % were used as a positive and negative control respectively. The percentage of metabolic activity was calculated as the ratio of mean sample absorbance of triplicate readings with respect to mean absorbance of control wells using the following equation:

Metabolic activity (%) = S-T / C-T * 100

Where, S is the absorbance obtained with the tested samples, T is the absorbance observed with Triton X100, and C is the absorbance observed with control. Cell survival was expressed as the percentage of cell viability of treated cells in comparison with that of control cells (cells without samples).

2.2.5.2 Trypan Blue Exclusion Assay

Cells were seeded into 12-well plates and incubated for 24 hours at 37˚C with 5% CO_2. Cells were treated with different concentrations of IONPs (22, 50 and 80 nm) for 24 hours. After that, cells were washed twice with PBS and trypsin was added to control and treated cells for cell detachment from the plate. Cells were re-suspended in fresh culture medium and equal volume of each cell suspension and 0.5% w/v trypan blue solution were mixed and used for cell counting by haemocytometer.

Blue stained cells were counted as nonviable cells and unstained cells as viable cells. Cell survival was expressed as the percentage of viability of treated cells in comparison with that of control cells (cells without samples). All experiments were repeated at least three times.

2.2.6 Cellular Uptake of IONPs

Calu-3 cells (2×10^5) per well was seeded on six well culture plates and treated with EMEM culture medium (2 ml) and incubated over two nights until 75% confluence. After that, culture medium was removed and replaced with medium containing coated IONPs of different amounts. Treated cells were placed in a humidified CO_2 incubator maintained at 37˚C. In addition, untreated cells and culture medium without cells were used as controls in order to rule out the possibility of presence of iron in both. After 0.5, 2, 4 and 24 hours, the medium containing IONPs was removed and saved for quantification of unbound IONPs in the culture medium using ferrozine assay. Cells were washed twice with PBS (1 ml) to remove unbound particles, which were not entrapped by the cells, and the final wash of PBS was removed. Now, cells were lysed with 0.2 M NaOH (500 µl) and the IONP content of the cells was determined using the ferrozine assay as described in section (2.2.2.6).

2.2.7 Microscopy Studies

2.2.7.1 Confocal Laser Scanning Microscopy

Principle

Nowadays, confocal microscopy is possibly the most widely used optical method in biological research. This method creates better (and more informative) images than wide field microscopy. Confocal microscopy (LSM 510 Meta, Zeiss) exhibits several advantages such as producing a detailed picture of sample from a very small sample area due to rejection of the light either from the out of focus planes or light scattering from the optical instrument. Also, the samples can be sequentially scanned point by point or multiple points at once, resulting in an acquired optical section with high contrast and resolution in x, y and z planes. A number of images generated with the focal plane shifted in small steps can be combined into a 3-D image stack, which is available for digital processing. For each imaging, a single laser is used to irradiate the sample and two corresponding band pass filters are set to separate the scattered light from the sample light and the fluorescence. The excitation and emission spectra of fluorescence as well as the wavelength of laser need to be taken into account. According to the wavelength range of the two filters, two pseudo-colours were used for the two images of the scattered light and fluorescence, and were then merged to make a compound image. Consequently, the compound cellular image of LSCM provides more information by combining the two biomarkers (nanoparticles and dyes). Biological samples usually have thickness of a few micrometres at least. One can get an image of a thin slice of the sample (optical section, e.g.

0.1 µm) without physically slicing the sample. We can then move the focus along the Z-axis to get clear images of sections above or below. Thus, for a cell 3µm thick, we can have 30 hi-resolution images 0.1 µm thick from bottom to top (z-sections). These images can then be stacked one on top of the other (z-stacking) to create a single 2D image of the sample. Microscopy was performed using laser lines with 543 nm filter (RBITC), 488 nm filter (LysoTracker) and 633 nm filter (Draq-5).

2.2.7.1.1 Fixed Imaging Method

For assessing the cellular uptake of coated IONPs, calu-3 cells of density 30,000 cells/well were grown to form a monolayer on eight-well chambered cover glasses in 300 µl of EMEM medium and allowed to attach in a humidified incubator at 37 ˚C and 5% CO_2 for 48 hours (75% confluence). Different amounts of iron (. After that, EMEM was aspirated and different amounts (25 and 50 µg) of coated IONPs of varied sizes in EMEM (300 µl) were added after filtration through a 0.2 µm syringe filter. The nanoparticles were incubated with the cells for 2 or 4 hours. After the period of uptake, the medium was aspirated and the medium saved for quantification of unbound coated IONPs using the ferrozine assay. Cells were then washed twice with PBS (200 µl) gently (using a Gilson) and then fixed with 4% paraformaldehyde (100 µl). After fixation, the fixative was removed by gentle aspiration and washed with 200 µl PBS once again. Draq-5 (5 mM, 200 µl) was added to the cells, and incubated for 20 min at room temperature to stain the nucleus. The stain was protected from the light during this incubation period. Finally, the excess of Draq 5 was removed (no wash was needed), mountant glycerol was

added and cells were kept in a fridge until imaging. A slice of 1 µm thickness was imaged from the middle of the sample by an individual confocal optical section. The stained fluorescent nanoparticles appear as red, lysosome (green) and nucleus is visualised (blue). One sample of cells without added particles served as negative control.

2.2.7.1.2 Live Imaging Method

Calu-3 cells were labelled with 50 nM LysoTracker® green DND-26. Calu-3 cells of density 30,000 cells/well were grown to form a monolayer on eight-well chambered coverglasses in 300 µl of EMEM medium and allowed to attach in a humidified incubator at 37 ˚C and 5% CO_2 for 48 hours. After that, EMEM was aspirated and pre-warmed EMEM (300 µl), was added and incubated with IONPs (50 µg) for 2 hours. After incubation, culture medium was removed and samples were rinsed two times gently with PBS using a Gilson. Draq-5 (5 mM, 200 µl) was added to the cells, and incubated for 20 min at room temperature to stain the nucleus (protect from the light to avoid colour bleaching). After incubation, excess Draq-5 was removed and LysoTracker green (200 µl, 50 nM) was added to the cells and incubated at room temperature for 30 minutes. Cells were then washed with PBS and left in PBS for imaging immediately. A slice of 1 µm thickness was imaged from the middle of the sample by an individual confocal optical section.

2.2.7.2 Electron microscopy

2.2.7.2.1 Evaluation of time dependent uptake of IONPs by calu-3 cells growing in monolayer culture using TEM

Calu-3 cells of density 2 x 10^5 cells/cm^2 in EMEM was seeded as outlined in section 2.2.4.4. On the day of the transport experiment, the transwell TEER was measured in culture medium to confirm the presence of a polarized monolayer. After that, medium was aspirated from the insert and 500 µl of sample was added (50 µg) after filtering through a 0.2 µm sterile filter and incubated under the same conditions for increasing time intervals: 10 minutes, 2 and 4 hours before dehydration and embedding. One sample of cells without added particles served as negative control.

2.2.7.2.2 Dehydration and Embedding of Cells

In preparation for TEM imaging, the calu-3 cells that were incubated with different IONPs sizes (for 10 minutes, 2 and 4 hours) were rinsed with cacodylate (0.1 M) buffer three times and then fixed in 3% glutaraldehyde in cacodylate (0.1 M) buffer for an hour. The cells were washed for 5 minutes in distilled water and after that dehydrated in a graded series of ethanol (50%, 70%, 90% and 100%). Each insert was removed using a scalpel and cut in half, and both halves put in a labelled glass vial containing 70% ethanol and left for 5 minutes. The samples were infiltrated with resin at 1:3 (resin to propylene oxide mixture) for 30 minutes and after that at 1:1 (resin to propylene oxide mixture) for an hour. After that, they were soaked three times in pure resin for one hour each and then placed in a vacuum oven at 60˚C for 2 days for polymerisation of resin. The polymerised blocks were then cut into sections (80–100 nm thick). The sections were placed on formvar-coated

copper grids stained with saturated Uranyl Acetate for 5 minutes and rinsed in distilled water approximately 10 times. After that, the sections stained with Reynolds lead citrate for 5 minutes and rinsed again with water before visualisation. Samples were imaged using a Tecnai Biotwin T12 transmission electron microscope (TEM) which runs at an accelerating voltage of 100Kv. The images were captured using a Megaview II Soft Imaging Software camera system.

2.2.8 In Vitro Transcytosis Study

Transepithelial transport of coated IONPs with varied size was carried out using 12 well plates. Calu3-cells of density 2 x 10^5 cells/cm^2 in EMEM was seeded as outlined in section 2.2.4.4. On the day of the transport experiment, the transwell TEER was measured in culture medium to confirm the presence of a polarized monolayer. After that, medium was replaced with pre-warmed (37˚C) FluoroBrite Dulbecco's Modified Eagle Medium (FB-DMDM) which is a DMEM-based formulation with background fluorescence that is 90% lower than that emitted by standard DMEM. It is designed to enhance the signal of fluorescence to allow visualisation of even the weakest fluorescent signals. FB-DMEM was incubated at 37 ˚C, 5% CO_2 for 30 minutes. TEER was measured again to ensure the cell layers maintained their integrity on FB-DMEM medium. Medium was aspirated from the insert and 500 µl of sample was added (50 µg) and then incubated under the same conditions. At every hour for four hours, a 200 µl sample was taken from the basolateral compartments and placed into a 96-well plate, then the same volume of FB-DMEM was added to replace the removed volume, and the plate was

returned to the incubator. At the end of the time, the medium was aspirated from the transwell and FB-DMEM was added again for further TEER measurements. Serial dilution was done for a total 24 dilutions including undiluted sample stock for creating the calibration curve. Coated IONPs were quantified using ferrozine assay as described in section 2.2.2.6. The apparent permeability coefficients P_{app} for IONPs through the cell monolayer was calculated using the following equation:

P_{app} (cm/s) = (V_R/ ($A*C_O$))*($\Delta C_R/\Delta t$) where, V_R = volume of the receiver compartment (1.5cm^3), A = surface area of the transwell membrane (1.12cm^2), C_O = apical donor concentration at start and $\Delta C_R/\Delta t$ = change in [nanoparticle] in receiver compartment over time (permeability rate).

2.2.9 Relaxivity Measurement

Relaxivity is a measure of the ability of a MRI contrast agent to increase the relaxation of the surrounding hydrogen protons that can then be used to enhance contrast in MR images. For the relaxivity measurements, aqueous suspensions of various IONP concentrations were prepared in water. IONP suspensions with sizes 22, 50 and 80 nm, with varying concentrations of 0.01, 0.03, 0.06, 0.1, 0.2, 0.4, 0.89 and 1.79 mmol/L were used. The T1 and T2 relaxation times of hydrogen protons in the aqueous suspension of the IONPs were measured at room temperature using a 1.5T Philips Achieva MRI scanner (Philips Healthcare, Best, Netherlands) Figure 2-4. The specific relaxivities were calculated according to:

$$1/\Delta T1 = r1.\,[C] \quad \text{and} \quad 1/\Delta T2 = r2.\,[C]$$

Since ΔT1 and ΔT1 are relaxation rate in seconds, [C] is the concentration of contrast agent and r1 and r2 represent relaxivity. The relaxation rates of a contrast agent in a solution are obtained by plotting changes in relaxation rates (1/T1) and (1/T2) at different concentrations.

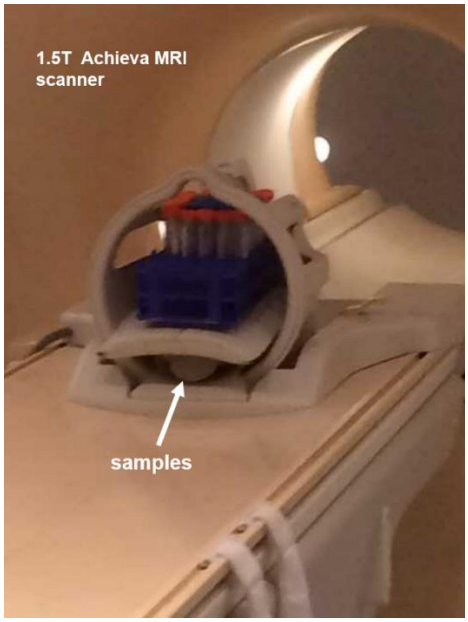


Figure 2-4: A 1.5T Philips Achieva MRI scanner image of sample suspensions of different polymer coated IONPs sizes (22, 50 80 nm).

2.2.10 Statistical Analysis

Data of at least three independent experiments are presented as means ± standard deviation. Statistical significance was tested using Prism 7 (GraphPad Software, La Jolla, USA) All experiments were performed at least three times and data are expressed by One way or Two-way ANOVA with a Tukey's or Sidak multiple comparison test, where *= significant ($p < 0.05$), **= very significant ($p < 0.01$), ***= extremely significant ($p < 0.001$), and ****= extremely significant ($p < 0.0001$). In

order to determine particle size from TEM measurements, the software Gatan Digital Micrograph was used.

3 Physicochemical Characteristics of Iron Oxide Nanoparticles

3.1 Introduction

Iron oxide nanoparticles have been investigated as a promising tool for use in cellular therapy, cell labelling, targeting, contrast enhanced-MRI, and tumour hyperthermia due to their biocompatibility, unique size, physical properties and specific targeting abilities, and this has led to their application in the fields of biomedicine, ophthalmology and electronics [6, 157, 181-184].

It is crucial to find a suitable method to prepare IONPs with appropriate sizes for the particular work as there are many methods producing different sizes. Massart reported the first controlled synthesis of IONPs [80, 185]. Various methods have been used for IONP synthesis such as hydrothermal synthesis [186, 187], microemulsion [188], sonochemical [85, 189] and thermal decomposition. However, these methods are complicated, time consuming and use a large amount of surfactant [8, 78, 83-85, 190, 191]. A co-precipitation chemical method is generally considered as the most effective way to prepare IONP suspensions as this method is simple, inexpensive in comparison to other preparation methods, uses safe materials and it is an efficient chemical method for producing different size nanoparticles [2, 77, 184, 192]. A study was carried out by Abushrida who modified the co-precipitation method and produced IONPs with narrow size distribution and a mean diameter 13 nm.

The main problem with IONPs is poor water solubility and the tendency of aggregation in an aqueous solution or at biological salt concentration. This is important because nanoparticles size and state of aggregation has an effect on cellular biological properties such as intracellular targeting and localisation which can limit in vivo and in vitro applications [96, 193]. To address these problems, it is essential to engineer the nanoparticles' surface with biocompatible materials for medical applications [10]. IONPs without any coating materials possess high surface energy due to their high surface area to volume ratio, which results in particle aggregation in biological solutions [96]. The nature of the surface coatings and modification methods determine the physical and biological properties such as the overall size, surface charge, coating density [194, 195]. IONPs were stabilised by electrostatic repulsion forces. However, the presence of charge on the surface of particles is not enough to prevent aggregation in biological solutions due to presence of salts that can neutralise the charges [193, 196]. Highly hydrophobic nanoparticles would not be able to reach the in vivo targeted cells in a high enough yield. This is because hydrophobic nanoparticles tend to be opsonised by protein adsorption and rapidly cleared from systemic circulation by the phagocytic system, ending up in the liver or the spleen. Nanoparticles which are quickly cleared will fail to reach the target.

PEG is a biocompatible material frequently used to modify nanoparticle surfaces. This modification provides steric stabilisation of particles by forming a hydrophilic layer around the particle surface which results in a neutral charge and a barrier that prevents the particles from aggregating

as well as producing well dispersed particles. The steric stabilisation leads to reductions in immunogenicity and antigenicity. PEG can be synthesised with terminal functionality and so enabling conjugation with hydrophobic polymers, such as PGA. Therefore, the presence of PEG-PGA layer on the surface of iron oxide core can enhance the colloidal stability of particles or the rate of precipitation will be decreased depending on the degree of coverage of coating materials on the particles and the thickness of the coating layer [197]. When using the PEG–PGA block copolymer, the iron oxide nanoparticles are essentially covered by two layers. The inner layer comprises the hydrophobic PGA which can interact with the surface of the particle. The outer layer is composed of the surface anchored hydrophilic PEG which provides steric stabilization.

A modified interfacial deposition method was used for IONPs coating by polymers in order to enhance the stability of these particles. Abushrida has previously used this method for coating IONP. He coated IONP surfaces by dropwise addition a small amount of polymer and organic solvent to give nanoparticles with a thin polymer coating and avoid production of polymer nanoparticles and aggregates of IONPs in polymer. However, a mixture of coated particle sizes was produced.

Nano-sized IONPs has recently attracted much attention in order to enhance the cellular uptake for medical applications. In general, most researchers agree that the nanoparticles efficiently enter mammalian cells compared to micro-sized particles. However, little work has been

performed to establish the effects of physicochemical characteristics (size) of nanoparticles on cellular uptake.

This chapter focuses on the production of nanoparticles with a small size, and coating with PGA 40%C_{18}, PEG-PGA-SA and PEGylated PGA 40%C_{18} using a modified IDP in order to produce nanoparticles with a narrow dispersity and without aggregation. In addition, the particle size and surface charge of IONPs will be considered in order to investigate the influence of polymer coating materials on nanoparticle physicochemical characteristics.

3.2 Aims of the Chapter

- To synthesise IONPs with different particle sizes not exceeding 100 nm.
- To produce nanoparticles with homogenous properties.
- Coating IONPs with PGA 40%C_{18}, PEG-PGA-SA and PEGylated PGA 40%C_{18} and select the best polymer that produces coated IONPs with the thinnest most reproducible polymer coating. This will give a starting point to identify how the structure of polymers could affect particle sizes.
- Determination in detail the influence of the amount of the polymer coating of nanoparticles required for colloidal stability and biological applications.

3.3 Results

Coated and uncoated IONPs were characterised in terms of their size, charge and shape using a variety of different techniques including DLS, zeta potential and TEM.

3.3.1 Synthesis of IONPs

IONPs were successfully prepared using a modified co-precipitation method whereby Fe_3O_4 was precipitated from Fe^{3+} and Fe^{2+} salt mixtures in alkaline medium. The reaction process was fast and was carried out in oxygen free conditions to prevent magnetite from being oxidised to ferric hydroxide. The reaction conditions such as pH needed to be controlled during the synthesis process in order to obtain defined and homogeneous particle size. To adjust the pH during the synthesis process, the amount of NaOH was varied resulting in nanoparticles of different hydrodynamic radii. The results are shown in Figure 3-1 and Figure 3-2.

3.3.1.1 The Effect of pH Variation on the Size of IONPs

The influence of pH on nanoparticle sizes was tested in the pH range 0.5–12. The pH of the final product is the most important factor that should be controlled during the preparation process to obtain IONPs of different sizes as shown in Figure 3-1. An increase in the hydrodynamic radii (Rh) of nanoparticle was observed at high pH, however the smallest radii could only be obtained at very acidic pH. At pH 0.5, the size of IONPs were 10 nm and gradually increased to 14, 18 and 25 nm at pH 1, 3 and 4. However, the Rh was greatly increased to 62 and 105 nm at pH 6 and 12.

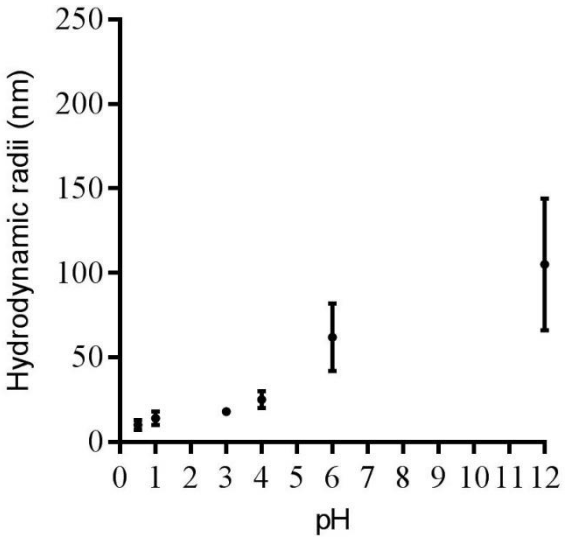


Figure 3-1: Variation in IONP hydrodynamic radii as a function of pH during the synthesis process. Different sized nanoparticles were obtained simply by varying the sodium hydroxide amount and with variation in the pH of precipitates. The particle size of the nanoparticles was determined by DLS. IONPs produced over the pH range 0.5-4 were of smaller size, as compared to those formed over the pH range 6 and 12, as IONPs were larger. The Rh of each sample is expressed as the mean particle hydrodynamic radius ± standard deviation of 5 readings.

3.3.1.2 Particle Sizes Distribution of Uncoated IONPs

IONPs of Rh 10, 18 and 25 nm that were produced at pH 0.5, 3 and 4 were selected for the present study. For all these radii of IONPs, a population of particles with low polydispersity was observed. The intensity plot for nanoparticle hydrodynamic radii is the most suitable indication of how many populations of nanoparticles are present in the sample. As seen in the Figure 3-2, all peaks showed relatively narrow particle radii distribution with one population of particles and very low levels of aggregation not exceeding 5% of population.

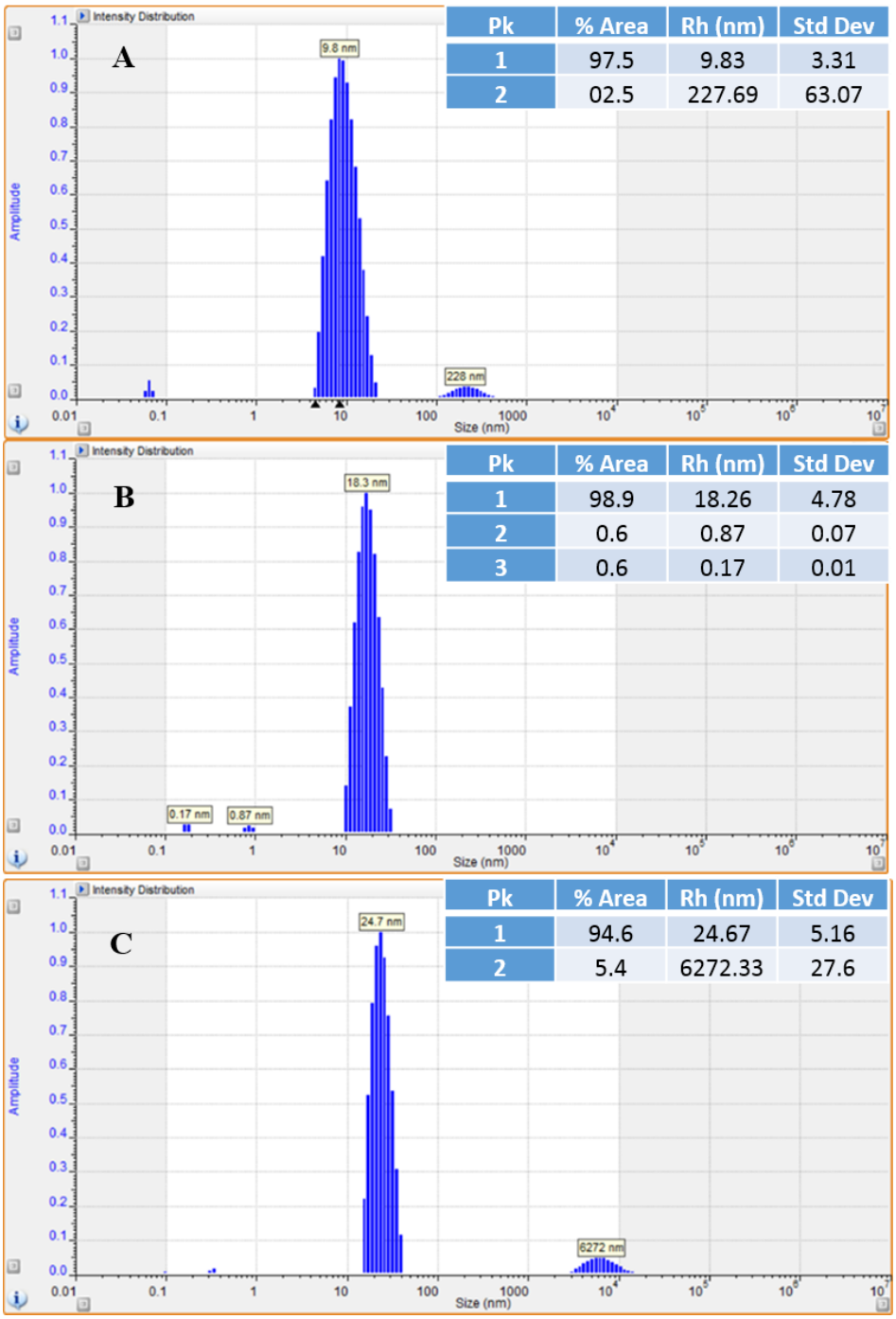


Figure 3-2: The hydrodynamic radii (Rh) intensity of uncoated IONPs by DLS. NPs were prepared by the co-precipitation method at different pH where (A) at pH 0.5, (B) at pH 3 and (C) at pH 4. NP suspension was diluted with ultrapure water to an appropriate concentration to give 300-600 kcps. The Rh of each sample is expressed as the mean particle hydrodynamic radius ± standard deviation of 10 readings.

3.3.1.3 Zeta Potential

The surface charge of the iron oxide nanoparticles is an important parameter for medical applications in vivo and vitro. Net charge of IONPs of different hydrodynamic radii 10, 18 and 25 nm in pre-filtered PBS buffer (15 mM, pH 7.4) was determined to be positive at 37 ± 5 mV, 40 ± 7 mV and 42 ± 8 mV respectively (as will show in Figure 3-10). All the samples were measured seven times and the mean values of zeta potential were calculated.

3.3.1.4 Dispersion and Stability of Uncoated IONPs

The aggregation and sedimentation of IONPs can significantly affect the stability of the final product of IONPs after coating. Particle–particle interactions are the major driving force for aggregation and deposition of nanoparticles, though other interactions such as steric, magnetic and hydration forces can also affect aggregation [29, 30].

The size of IONPs need to be monitored by DLS over days, weeks or months. The sharp intense peaks as appeared in DLS results of IONPs (Figure 3-2) confirms the lack of aggregation. Uncoated IONPs, which were routinely prepared at pH 0.5 and 1, showed small particle size with no obvious change in size over long time, which have been confirmed by DLS before every experiment during three years. However, IONPs that were prepared at pH 3 tend to aggregate after days.

3.3.2 Particle Size of Coated IONPs with Different Polymers

The smallest hydrodynamic radii of IONPs (10 nm at pH 0.5) was chosen as starting point for coating with different amount of different polymers to

investigate the effect of various polymers on particle size and to identify a polymer that can produce thin coating layers. PGA 40%C_{18}, PEG-PGA -SA and PEGylated PGA 40%C_{18} were used for coating IONPs using a modified Interfacial deposition method. The PEGylated succinic acid modified PGA is a negatively charged polymer due to presence of excess of the pendant carboxyl groups. This polymer also has a high loading of PEG groups, which are pendant on the succinyl groups. The function of the carboxyl group is to bind to cationic IONP surfaces. The approach of introducing carboxylic acid functionality in the form of succinic acid moieties is to compare the effects of a more hydrophilic PGA polymer structure in producing small particle sizes. In contrast, PGA 40%C_{18} contains not only the very hydrophobic C_{18} moieties, but also some hydrophilic hydroxyl pendant groups, which may interact with IONP surfaces. Additionally the PGA 40%C_{18} polymer has terminal carboxyl groups. In PEG-PGA 40%C_{18} most of these terminal free carboxyl groups will disappear through conjugation to PEG.

3.3.2.1 PGA 40%C_{18} Coated IONPs

The Rh average of PGA 40%C_{18} coated IONPs differs from uncoated nanoparticle radii, being almost 8 times larger. Using different amounts of PGA 40%C_{18} polymer did not decrease the particle radii as shown in Figure 3-3. The Rh of 0.05 mg coated particles was 86 nm, whereas the average of Rh of 0.1, 0.2 and 0.3 mg coated IONPs was 91 nm, 101 nm, and 121 nm, respectively. All preparations showed very low levels of aggregation comprising just 5-14% of the population. Decreasing the amount of polymer used did not decrease the hydrodynamic radii of

uncoated particles. However, the biggest increase was with polymer concentration 0.3 mg. These experimental results indicated that the presence of coating polymer around the particle resulted in an increase of the Rh with increasing polymer amount.

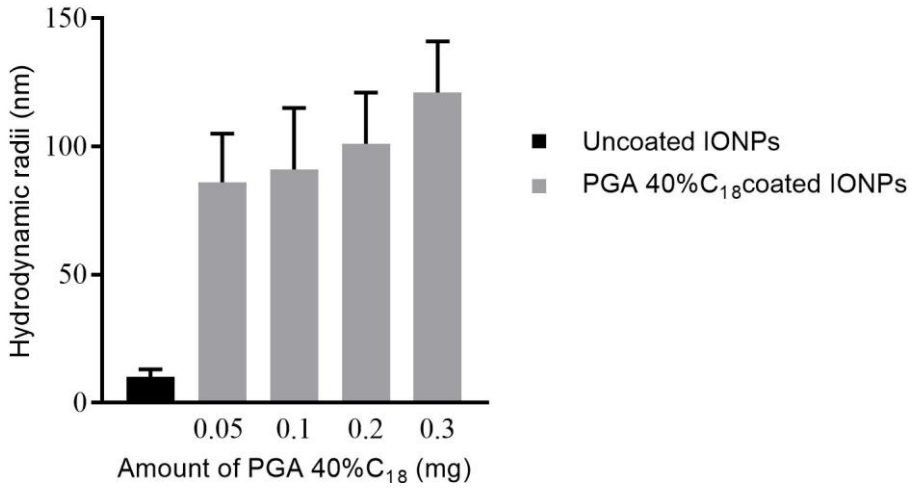


Figure 3-3: Hydrodynamic radii of PGA 40%C_{18} coated IONPs: NPs of radius 10 nm were coated with different amounts of polymer using the interfacial deposition method. NP suspension was diluted with ultrapure water to an appropriate concentration to give 300-600 kcps. Particle size was the mean hydrodynamic radius and measured by Dynamic light scattering instrument. The Rh of each sample is expressed as the mean particle hydrodynamic radius ± standard deviation of 10 readings.

3.3.2.2 PEG–PGA-SA Coated IONPs

A considerably different size distribution was seen upon addition of different amounts of PEG-PGA-SA. The hydrodynamic radius of particles was 140 nm with 0.025 mg PEG-PGA-SA as seen in Figure 3-4. Increasing amount of polymer resulted in particle radii of 119 nm and 124 nm respectively in the amounts of 0.05 and 0.1 mg, with a subsequent increase again to bigger particles of about 144 nm with higher amount of PEG-PGA-SA.

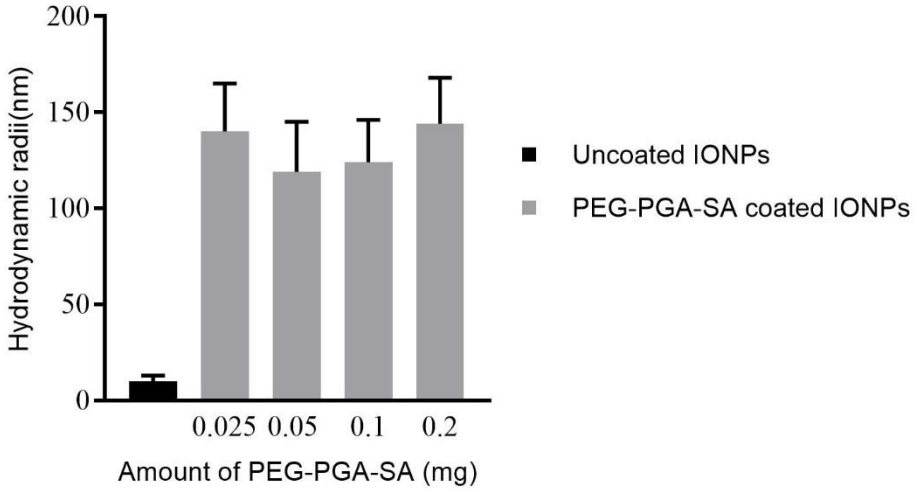


Figure 3-4: Hydrodynamic radii distribution of PEG-PGA-SA coated IONPs: NPs of radius 10 nm were coated with different amounts of polymer using the interfacial deposition method. NP suspension was diluted with ultrapure water to an appropriate concentration to give 300-600 kcps. Particle size was the mean hydrodynamic radius and measured by Dynamic light scattering instrument. The particle size of each sample is expressed as the mean particle hydrodynamic radius ± standard deviation of 10 readings.

3.3.2.3 PEGylated PGA 40% C_{18} Coated IONPs

Coating IONPs (10 nm) with PEGylated PGA 40%C_{18} led to significantly smaller particles than that produced from coating the IONPs with PGA 40%C_{18} and PEG-PGA-SA as shown in Figure 3-5.

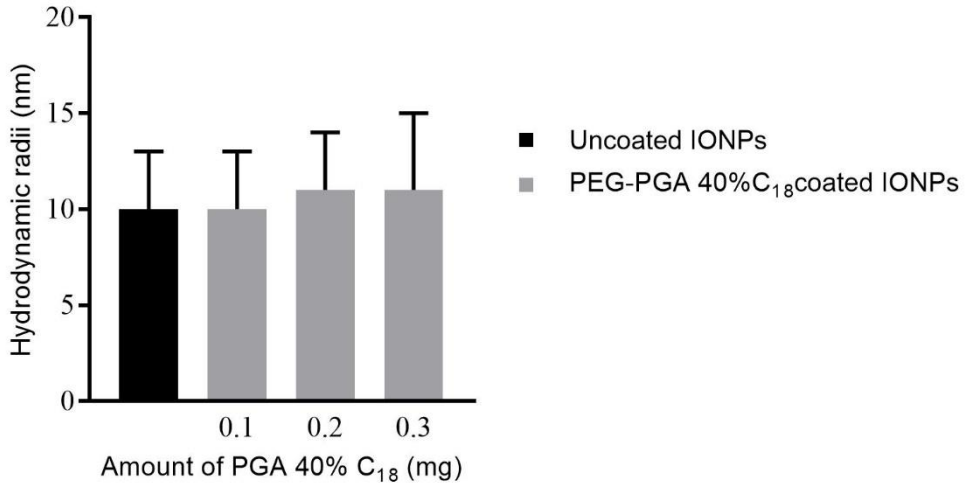


Figure 3-5: Hydrodynamic radius distribution of PEG-PGA 40%C_{18} coated IONPs: NP of radius 10 nm were coated with different amounts of polymer using the interfacial deposition method. NP suspension was diluted with ultrapure water to an appropriate concentration to give 300-600 kcps. Particle size was the mean hydrodynamic radius and measured by Dynamic light scattering instrument. The particle size of each sample is expressed as the mean particle hydrodynamic radius ± standard deviation of 10 readings

Different amounts of PEGylated PGA 40%C_{18} (0.1, 0.2 and 0.3 mg) were used to determine appropriate conditions that could be used to obtain well dispersed particles with optimum surface coating. Particles with a complete but thin layer of polymer are required. i.e. small particle sizes have large surface area which require higher amount of polymer to increase the stability. DLS results (Figure 3-6) showed small hydrodynamic radii distributions. The average radius of IONPs after addition of PEGylated PGA 40%C_{18} was 11 nm irrespective of the

amount of PEG-PGA 40%C_{18} added which indicates that the nanoparticles were coated with thin layer of polymer and well dispersed in solution. All coated IONPs exhibited a single main population. The distribution of PEGylated PGA 40%C_{18} coated IONPs used in the present study showed one prominent narrow peak with very low level of aggregates. Although, the hydrodynamic radii of the coated IONP were not significantly different to that of uncoated IONPs ($P>0.05$) as shown in Figure 3-2A.

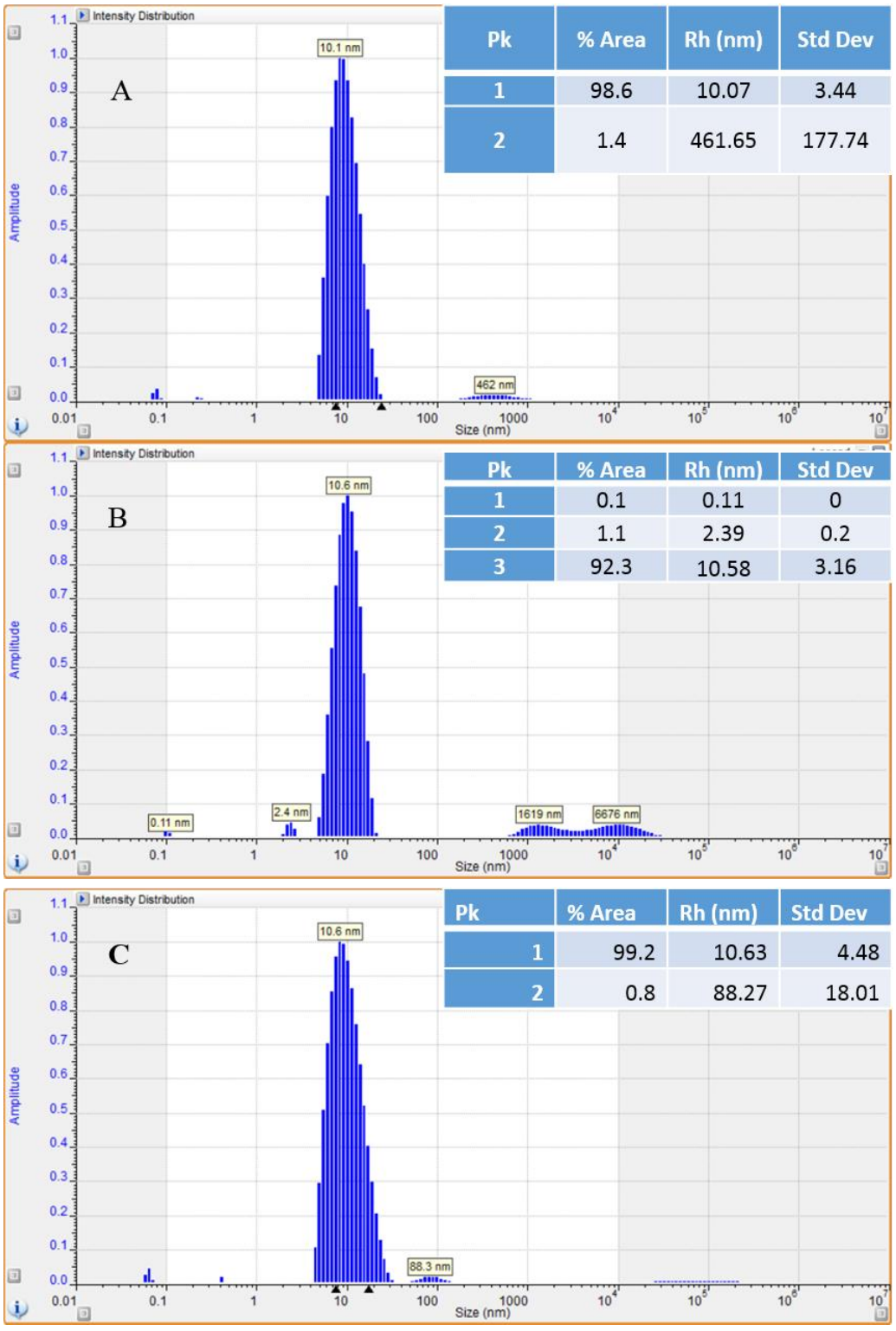
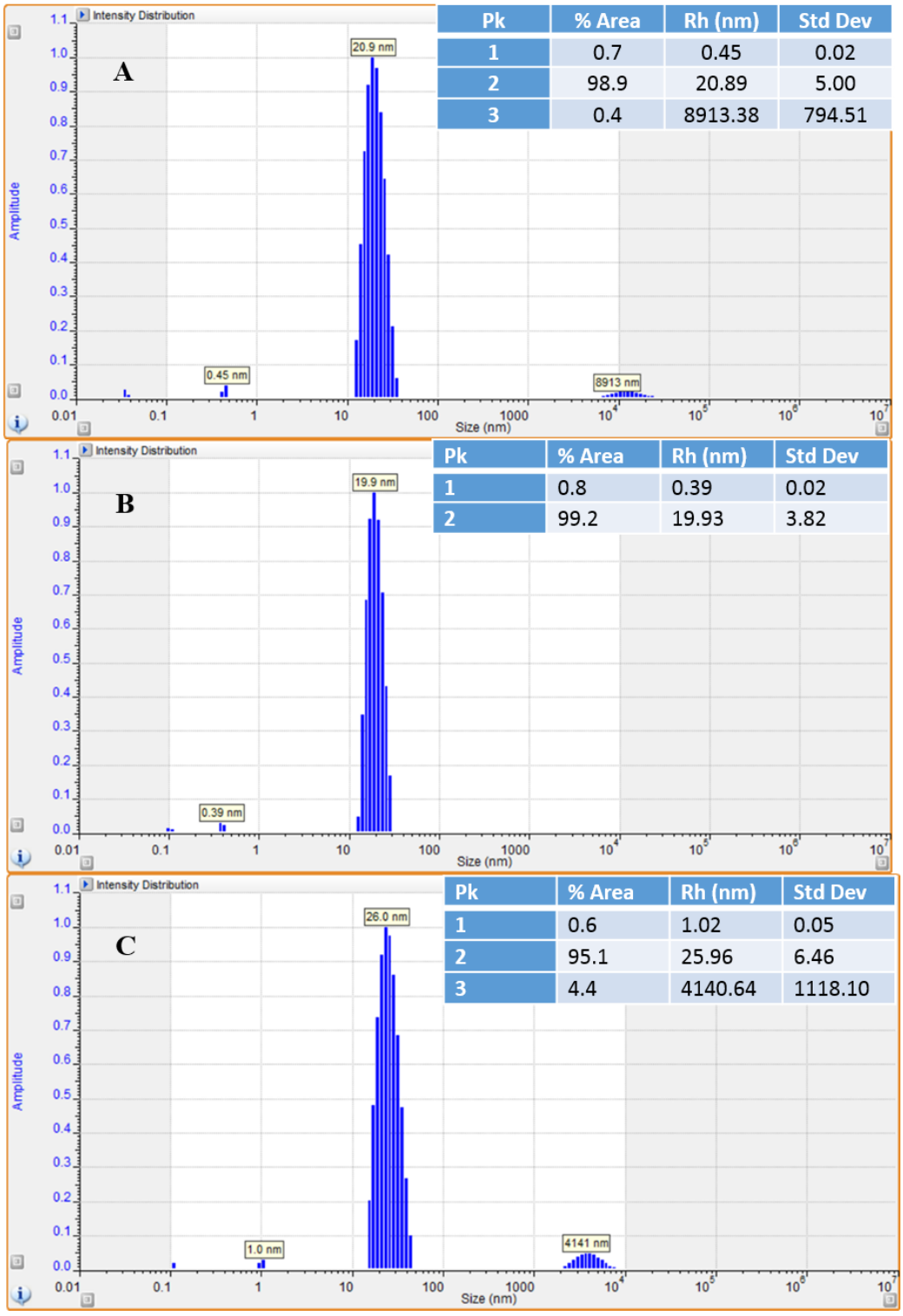


Figure 3-6: The hydrodynamic radii (Rh) intensity of PEGylated PGA 40% C_{18} coated IONPs by DLS. NP of radius 10 nm were coated with different amounts of polymer using the interfacial deposition method where (A) 0.1 mg (B) 0.2 mg and (C) 0.3 mg PEGylated PGA 40% C_{18}. NP suspension was diluted with ultrapure water to an appropriate concentration to give 300-600 kcps. The Rh of each sample is expressed as the mean particle hydrodynamic radius ± standard deviation of 10 readings.

Due to the successful of coating IONPs of small size (10 nm) with a thin layer of PEGylated PGA 40%C_{18}, IONPs of average hydrodynamic radii 18 and 25 nm that were produced at pH 3 and 4, were coated with different amounts of the same polymer in order to obtain coated nanoparticles of different particle sizes. Figure 3-7 showed the different particle sizes of the formulation obtained by coating IONPs of radius 18 nm with different amount of PEGylated PGA 40%C_{18} ranging from 0.05 to 0.2 mg. The addition of 0.05 and 0.1 mg coating materials into the nanoparticles led to an overall trend of a small but insignificant increase in nanoparticle hydrodynamic radius (to 21 nm and 20 nm respectively), whilst the nanoparticles coated with 0.2 mg PEGylated PGA 40% C_{18} had a radius of about 25 nm which was slightly different from the other coated nanoparticles.



Pk	% Area	Rh (nm)	Std Dev
1	0.7	0.45	0.02
2	98.9	20.89	5.00
3	0.4	8913.38	794.51

Pk	% Area	Rh (nm)	Std Dev
1	0.8	0.39	0.02
2	99.2	19.93	3.82

Pk	% Area	Rh (nm)	Std Dev
1	0.6	1.02	0.05
2	95.1	25.96	6.46
3	4.4	4140.64	1118.10

Figure 3-7: The hydrodynamic radii (Rh) intensity of PEGylated PGA 40%C_{18} coated IONPs by DLS. NP of radius 18 nm were coated with different amounts of polymer using the interfacial deposition method where (A) 0.05 mg (B) 0.1 mg and (C) 0.2 mg PEGylated PGA 40% C_{18}. NP suspension was diluted with ultrapure water to an appropriate concentration to give 300-600 kcps. The Rh of each sample is expressed as the mean particle hydrodynamic radius ± standard deviation of 10 readings.

The addition of PEGylated PGA 40% C_{18} to IONPs of radius 50 nm led to an increase in the hydrodynamic radius with a bimodal size distribution as in Figure 3-8. The average particle radius of IONPs was observed to rise significantly as a small but increasing amount of PEGylated PGA 40%C_{18} were added. The 0.05 mg of coating materials had a high percentage of PEGylated PGA 40%C_{18} IONPs of around 37 nm in radius, but there was also small percentage of aggregated particles (Figure 3-8A). The 0.1 mg PEGylated PGA 40%C_{18} IONPs batch also had a bimodal size distribution, with a majority of the nanoparticles formed at about 40 nm and a low population of aggregated particles compared to 0.05 mg PEGylated PGA 40%C_{18} IONPs. Increasing the amount of coating materials used up to 0.2 mg led to a further increase in the particle radius of about 45 nm. According to Figure 3-8C, the peak showed relatively wide particle size distribution with two populations of particles (polydispersity typically around 0.3), a minority of the population (about 17%) was aggregated particles.

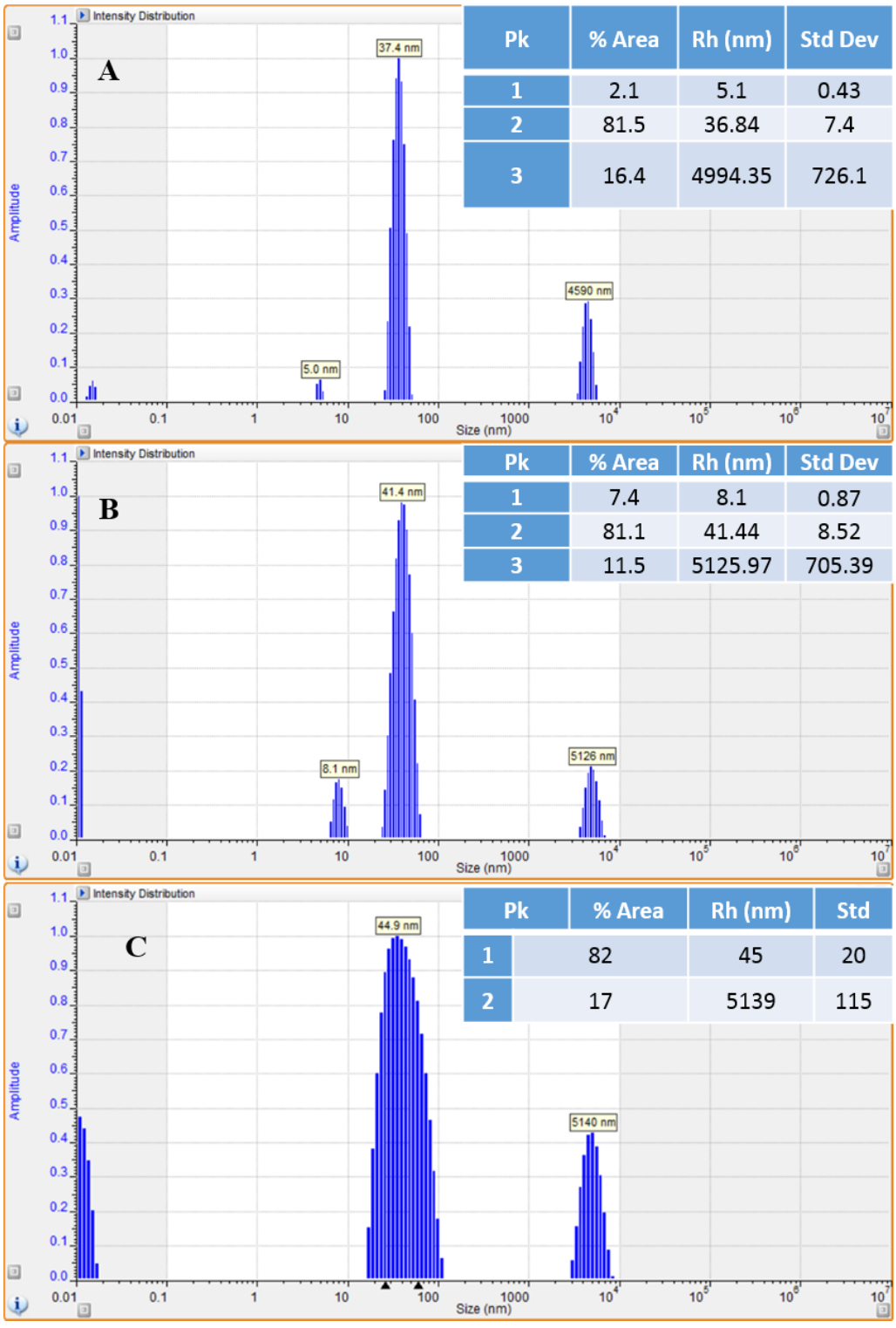


Figure 3-8: The hydrodynamic radii (Rh) intensity of PEGylated PGA 40% C18 coated IONPs by DLS. NP of radius 25 nm were coated with different amounts of polymer using the interfacial deposition method where (A) 0.05 mg (B) 0.1 mg and (C) 0.2 mg PEGylated PGA 40% C18. NP suspension was diluted with ultrapure water to an appropriate concentration to give 300-600 kcps. The Rh of each sample is expressed as the mean particle hydrodynamic radius ± standard deviation of 10 readings.

3.3.3 TEM Images

In order to determine more precisely the morphology and size of iron oxide particles at the nanoscale level, TEM studies were performed. The size distribution of IONPs nanoparticles is an important parameter relating to their biological application and performance. The TEM images showed the morphology and size of different PEGylated PGA 40%C_{18} coated IONP formulations (Figure 3-9). The measurement of coated particles was carried out randomly to detect the shape and the size of the majority of particles. These particles were observed to be morphologically ovoid in shape and uniform without aggregation and were recorded as smooth. In Figure 3-9A, the IONPs coated with 0.3 mg PEGylated PGA 40%C_{18} showed a large number of small size particles of about 8 ± 3 nm which is relating to the major axis with a slightly oval shape and well dispersed in polymer. TEM image presented in Figure 3-9D using 0.2 mg PEGylated PGA 40% C_{18} coated IONPs shows a particle size diameter of about 47 ± 10 nm. It can be seen from the Figure 3-9G that, 0.1 mg PEGylated PGA 40%C_{18} coated IONPs showed particles size approximately 47 ± 11 nm however, some small coated IONPs can still be seen. It was difficult to distinguish the light colour of polymer layer around a dark core which may due to the thin polymer shell around the particles. However, at a higher magnification, the crystal lattice of IONPs can be observed with the coating layer. The lattice planes of individual particles of all formulations were well crystallized and an amorphous layer of PEGylated PGA 40%C_{18} appears to be

homogeneous with a fairly constant thickness, probably close to 1 nm (Figure 3-9B, E and H).

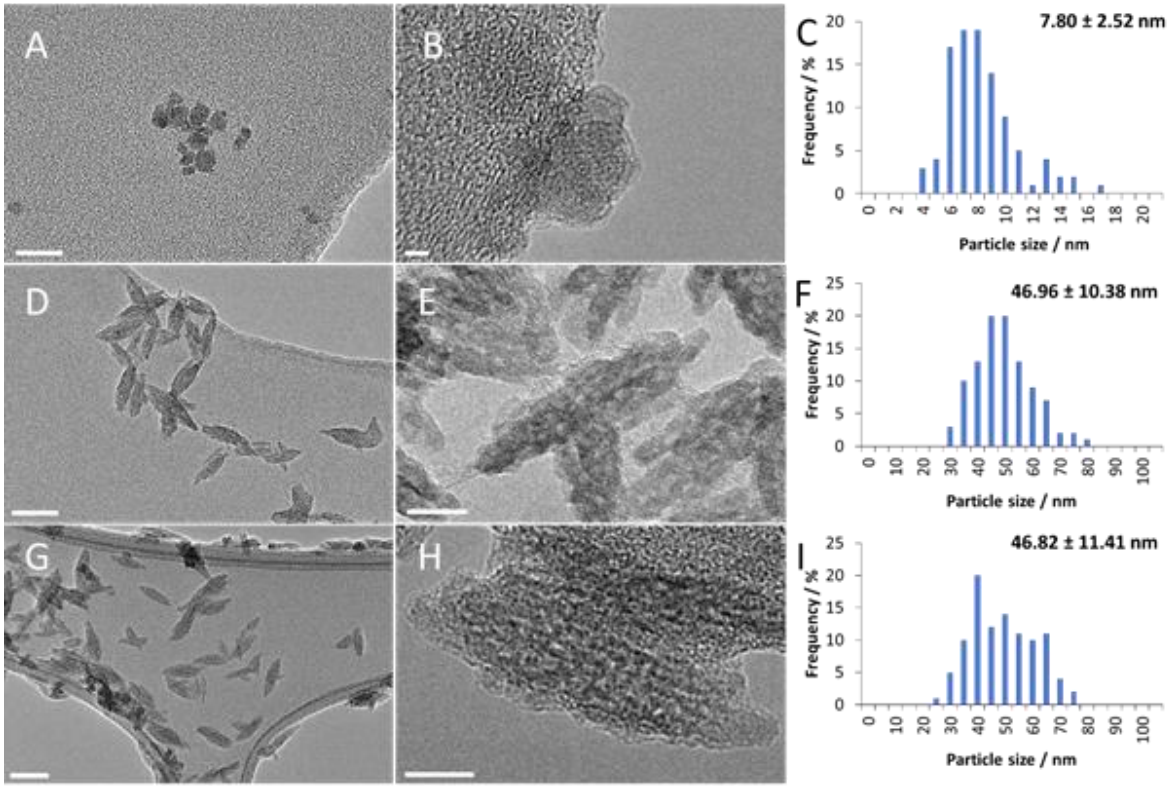


Figure 3-9: TEM images (A, D, G) and particle size distribution graphs (C, F and I) of different batches of PEGylated PGA 40% C_{18} coated IONPs where (A and C) 0.3 mg, (D and F) 0.2 mg and (G and I)) 0.1 mg PEGylated PGA 40% C_{18} coated IONPs. Particle size and standard deviation values are inset (N = 100). Higher magnification of each formulation of PEGylated PGA 40% C_{18} coated IONPs, shows visible lattice planes of individual IONPs (darker structured area) embedded in a polymer matrix (lighter more granular appearance) (B, E and H). Scale bars are (A) 20 nm, (B) 2 nm (D and G) 50 nm and (E and H) 10 nm.

3.3.4 Surface Charge of IONPs

The surface charge of uncoated and PEGylated PGA 40%C_{18} coated IONPs were studied by zeta potential measurements. The uncoated and coated IONPs were suspended in pre-filtered PBS buffer (15 mM, pH 7.4). These measurements were performed at 25 ˚C with a scattering angle of 90˚. Figure 3-10 shows the zeta potential of uncoated IONPs of different hydrodynamic radius (10, 18 and 25 nm) and different amounts of PEGylated PGA 40%C_{18} coated IONPs (0.05 mg, 0.1 mg, 0.2 mg and 0.3 mg). The results of zeta potential measurement indicated that the surface charge of coated nanoparticles changed to negative from the positive values found for uncoated nanoparticles. Uncoated IONPs of hydrodynamic radius 10 nm had a positive zeta potential of + 37 mV and changed to – 40 mV for 0.1 mg PEGylated PGA 40% C_{18} coated IONPs. However, for 0.2 and 0.3 mg coating, the zeta potential was slightly decreased to -36 and -31 mV respectively, although the decrease was not statistically significant (Figure 3-10A).

For uncoated IONPs of hydrodynamic radius 18 nm, the zeta potential values were + 40 mV and changed to – 33 mV with 0.05 mg PEGylated PGA 40% C_{18}. A slight increase in surface charge was observed with 0.1 mg of polymer, which gave value of - 35 mV however, the value of zeta potential with 0.2 mg PEGylated PGA 40% C_{18} was slightly decreased to – 31 mV, however these changes are not statistically significant (Figure 3-10B).

Figure 3-10C shows zeta potential of uncoated IONPs of hydrodynamic radius 25 nm of + 42 mv. The surface charges of 0.05 and 0.1 and 0.2 mg PEGylated PGA 40% C_{18} are – 40, – 38 and – 31 mV respectively.

All formulations exhibited a net positive charge with uncoated IONPs with a slight increase in zeta potential value as the size increase. However, increasing added amount of PEGylated PGA 40% C_{18} on the surface of IONPs consistently showed a slightly decrease in zeta potential, although these differences were small and within experimental error.

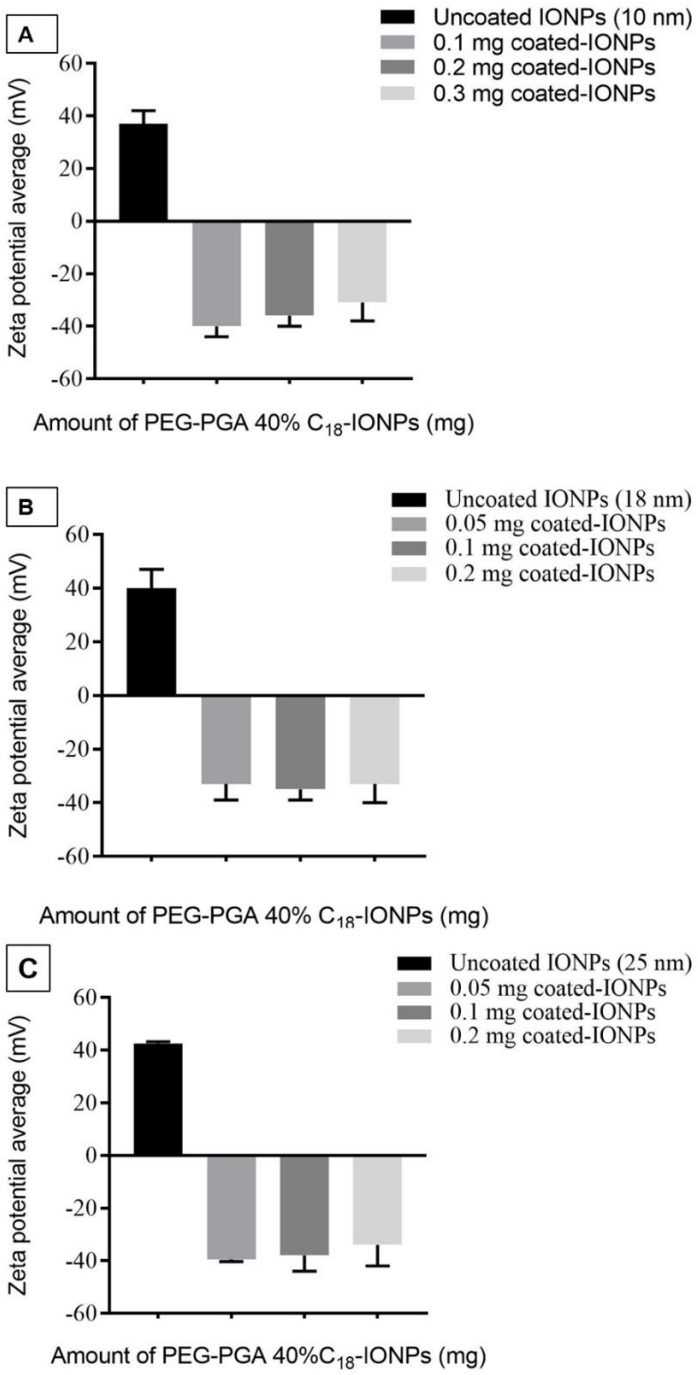


Figure 3-10: Surface charge of uncoated and PEGylated PGA 40% C_{18} coated IONPs where, (A) zeta potential of Rh 10 nm, (B) zeta potential of Rh 18 nm and (C) zeta potential of the biggest Rh (25 nm) of uncoated and coated with PEGylated PGA 40%C_{18} of different amounts. The zeta potential of all formulations was evaluated by one way ANOVA with a Sidak's multiple comparisons ($p > 0.05$). The zeta potential of all formulations was not significantly decreased when the amount of PEGylated PGA 40% C18 is increased. Zeta potential measurements were performed in PBS (15 mM) at pH 7.4 using Zeta sizer (Malvern Instruments,Malvern,UK). Results are expressed as the mean ± standard deviation of 5 readings.

3.3.5 Colloidal Stability of PEGylated PGA 40%C_{18} Coated IONPs

This study is crucial to obtain colloidal IONP that are stable against aggregation in a biological medium. Various concentrations of NaCl were added to uncoated and PEGylated PGA 40% C_{18} coated IONPs in order to determine their stability. Nanoparticles need to be stable at physiological salt concentration, which is 150 mM, but the concentration of NaCl was raised up to 480 mM in this experiment to check whether the stability was well in excess of this value. Turbidity measurements were performed by determining the optical density of suspended particles. Figure 3-11A, B and C show the colloidal stability of uncoated IONPs of different hydrodynamic radius (10, 18 and 25 nm) and coated IONPs with different amount of PEGylated PGA 40% C_{18} (0.05, 0.1, 0.2, 0.3 mg). Uncoated and coated IONPs were treated with an increasing concentration of aqueous sodium chloride solution, and the turbidity of the corresponding dispersion after rapid mixing was determined using optical density at 562 nm. All coated IONPs were found to show no increase in turbidity with increasing salt concentration, while uncoated particles showed increasing turbidity from even the smallest concentrations of added salt. This showed that all of the PEGylated PGA 40%C_{18} coated IONs formulations were stable and resistant to aggregation caused by NaCl addition. The main differences between different amounts of PEGylated PGA 40%C_{18} that was used to coat IONPs were found in the range 100-480 mM salt concentration. It was found that the PEGylated PGA 40% C_{18} IONPs that were produced from coating IONPs of small radii of 10 and 18 nm (Figure 3-11A and B) were

significantly more stable than that obtained from coating the large particle size of radius 25 nm (Figure 3-11C). However, uncoated particles were unstable at all concentrations of NaCl. This result is an indicator of the effectiveness of the application of coating materials on these IONPs.

.

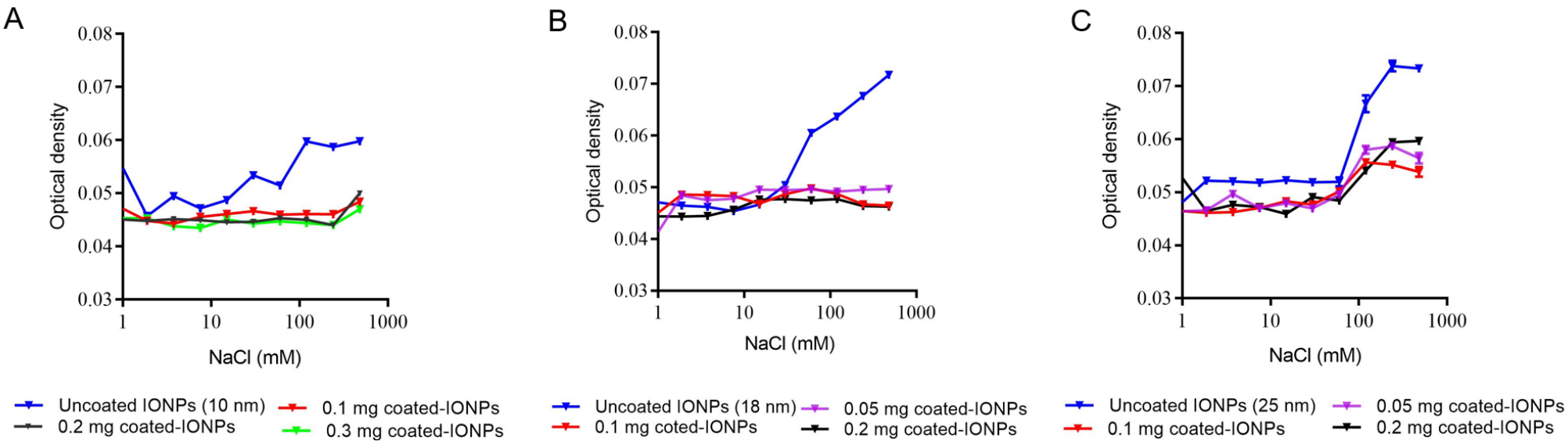


Figure 3-11: Stabilities of different formulations of uncoated and coated IONPs with different amount of PEGylated PGA 40% C_{18} (0.05, 0.1, 0.2 and 0.3 mg), where (A, B and C) stability of PEGylated PGA 40% C_{18} IONPs resulting from coating IONPs of hydrodynamic sizes 10, 18 and 25 nm respectively. Coated and uncoated IONPs (25 µg/ml) were mixed with different concentrations of NaCl. The absorbance was measured at 562 nm using a TECAN plate reader. For the IONPs absorbance at 562 nm, a significant difference was found between the uncoated and PEGylated PGA 40%C_{18} of different sizes ($P < 0.0038$), however according to a Tukey's multiple comparisons (2 way ANOVA), there were no significant differences between 0.05, 0.1, 0.2 and 0.3 mg PEG-PGA coated IONPs ($P>0.05$).

3.3.6 Quantification of Uncoated and PEGylated PGA 40%C_{18} Coated IONPs

Iron quantification is critically important when exploring the biomedical application of IONPs, cell-based therapy, MRI contrast agents or drug delivery. To know directly the amount of uncoated and coated IONPs in solution or taken up by cells, a ferrozine assay was used. This assay is often used in determining the iron concentration of IONPs based on the absorbance of the ferrozine-Fe^{2+} complex at 562 nm. The main advantages of using iron assays is that several samples can be measured at once. It is impossible to estimate iron content accurately by calculation due to the losses during the several filtrations, washing and centrifuge processes, so the ferrozine assay provides an accurate estimate to ensure the same quantity of nanoparticles is used in biological assays. In addition, during production of several batches of PEGylated PGA 40%C_{18} coated IONPs, the amount of nanoparticles will be different from the total amount of iron used in the first steps of coating process. In order to measure the iron concentration of an IONP, a standard curve (Figure 3-12) of absorbance at 562 nm as a function of Fe^{3+} amount was created according to a previous protocol (section 2.2.2.6). According to the calibration curve, IONPs of hydrodynamic radius 10 nm were calculated to be at a concentration of 3 mg/ml with respect to iron and 1.5 mg/ml after coating with PEGylated PGA 40%C_{18}. However, the concentration of IONPs of radii of 18 and 25 nm was 6.3 mg/ml initially and 3.5 mg/ml after coating with the same polymer.

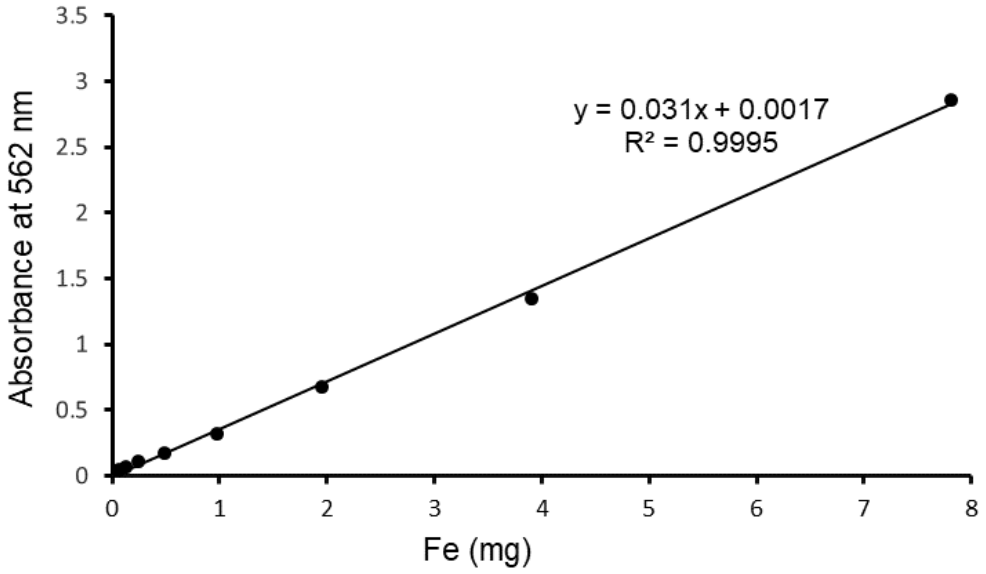


Figure 3-12: Iron calibration curve in water. The calibration curve was created using standard amount of iron ranging from 7.81 to 0.06 mg and reacted with ferrozine reagent. The absorbance was measured using a TECAN Spark plate reader. All samples are taken triplicate and averages calculate.

3.4 Discussion

The particle sizes were measured in terms of their hydrodynamic radii (Rh) using DLS. These will be converted to diameters and all particle sizes will be discussed as diameters for all DLS results

3.4.1 IONPs Preparation and Characterisation

Various IONP sizes ranging from 20 nm up to 80 nm were successfully prepared using the modified co-precipitation method whereby Fe_3O_4 was precipitated from Fe^3 and Fe^{2+} salt mixtures. The reaction process was fast and was carried out in oxygen free conditions to prevent magnetite from being oxidised to ferric hydroxide. Reproducibility of IONPs with the required size need to be consistent. IONP suspensions were produced three times with same particle size range using the same experiment

conditions. It was important since the size of the particles needed to be similar in order to investigate the effect of particle size on the interaction and uptake of the IONPs. Uniform particles are usually obtained by different methods. A homogeneous precipitation reaction, which involve processes of nucleation and growth [198-200]. The nucleation occurs due to the addition of excess solute at high temperature which leads to supersaturation [201]. After that, the nucleation stops once the concentration of solute drops then the nucleus grows due to the diffusion of the solute from the solution to the nucleus surfaces, and an equilibrium is achieved. Budhian et al (2008) reported that the nanoprecipitation does not require a source of external energy and would be easy to scale up relative to homogenization and sonication, which require an extra energy source [202]. IONPs with a narrow size distribution can also be obtained by controlling co-precipitation method conditions such as pH, temperature and stirring rate needed [78, 199]. In the present work, the particles synthesized with the co-precipitation method show a small size and narrow particle size distribution under controlled conditions with uniform particles of ovoid shapes and there was a very low percentage of aggregates. IONPs have been produced with different sizes by varying the amount of NaOH.

Many studies have been reported on the production of IONPs with different size and shape by using a co-precipitation technique. The type of polymer and materials that are used in the synthesis process played a significant role in the determination the size and form of the resulting particles. Mahmoudi et al (2009) [203] used a synthesis process

performed by addition of polymer during the IONP production process. The mole fraction of ferric and ferrous used by Mahmoudi was 2:1 and the precipitation process carried out by addition of iron salts and 1 M HCl to a solution of NaOH and PVA polymer under argon atmosphere and high temperature. The resulting size distribution and shapes of IONPs with or without PVA coatings was dependant on the stirring rate and amount of polymer. The hydrodynamic size obtained by Mahmoudi et al (2009) was 30 nm in diameter and TEM results of PVA coated IONS showed different particle shapes including spherical, elongated, beads, rod shaped with an average particle size diameter 86 nm. Hradil et al (2007) [204] used ammonium hydroxide to precipitate iron salt (2:1 molar ratio ferric to ferrous) in the presence of dextran solution. DLS results showed that particle size coated with dextran was 92 nm in diameter and reached to 120 nm after increasing the dextran/iron oxide ratio. The TEM (Figure 3-9) showed an approximately round particle with sizes of about 10-15 nm in diameter which was completely different from that found from DLS.

According to a study by Amiri et al (2011), SPIONs of magnetite with a mean diameter of 5 nm and narrow size distribution were synthesised by the co-precipitation method using an ultrasonic bath and homogenization rates at a high stirring speed [205]. Small particle sizes have also been obtained using a co-precipitation method by reaction of $FeCl_3$ salt in the presence of potassium iodide, ammonia solution and alcohol at room temperature and with stirring for more than 5 hours [206]. SPIONs with a diameter of 5 -20 nm were synthesised chemically using

a pH solution between 8 and 14 [207]. Another study carried out by Abushrida who used aqueous $FeCl_3$ and $FeCl_2$ solutions at a concentration ratio 2:1, and pH between 0.5 to 1, yielded IONPs with diameters from 3 to 15 nm using the co-precipitation method.

3.4.2 Optimised Conditions for Synthesis IONPs with Controlled Sizes

3.4.2.1 Effect of pH Variation on Particle Sizes

In general, results from the DLS study demonstrated the size of uncoated IONPs (Fig.3-1) increased remarkably, when colloidal pH was increased to 6 and above. DLS measurements generally showed a small particle size with no evidence of aggregation at pH 0.5. This is because at very acidic pH values, nanoparticles are highly charged preventing their aggregation by increasing electrostatic repulsive forces that limit the attraction of colloids [158]. At pH 3-4, the charge on the nanoparticles was reduced, resulting in formation of relatively larger particles with a low percentage of aggregation. Further increases in pH (6 and 12), lead to a significant reduction in surface charge, resulting in much larger particle sizes due to the aggregation. This is in a good agreement with the report by Gnanaprakash et al [208], that the average particle diameter of IONPs increased with increase in pH. Another study found, there was an increase in the concentration of ferrous ions at a low pH value, which led to a decrease in oxidation ratio and smaller magnetite particles are more likely to form [209].

In the present study, controlling the pH during the synthesis process of IONPs played a key role in adjusting the size of nanoparticles, for this

reason it was possible to produce IONPs with controlled size that can be used subsequently for further study. Filtration of the IONPs after synthesis using 0.2 µm filters was also important to remove large aggregates, and to produce a sterile formulation for the in vitro experiments.

3.4.3 Surface Charge of IONPs

Surface charge of nanoparticles gives an indication of their colloidal stability. In general, highly positively or negatively charged particles show good dispersion stability and consequently no particle agglomeration during storage [210]. Zeta potential of the all uncoated IONPs of different sizes are shown in Figure 3-10. It can be seen, net charge of IONPs in PBS (15 mM, pH 7.4) was determined to be positively charged. The positive charge of uncoated IONs was probably due to $Fe—OH_2^+$ formation in acidic medium as discussed by Lucas et al [211]. An increase of surface charge with increase in size was observed due to an increase in the number of functional groups on the surface of IONPs. The high values of the zeta potential of uncoated IONPs provide a strong electrostatic repulsion force between the nanoparticles, providing a good colloidal stability of the suspension at low salt concentrations.

3.4.4 Stability of IONPs

The stability of nanoparticles is defined in terms of their ability to stay in the same chemical composition, shape and size over time or under different conditions such as temperature, light, humidity. Aggregation of nanoparticles is the main stability problem.

Surface properties of nanoparticles play an important role in their stability as highly positively or negatively charged particles have a high density of charge around the particles resulting in more stable particles in water with no aggregation due to electrostatic stabilisation [78, 212-214].

It was important in this work to maintain the IONPs at their original size without aggregation before the coating process. For this reason, the size and appearance of uncoated IONPs was examined routinely over time before further characterisation in order to investigate how long they can be maintained without aggregation.

3.4.5 Size Distribution of Polymer Coated IONPs

The uncoated nanoparticles were investigated and were found to be unstable in physiologically relevant solutions. In order to achieve good dispersity and to maintain the size stability of particles produced, polymers were added to act as a stabilizing agent. Polymers contribute to stabilizing the whole particle and providing homogeneity and good dispersity in biological medium. It is for this reason that many NP preparation methods incorporate stabilisers or polymers during the coating process.

According to literature reports, there are different methods for producing successful stable dispersions of IONPs [4, 215]. However, most of them fail in achieving a small particle size. Mahmoudi et al (2009) used a synthesis process performed by addition of polymer during the IONP production process and he found the size of PVA coated IONPs were affected by the polymer/iron and the stirring rate [203]. A study by Yallapu

et al. (2011) who illustrated that, multi-layer β-cyclodextrin and F127 polymer coated IONPs were produced and offer good stability, but their effective utility was limited due to a larger particle size [216].

In this study, uncoated IONPs were produced initially so that different polymers and coating methods could be investigated using the same batch of IONPs. These particles were successfully coated with PGA 40%$C_{18,}$ PEG-PGA-SA and PEGylated PGA 40% C_{18} using modified IDP method. The main purpose of using different polymers was to determine an appropriate polymer that could produce a small particle size and have suitable properties for use in vitro environment. The IDP method was used previously for producing polymer coated nanoparticles [178]. The main advantages of this method are that it is reproducible, low cost, and simple, can produce particles in the nanometre size range, and also allows nanoparticles to be prepared without any surfactant or residual solvents being left in the system, which is important in terms of toxicity and safety in biological systems. When the organic phase was added to the aqueous phase by, the diffusion process started to occur and the tension at the aqueous–organic interface decreased. This resulted in the formation of tiny droplets of the organic phase in the aqueous phase, ultimately leading to the formation of a precipitation of the polymer on the surface of nanoparticles. On comparing the coated particles produced by Modified IDP method in this project using the pump technique, successful coating process was achieved because it allow even mixing of polymer with IONPs and showed good yield of coated particles with a narrow size distribution and small particle size. However, the dropwise method of

coating process using IDP that used by Abushrida showed two different populations of particle size with aggregation among the particles. The use of this procedure in the absence of iron oxide nanoparticles gives large polymer nanoparticles in the size range 150–200 nm, but using a small amount of polymer in the presence of iron oxide nanoparticles, small nanoparticles consisting of IONPs with a thin polymer coating are obtained. The process of association between polymer and particles is possibly through hydrogen bonds between the reactive carboxyl group of the polymer and hydroxyl groups on the surface of the iron oxide nanoparticle which provide a core for nanoparticle growth. Additionally the hydrophobicity of the C_{18} chains are also most likely to have an effect as previous work by Abushrida showed that PGA 40%C_{18} formed more effective layers than unmodified PGA. The polymers form a stable layer on the IONPs surface because they are insoluble in water. The amount of polymer used in the present work ranged between 0.05 mg to 0.3 mg, because a lower amount was insufficient in the coating process and using more than 0.3 mg polymer resulted in particle size increases. Basically, coating of nanoparticles depend on the “diffusion–stranding” process between two equilibrated liquid phases which involves addition of polymer dissolved in acetone into aqueous suspension under magnetic stirring [178, 217]. The solvent evaporates and the polymer is precipitated which result in the formation of core shell structured nanoparticles [218]. The particle size and size distribution of resulting nanoparticles in aqueous solution were determined by DLS.

PGA 40%C_{18} and PEG-PGA-SA led to significant increases in the size of IONPs. This could indicate that the presence of coating materials around a particle has resulted in an increase in particle size or may indicate aggregation of NP. In addition, the percentage of acylation of the PGA polymers increases the hydrophobicity of the polymer, which is likely to lead to an increase in the aggregation of polymer molecules rather than an increase in the number of particles formed [112, 219]. Indeed, an increase in length of hydrocarbon chain can influence the viscosity of the organic phase [217]. When PGA 40% C_{18} or PEG–PGA-SA are dissolved in acetone, a more viscous organic phase is produced due to the higher length of polymer side chains which could lead to a greater volume of polymer chains per unit volume of solvent. Increasing the viscosity of the organic phase could increase mass transfer resistance. Thus, the diffusion of polymer-solvent phase to the aqueous phase is decreased resulting in formation of polymer particles, which increase particle size. Additionally, we need to consider why PEG-PGA 40%C_{18} polymer resulted in a well controlled thin layer of polymer and unaggregated particles were produced whereas much larger particles resulted with PEG-PGA-SA. Explanation of producing large size of IONPs coated with PEG-PGA-SA that the structure of this polymer contains many PEG units on the surface of IONPs, which are highly dissolve in water rather than the formation of hydrophobic layer around the particle surface. This led to particle aggregations inside the polymer rather than the formation of single coated particles. However, PEG-PGA 40%C_{18} polymer contains only one PEG end, which attached to the PGA 40%C_{18} chain and allow

the hydrophobic part to be clumped around the particle to form thin layered particle rather than aggregates.

Small IONP size was obtained after coating IONPs with PEGylated PGA 40% C_{18}. Basically, the presence of PEG on PGA coated IONPs resulted in production of a very thin hydrophilic layer around the particles that increases the distance between the surface of the particle and therefore reduces the likelihood of aggregation so that only individual particles are dispersed in the PEGylated PGA 40% C_{18} matrix. TEM images showed smaller size than that measured by DLS. The size of nanoparticles of all formulations by TEM was approximately 8-47 nm and showed ovoid shaped particle (Figure 3-9), however the sizes of particle measured by DLS were 22 to 80 nm respectively. The particle size viewed by TEM was smaller than that measured by DLS, which can be attributed to the dehydrated state of the particles measured using TEM. In addition, the possibility of some low level nanoparticle aggregation in aqueous solution could lead to larger DLS values than with TEM. Shape can also have an effect on the particle size as in DLS analysis, an effective sphere radius is measured, which will be intermediate between the length of the particle core and the thickness. However, in TEM, the analysis of images was based on the length of the nanoparticles which is the major axis of each particle.

Controlling the size of nanoparticles is very important for in vivo and in vitro environment application. Large nanoparticles undergo opsonisation by plasma proteins. The adsorbed protein components affect the

biodistribution, degradation and elimination of the nanoparticles. Particle sizes also influence the biological stability, biodistribution, cellular uptake and toxicity of engineered nanoparticles. Previous investigations have shown that the effect of size of nanoparticles on cellular uptake, revealed different conclusions; One study was done by Calero, M., et al (2015) [220] showed uptake by two endocytic pathways depending on the size of superparamagnetic iron oxide nanoparticles (IONPs) surface stabilised with Dimercaptosuccinic acid (DMSA-IONPs) and reported that, larger particles were incorporated by micropinocytosis, while smaller nanoparticles were incorporated using the clathrin dependent pathway. Other studies reported the effect of nanoparticles size for in vivo application and they found nanoparticles of large size (>500 nm) undergo quick blood clearance and nonspecific uptake by macrophages, however small particle size (< 50 nm) and poly(ethylene glycol) (PEG) surfaces have been shown to be effective for the uptake by carcinoma cells as determined by the use of gold nanoparticles [108, 221, 222]

In the present work, Different size of PEGylated PGA 40% C_{18} IONPs were achieved in order for fully investigate the effect of size on the interaction and uptake of IONPs.

3.4.6 Surface Charges of coated IONPs

The change of charge from positive, in the case of uncoated particles, to negative after coating confirmed the presence of the coating materials surrounding the particle core. PEGylated PGA 40%C_{18} IONPs of different sizes showed a negative charge, most likely due to the presence of an

ionised carboxyl group of the polymer on the nanoparticle's surface, as reported previously by Kallinteri et al. [101]. The attachment of the PEG chain to the carboxyl group of PGA 40%C_{18} resulted in a decrease of the negative charges compared to non-PEGylated polymer. This may suggest that the polymer may start with a carboxyl group at each end rather than just one end on average. The zeta potential results (Figure 3-10) showed that the PEGylated PGA 40%C_{18} coated IONPs prepared in this work were negative after addition low amount of polymer however, there was a slight reduction in the negative charge surrounding the particles with increasing amount of PEGylated PGA 40% C_{18} which may due to the thickness of the coating materials (Figure 3-10A). The hydrophilic PEG layer on the surface of nanoparticles increases the distance between the particle surface and the slipping plane and the increased distance reduces the apparent charge on the surface of the particle i.e. the value of zeta potential. As increasing amounts of PEG-PGA was added, the PEG molecules become closer together on the surface, causing an extension of the PEG chain and a slightly decrease in the zeta potential.

3.4.7 Colloidal Stability of PEGylated PGA 40% C_{18} IONPs

According to previous studies, colloidal stability of the nanoparticles is a significant parameter since the aggregation of nanoparticles affect the biological function of particles in vitro [223, 224] and in vivo [225]. It was important to investigate and determine the stability of PEGylated PGA 40%C_{18} IONPs produced at different sizes in order to show the ability of this polymer to provide an effective coating layer. The stability of

PEGylated PGA 40%C_{18} IONPs formulation against particle aggregation at high NaCl concentration was probably due to both a strong interaction between the IONP core and polymer, and an effective PEG layer. The thickness of PEG-PGA polymer on the surface of nanoparticle core was enough to reduce charges around particles and act as a steric barrier against aggregation produced very stable particles.

Yue-Jian et al. (2010) reported that, there were no aggregates upon incubation of PEG-coated magnetic nanoparticles in distilled water and PBS buffer solution or a big different change in particle size after incubation in cell culture medium containing 10% serum protein for 24 hours which was mainly attributed to the antibiofouling property of the PEG coating layer [10].

In the present work, PEGylated PGA 40%C_{18} IONPs of size 22, 50 and 80 nm was selected for further investigation as they showed zeta potential with a negative charge that was slightly more negative than - 30 mV suggesting some contribution to stability by electrostatic interactions however, the PEG surface layer makes its greatest contribution to particle stability through steric stabilisation. The particles were stable without aggregation during storage at 4˚C. The good stability of PEGylated PGA 40%C_{18} coated IONPs could make them a useful candidate for cellular studies in addition to quantifying uptake and transport.

3.5 Conclusion

IONPs with different sizes have been prepared by a modified co-precipitation method under controlled conditions. Following synthesis, the IONPs were coated with PGA 40%C_{18}, PEG-PGA-SA and PEGylated PGA 40%C_{18} using a modified interfacial deposition method. However, only the PEGylated PGA 40%C_{18} produced nanoparticles with a small size, thin coating and acceptable morphology. The surface of IONPs changed to negative upon the addition of polymer. The properties of uncoated and coated IONPs was determined through DLS, TEM and zeta potential measurements and supplemented by stability studies in the presence of salt showing colloidal stability of the polymer coated IONP in physiological salt concentrations. It can concluded that the particle size depended on the type of the polymer used. In the following chapter, we will investigate the cellular uptake of Rhodamine B Isothiocyanate (RBITC) labelled PEGylated PGA 40% C_{18}. For the physicochemical properties presented in this chapter, particle radii have been used to define the particles as is usual for this type of work. However, for cell work where the overall diameter of the particle may be important we have used this measure of size to investigate the effect of IONP of diameters (22, 50 and 80 nm) on Calu-3 cells in order to identify the possible mechanism of internalization of these particles and will refer to them for the rest of the chapters as polymer coated IONPs.

4 Evaluation of Endocytosis and Transcytosis of Rhodamine B Isothiocyanate Labelled Polymer Coated Iron Oxide Nanoparticles

4.1 Introduction

A variety of cells can internalise protein, lipid and other substrate essential for cell function, but also nanoparticles by a process known as endocytosis [126, 137, 226]. Different types of endocytosis mechanisms have been proposed by previous studies including, caveolae or clathrin-mediated endocytosis, micropinocytosis and phagocytosis. During endocytosis, nanoparticles become encapsulated within vesicles and trafficked within the cell to the endo-lysosomal compartment where they may be enzymatically degraded, or affected by the acidic pH, or exocytosed. In a few exceptional cases, endocytosed material may be trafficked to another intracellular location, including the cytoplasm, endoplasmic reticulum, or cell nucleus [108, 136, 139, 227, 228]. Although it is largely assumed that nanoparticles enter cells by endocytic routes because they are not thought to be able to cross membranes, there is some evidence that some nanoparticles may enter the cells by passive diffusion across the membrane. If nanoparticles can cross the plasma membrane or the endocytic membrane, then they can probably cross any membrane and be fully distributed in the cell rather than being confined to the endocytic vesicles. This has been suggested by a few studies showing entry into cells through passive penetration of the plasma membrane [123, 181]. The interaction between the nanoparticles and plasma membranes is arguably the most critical step in membrane

penetration. For example, quantum dots are nanoparticles made of inorganic core materials, they can penetrate cells using different mechanisms including active and passive transportation. Osaki et al [229, 230] illustrated that the major route of QDs transport pathway is endocytosis. Passive diffusion of QDs into the cells is mostly due to electrostatic interaction with the plasma membrane. Le Bihan et al [231] investigated the accumulation of amorphous silica nanoparticles of size smaller than 20 nm into giant unilamellar vesicles. The resulting passage of these nanoparticles into the liposomes demonstrated that these nanoparticles could cross the lipid membranes without the need of supplementary energy. Recently, it has been shown that zwitterionic quantum dots can enter erythrocytes by passively crossing the cell membrane [181]. The route of entry into the cell is very important for determining the final intracellular location of the particle and its resultant efficacy. The uptake of nanoparticles via passive penetration of the plasma membrane directly transferred the particles into the cytoplasm which can be the preferred choice principally when designing a gene delivery system [181] or alternatively at least to define how the nanoparticle enters the cell as this may greatly affect its drug delivery properties. The physicochemical properties of nanoparticles can determine cellular internalisation and distribution which have been discussed in the introduction but briefly, they include nanoparticle size, shape, colloidal stability, surface charge and chemistry along with cell dependent factors including cell type.

In recent years, there has been a great interest in applying nanotechnology for biomedical studies, in particular for therapeutic and diagnostic purposes. How the size of nanoparticles can determine the pathway of cellular internalisation has become a question of absolute priorities in nanomedicine [232-234]. For this reason, cell culture is an important first line tool to screen uptake efficiently, to assist in determining the safety of nanoparticles and provide significant information to understand cell-particle interactions before moving to in vivo analysis [220, 235]. In this regard, evaluation of potential use of nanoparticles requires a precise knowledge of the internalisation mechanism.

Calu-3 cell line is one of the few cell lines that can form sheets of cells that are connected to each other by tight junctions. In addition, it is a well differentiated and characterised cell line which demonstrates many characteristics of the bronchiolar epithelium [236]. This cell line is suitable for assessment of drug permeation and in discovery studies. The airway epithelium is directly exposed to the external environment. Exogenous substances or medical therapies can be delivered to the epithelial cells themselves for local action as well as for systemic action which require drugs to be able to penetrate different biological barriers to reach the circulation. Thus, determination of how drugs can cross the barrier would be very useful for the development of systemic delivery.

The potential impact of particle size of NP on their interaction with cells has motivated many studies on the uptake of nanoparticles however

different conclusions were revealed. A study [221] comparing between 14, 30, 50 74 and 100 nm gold nanoparticles found that the particle size of 50 nm showed the highest uptake, as indicated in other studies [229, 238], however another group reported that gold nanoparticles of size 20 nm gave the best results [239]. Differences in particle type, size, shape and cells make it difficult to draw definite conclusion cross these studies.

IONPs have attracted enormous scientific interest due to properties that make them useful for a large variety of biological applications. The main advantages are the ability to be synthesised at varied size, biocompatibility, non-toxicity, biodegradability and their chemical stability [9, 10, 13, 240]. Most importantly, IONPs can be traced in vitro by TEM due to their higher detection sensitivity [29, 30, 61].

A study by Abushrida (2012) who worked in the same research group as me, found PEGylated PGA40%C_{18} coated IONPs of small size (~20nm diameter) were not taken up into C6 (glioma tumour cells) by the normal endocytic pathway and they were observed in huge amounts in the cytoplasm and all subcellular compartments throughout the cells. Also an unusual feature of the uptake was noted. Fluorescent patches appeared over the nuclei which was particularly noticeable with high concentration particle uptake. It was therefore unclear whether the mechanism of transport was by endocytosis or a translocation across membranes [176]. In addition, do other particle sizes have the same unusual feature? For this reason, IONPs of different sizes were used as a model for endocytosis and transcytosis study because it allows us to track the

intracellular localisation in different cell type and determine the uptake pathway by electron microscope which cannot be performed with other polymer nanoparticles.

RBITC was chosen as the a fluorescent label due to its photostability against quenching [241]. Polymer coated IONPs were labelled with RBITC to investigate and evaluate the cellular internalisation of fluorescently labelled nanoparticles of different sizes (22, 50 and 80 nm) through a lung epithelial cell line (Calu-3 cells).

4.2 Aim

The aim of this chapter is to examine the effects of labelled coated IONPs with varied particle sizes (22, 50 and 80 nm) on cellular uptake using an in vitro Calu-3 model. For a better understanding of cellular uptake, it is important to visualise and quantify IONPs inside the cells to determine an optimal nanoparticle dose at which the cellular uptake reaches a maximum level. The study will explore the cellular localisation of the labelled nanoparticles within the in vitro model. Possible mechanism of internalisation of these sizes will be identified. The effects of internalisation on the cells will be investigated through an examination of cell morphology, viability and metabolic activity. The present study will also evaluate the effect of polymer coated IONP's size on permeability across an in vitro cell culture model of the of lung epithelial barrier.

4.3 Results

4.3.1 Physicochemical Properties of RBITC Dye Labelled IONPs

In order to allow tracking of polymer coated IONPs uptake into cells and investigate the subsequent subcellular localization by fluorescence or confocal microscopy, RBITC was chemically bound to the terminal carboxyl functional group of the polymer. Furthermore, those dye molecules are not easily photo-bleached as indicated in the literature due to the restricted movement of dye molecules after being attached to functional groups [242, 243]. The surface of sterically stabilised polymer coated IONPs contains an abundance of negatively charged carboxylic groups, which can be readily conjugated with a fluorescent dye to produce monodisperse nanoparticles. While it is well known that amine groups can react with isothiocyanate groups of RBITC producing dye conjugated polymer encapsulated IONPs [244, 245], the potential reaction with Carboxylic groups is less well known. Because it has been shown that the RBITC has a very slow release from PGA nanoparticles [165], it is assumed that the RBITC is probably conjugated to the polymer by this carboxyl group.

It was essential to ensure that the dye incorporation process did not cause alteration in physicochemical properties of nanoparticles, which include the size, surface charge and the stability of coated IONPs. The particles sizes and surface charges are almost not changed (appendix, Figure **I** and Figure **II**). More notably, the labelled particles were still stable in HEPES, at pH 7.4 with almost no leaching of the encapsulated dye from the nanoparticles or aggregate. It was important for accurate

and consistent monitoring of IONPs for biological applications to control the amount of dye conjugated to particles by adjusting the ratio between the dye and polymer coated IONPs.

4.3.2 Amount of RBITC Incorporated to the Coated IONPs

This study aimed to calculate the amount of entrapped dye in the polymer matrix. The labelling process of polymer coated IONPs with RBITC was described in Section (2.2.1.3). The amount of incorporated dye was obtained from the calibration curve displayed in Figure 4-1. The hydrophobic properties of the polymer and the interaction between the polymer and RBITC have an effect on the loading capacity. Incorporation of RBITC to the polymer coated IONPs of different sizes was in the range from 0.08-0.15%, suggesting that the dye used for labelling became entrapped into the nanoparticle matrix. The level of fluorescence was analysed fluorometrically in order to calculate the fluorescence intensity of the different particle sizes and monitor the optimum concentration of labelled nanoparticles as the presence of excessive particles in the sample may have an effect on the fluorescence of RBITC. A sufficient fluorescence intensity of RBITC labelled nanoparticles is important for cellular uptake and permeability studies of IONPs.

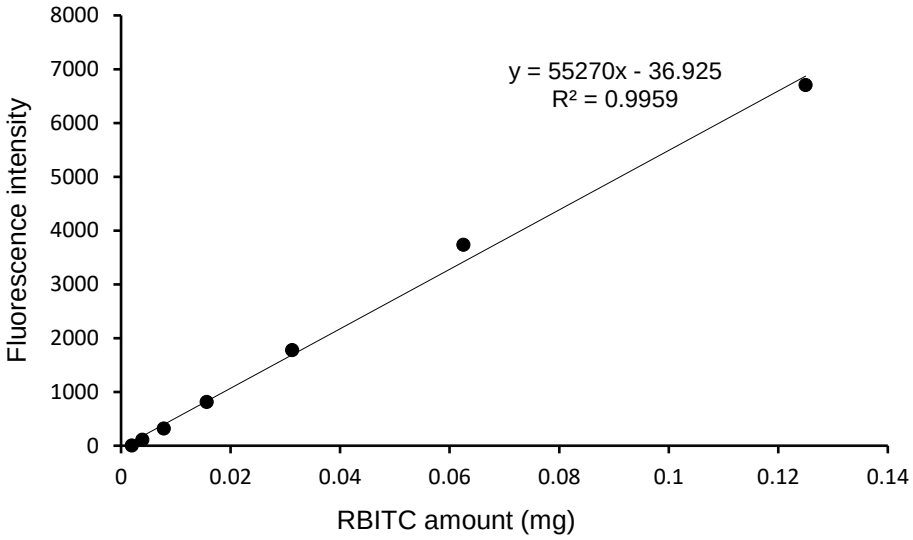


Figure 4-1: Calibration curve for RBITC in HEPES. The calibration curve was created by preparing a dilution series of a RBITC stock solution ranging from 0.002 to 0.125 mg. The fluorescence intensity was measured using a Dynal MFX Fluorimeter, at Ex 554 nm and Em 575 nm.

4.3.3 Cell viability study of different coated IONPs size

Cytotoxicity of polymer coated IONPs was determined by using trypan blue and MTT assay in order to investigate the morphology and metabolic activity of Calu-3 cell after addition of different concentrations of different coated nanoparticle sizes.

4.3.3.1 Metabolic Activity (MTT) Assay

Nanoparticles often affect the metabolic activity of cells, cell apoptosis, cell membrane integrity and proliferation. Therefore, the potential of in vitro toxicity of IONPs is initially determined by the viability of cells. The MTT assay is a colorimetric assay for assessing cell metabolic activity and can measure cytotoxicity of nanoparticles. NAD(P)-dependent cellular oxidoreductase enzymes reflect the number of live cells present and these enzymes are capable of reducing tetrazolium dye MTT 3-(4,5-

dimethylthiazol-2-yl)-2,5-diphenyltetrazolium bromide to its insoluble formazan, which has a purple colour. MTT assays are usually done in the dark because it is sensitive to the light. Cytotoxicity was tested on the Calu-3 epithelial cell line that was treated with varying doses (200, 100, 50, 25 and 10 µg/ml) of polymer coated IONPs of different sizes (22, 50 and 80 nm) for 24 hours. Statistical ANOVA analysis test indicated that, there was insignificant difference upon increasing the dose of nanoparticles of size 50 and 80 nm as seen in Figure 4-2. However, nanoparticles of size 20 nm exhibited a significant decrease in the number of viable cells at a concentration of 200 µg/ml.

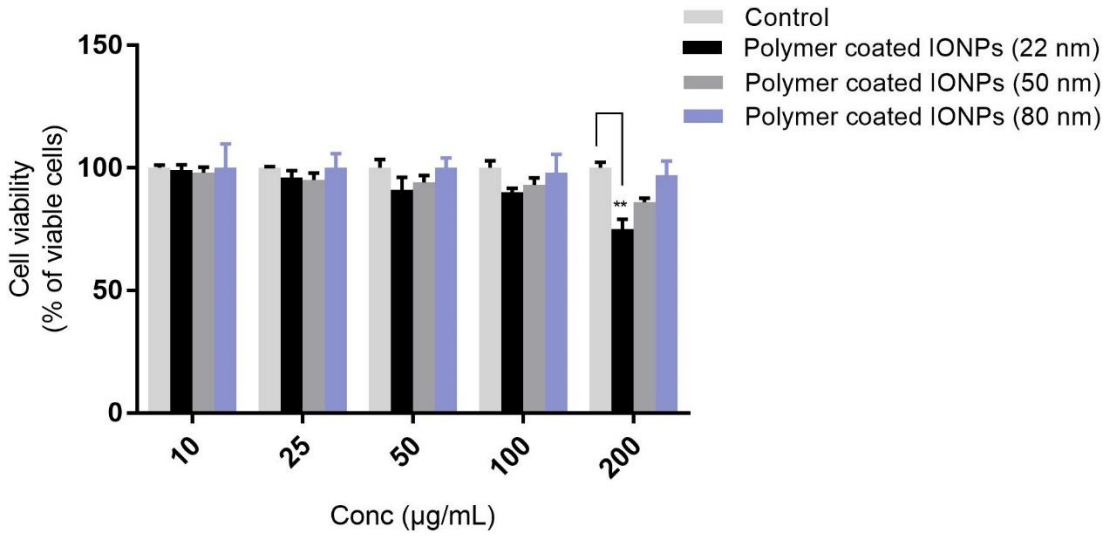


Figure 4-2: Viability of Calu-3 cells incubated with increased dose of PEGylated PGA 40%C_{18} IONPs of different sizes (22, 50 and 80 nm) for 24 hours as determined by the MTT assay. Results presented as % viability and shown as the mean ± S.E.M (N=3). A Tukey's multiple comparison test (2 way ANOVA) was used for statistical analysis. ** indicated that the viability of Calu-3 cells is significantly lower than the control with $p<0.01$.

4.3.3.2 Trypan Blue Exclusion Method

The trypan blue exclusion test was used as the gold standard method to validate the cell viability data that was obtained by MTT assay. This method depends on the counting of viable cells using a haemocytometer. The main advantage of this method is the lower probability of interference occurring. The trypan blue assay results as seen in (Figure 4-3), clearly showed that the all sizes of polymer coated IONP possessed a minor cytotoxic effect in Calu-3 cell line with no significant differences between different particles sizes in the concentration range 10-100 µg/ml up to 24 hours of treatment (>95% viability in relation to the control sample). A statistically, insignificant reduction of about 8% in the number of viable cells was observed with the increased concentration (100 µg/ml) of incubated nanoparticles of size 22 nm. These results correlated well with visual examination when observed under microscope. The maximum concentration of NPs (50 µg/ml of medium) expected to be used for potential in vitro applications and the time of incubation was reduced to 4 hours for further studies to minimize the effect of NPs on the cell viability.

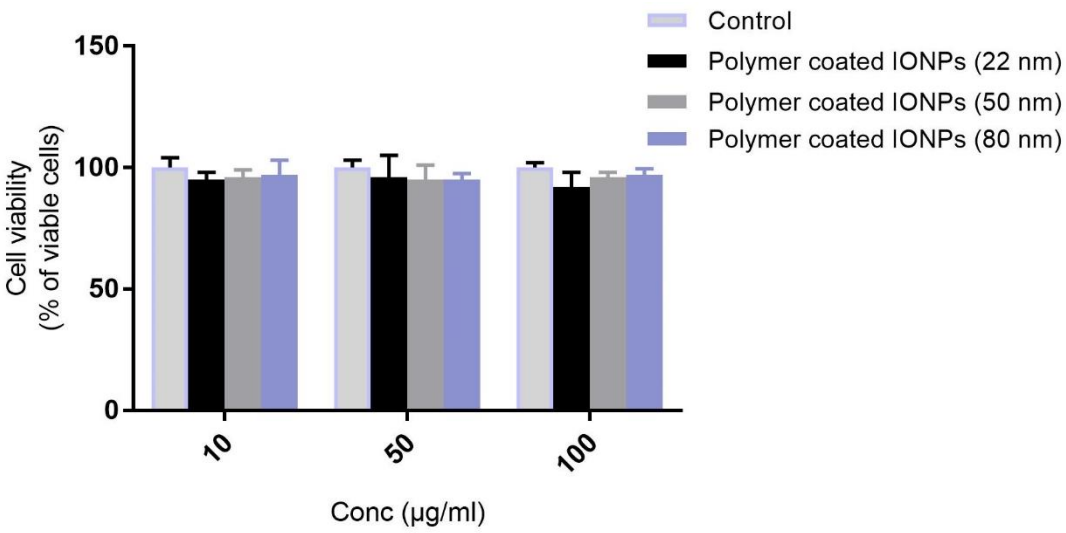


Figure 4-3: Viability of Calu-3 cells incubated with different concentrations of PEGylated PGA 40%C_{18} IONPs (10, 50 and 100 µg/ml) for 24 hours as determined by haemocytometer. Results are presented as % viability relative to control cells and shown as the mean ± SD (n=3). A Tukey's multiple comparison test (2 way ANOVA) was used for statistical analysis. The results showed that the viability of Calu-3 cells was not significantly lower than the control with $p>0.05$.

4.3.4 Interactions of Polymer Coated IONPs with Calu-3 cells

Quantitative measurements of nanoparticle uptake pose a technical challenge as it is difficult to accurately distinguish real nanoparticle uptake from the adsorption of nanoparticles at the cell surface. This is one of the limitation of this experiment. However, the purpose of this experiment was to obtain quantitative information on the amount of material associated with the cells, which could be later analysed in the context of localisation experiments using microscopy.

To determine the amount of polymer coated IONPs associated with Calu-3 cells, ferrozine was used due to its affordability and sensitivity to even low iron concentration [246]. Several studies have shown the potential of ferrozine assay in the quantification of IONPs [220, 247, 248].

Ferrozine forms a complex with reduced iron form to yield a coloured solution, which absorbs light at 562 nm, and using appropriate calibration standards created under the same conditions allow accurate quantitation of iron. This assay has been applied extensively in determining the concentration of polymer coated IONPs inside the cells at different incubation time as will be described in the following section:

4.3.4.1 Effect of IONP Amounts on Calu-3 Cellular Interaction

Nanoparticles need to be accumulated in the cells with a sufficiently high rate and extent. It has been proposed that the size of nanoparticles play an important role in their interaction with cells. Calu-3 cells were incubated with different amount of polymer coated IONPs of size 22, 50 and 80 nm for 2 hours. As can be seen in the Figure 4-4, the association of nanoparticles with Calu-3 cells was dependent on the amount of nanoparticles in culture medium. The association increased with increase the amount of IONPs, however a greater increase was detected after addition of 75 μg of nanoparticles with size 50 nm. NPs of small size (22 nm) showed a greater accumulation at lower amounts than NPs of size 50 and 80 nm. There was no further increase in the efficiency of cellular accumulation upon addition of a higher amount of particles of size 22 and 80 nm, suggesting that the cells were reaching saturation of accumulation, conversely the polymer coated IONPs of size 50 nm continued their accumulation in calu-3 cells with increasing concentration.

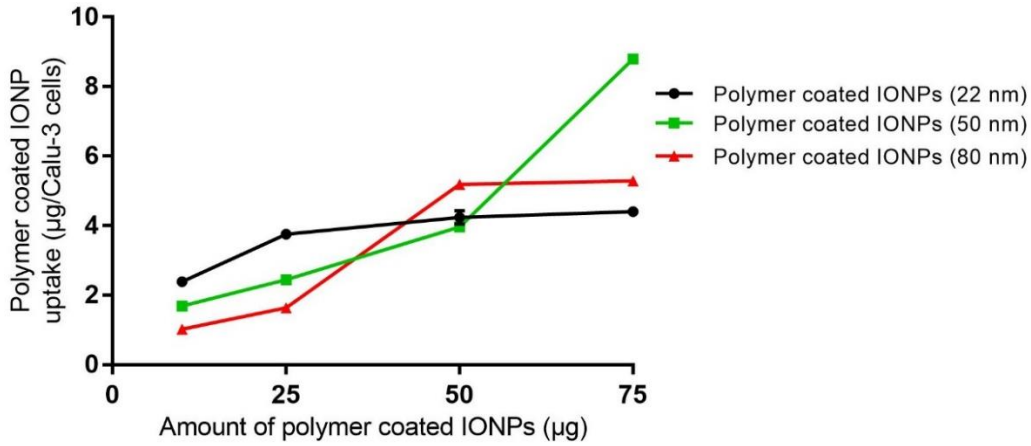


Figure 4-4: Schematic showing the effect of polymer coated IONP amount on accumulation of nanoparticles in Calu-3 cells. Calu-3 cells were incubated with different sizes of PEGylated PGA 40%C_{18} IONPs (22, 50 and 80 nm). The intracellular uptake was evaluated after 2 hours of incubation with different NP amounts (10, 25, 50 and 75 µg). Intracellular iron content was calculated by creating a standard curve of known NP concentration using the ferrozine assay. According to a Tukey's multiple comparison test (2 way ANOVA), there were significant differences between the accumulated amount of particles of size 22, 50 and 80 nm in Calu-3 cells with $P < 0.0001$, however cells incubated with 50 µg of particle with sizes 22 and 50nm showed insignificant differences of cellular accumulation with ($P = 0.1906$). Error bars represent mean ± S.E.M (N=3).

4.3.4.2 Effect of Incubation Time on Calu-3 Cellular Interactions

The previous section showed continued cellular loading of polymer coated IONPs of size 50 nm, however the particle of sizes 22 and 80 nm showed that the accumulation in cells had reached a plateau. Now, evaluation of the rate of accumulation with incubation time was important to indicate the kinetics of NP accumulation and to establish how long these polymer coated IONPs remain inside cells. Figure 4-5 shows results of cells incubated with polymer coated IONPs of size (22, 50 and 80 nm) for different time periods (30 minutes to 24 hours). The interaction of polymer coated IONPs with cells was dependent on the incubation time as it was possible to detect IONPs of varied sizes in Calu-3 cells

even after 30 minutes of nanoparticle incubation. After the first 2 hours of incubation, association of nanoparticles of size 22 and 50 nm with cells was lower compared to the NPs of size 80 nm. There was a significant decrease of nanoparticles of size 80 nm in the cells beyond 2 hours incubation period, however no noticeable change on cellular accumulation of particle of size 50 nm after 2 hours which may be attributed to the limited saturation level. The cellular interaction of nanoparticles of size 22 nm seems to gradually increase with time and reached a maximum accumulation point at the longest time period of 24 hours of incubation. To confirm the association of nanoparticle with the cells, untreated cells incubated for the same periods were also used. The results show that, the cells not incubated with nanoparticles showed insignificant increase in absorbance against the ferrozine assay (result not shown).

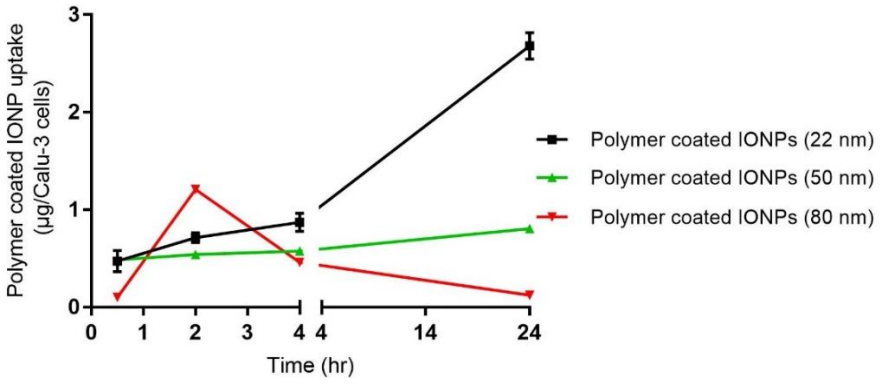


Figure 4-5: Effect of incubation time on polymer coated IONPs accumulation in Calu-3 cells. Calu-3 cells were incubated with different sizes of PEGylated PGA 40%C_{18} IONPs (22, 50 and 80 nm). The intracellular accumulation was evaluated after 30 minutes, 2, 4 and 24 hours of incubation with 50 µg NPs. Intracellular iron content was calculated by creating a standard curve of known concentration NPs using the ferrozine assay. According to a Tukey's multiple comparison test (2 way ANOVA), the amount of particles of size 22 nm that accumulated in Calu-3 cells within 24 hours was significantly higher than particles of size 50 and 80 nm with P <0.0001 within 24 hours. Error bars represent mean ± S.E.M (N=3).

4.3.5 Quantitative Determination of Unbound IONPs in Cell Culture Medium

The intracellular accumulation of polymer coated IONPs (50 µg) after different times was investigated as mentioned in the previous section. Further investigation was done for quantification of unbound IONPs in the culture medium (saved from previous experiments) using ferrozine assay. The quantity of polymer coated IONPs in cell culture media (EMEM) was investigated after the incubation of nanoparticles with cells for 2 and 4 hours. The previous experiment showed there was a continuous increase in the cellular accumulation of particle size 22 nm, however the accumulation of nanoparticles (50 nm) remained the same upon increasing the time of incubation and the amount of particles (80 nm) in the cell was reduced. These results were confirmed by this assay as in Figure 4-6. This shows the amount of particles of size 20 nm are decreased in the culture medium, however the level of particles of size 50 and 80 nm increased in the medium after 4 hours of incubation with Calu-3 cells. This order of relative amounts of the different particle sizes in the medium is in agreement with the cell accumulation data presented in Figure 4-5.

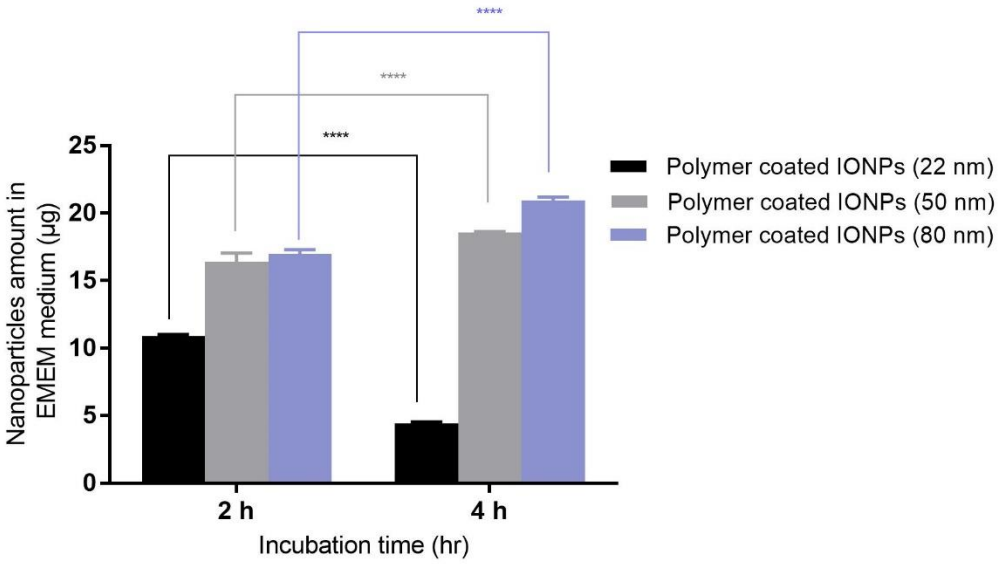


Figure 4-6: Analysis of different sizes polymer coated IONP contents in EMEM medium. Calu-3 cells were incubated with 50 µg PEG-PGA 40%C_{18} coated IONPs (22, 50 and 80 nm) for different times (2 and 4 hours). The unbound polymer coated IONPs content that were present in EMEM were analysed by ferrozine assay using a standard curve of known concentrations of NPs. According to a Tukey's multiple comparison test (2 way ANOVA), the amount of particles of size 22 nm in EMEM medium was extremely significant decreased after 4 hours, however the particles of size 50 and 80 nm was extremely significant increased (P <0.0001). Error bar represent mean ± standard deviation (n=3).

4.3.6 Microscopy Studies

The present study was conducted to investigate the subcellular localization of nanoparticles. Effects of particle size and treatment time on nanoparticle uptake will be clearly evidenced. These can be performed through using fluorescent nanoparticles and labelling the intracellular organelles such as lysosomes, endosomes and nucleus [249]. In this work, the RBITC-labelled polymer coated IONPs of different size (22, 50 and 80 nm) were used and their uptake into Calu-3 cells was investigated and quantified using confocal microscopy.

4.3.6.1 Dose dependent and intracellular distribution of RBITC labelled polymer coated IONPs in Calu-3 cells using confocal laser scanning microscopy

Calu-3 cells were incubated with EMEM medium containing polymer coated IONPs labelled with RBITC for 2 and 4 hours before washing and examination by confocal microscopy. The stained nucleus is visualised by Draq-5 (blue) and the fluorescent nanoparticles as red. Figure 4-7clearly shows the cellular intensity level of different concentrations of nanoparticles (5, 25 and 50 µg/ml) incubated with Calu-3 cells for 2 hours, which strongly support the previous quantitative measurements by the ferrozine assay. The cell-associated fluorescence increased with the dose of added RBITC-labelled nanoparticles of all sizes, however there was an apparent difference in pattern of nanoparticle distribution inside the cells. The confocal pictures clearly indicates no significant cell surface binding of nanoparticles. Cells incubated with nanoparticles of size 22 nm displayed a high fluorescence intensity of very finely distributed spots evenly distributed across the whole cell with no obvious bright spots of fluorescence corresponding to lysosomal distribution (Figure 4-7C-E). For nanoparticles of size 50 and 80 nm at the same nanoparticle concentrations, the appearance of the fluorescent spots was slightly more granular and there were some spots of higher fluorescence intensity, against the overall even distribution of fluorescence across most cells. For the cells that were incubated with nanoparticles of size 50 nm, an even distribution can be seen in some cells with some of points of fluorescence in other cells which may indicate different sorts of internalisation (Figure 4-7H and I). For labelled

nanoparticles of size 80 nm, many bright spots over all cells were detected, although there was no obvious perinuclear distribution (Figure 4-7L and M).

To confirm that cellular uptake resulted from fluorescently-labelled nanoparticles, two types of control were used. One was culture medium without labelled nanoparticles (control 1) and another was cells cultured with medium containing free RBITC (control 2) using the concentration incorporated into the coated nanoparticles . There was no significant autofluorescence with the medium control sample (Figure 4-7A) and no uptake of free dye was seen at the level of free dye expected in the nanoparticles (Figure 4-7B).

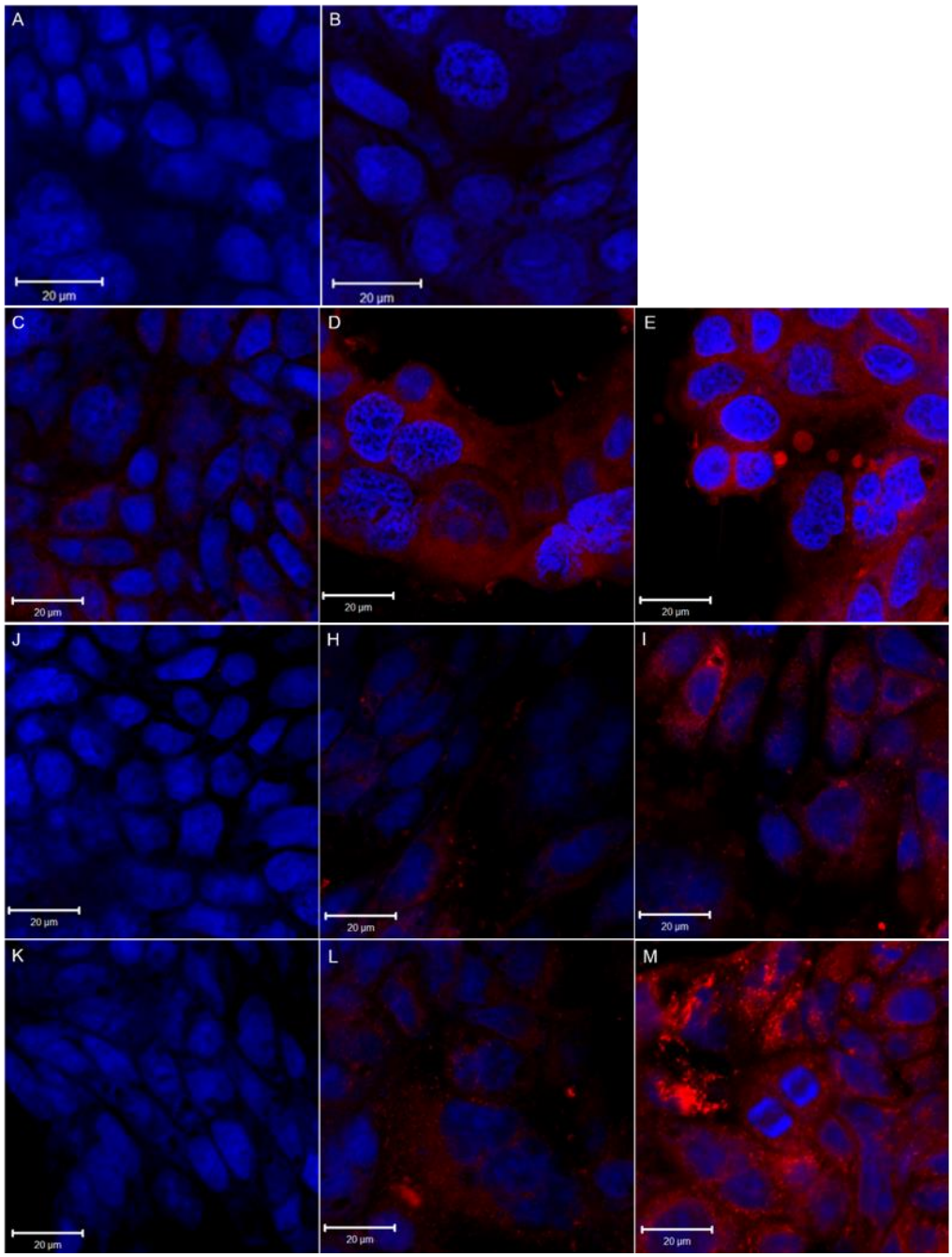


Figure 4-7: Confocal microscopy images of RBITC-labelled polymer coated IONPs incubated with Calu-3 cells for 2 hours, where, (A and B) are untreated cells and cells incubated with free RBITC. (C, D and E) cells incubated with (5, 25 and 50 µg/ml) NPs of size 22 nm, (J, H and I) cells incubated with (5, 25 and 50 µg/ml) NPs of size 50 nm and (K, L and M) cell incubated with (5, 25 and 50 µg/ml) NPs of size 80 nm (Scale bar 20 µm). A slice of 1 µm thickness was imaged from the middle of the sample by an individual confocal optical section.

A study of the influence of increasing the incubation time of nanoparticles on cellular uptake was then carried out. In this case labelled polymer coated IONP concentrations (25 and 50 µg/ml) were incubated with Calu-3 cells for 4 hours. Figure 4-8A and Figure 4-8B shows that for an incubation time of 4 hours, the uptake of small size nanoparticles (22 nm) into the Calu-3 cells is more intense than the incubation for 2 hours with a more granular appearance of the fluorescent spots. However, nanoparticles of size 50 nm exhibited low fluorescence intensity and no nanoparticles of size 80 nm were observed over any cells at 25 µg/ml, only a small amount of fluorescence visible on increasing the concentration to 50 µg/ml. The changes in intensity of fluorescence in cells incubated with nanoparticles of size 22 nm for 4 hours reflects the cellular accumulation of particle, seen in the quantitative determination of IONP uptake by ferrozine seen in Figure 4-5.

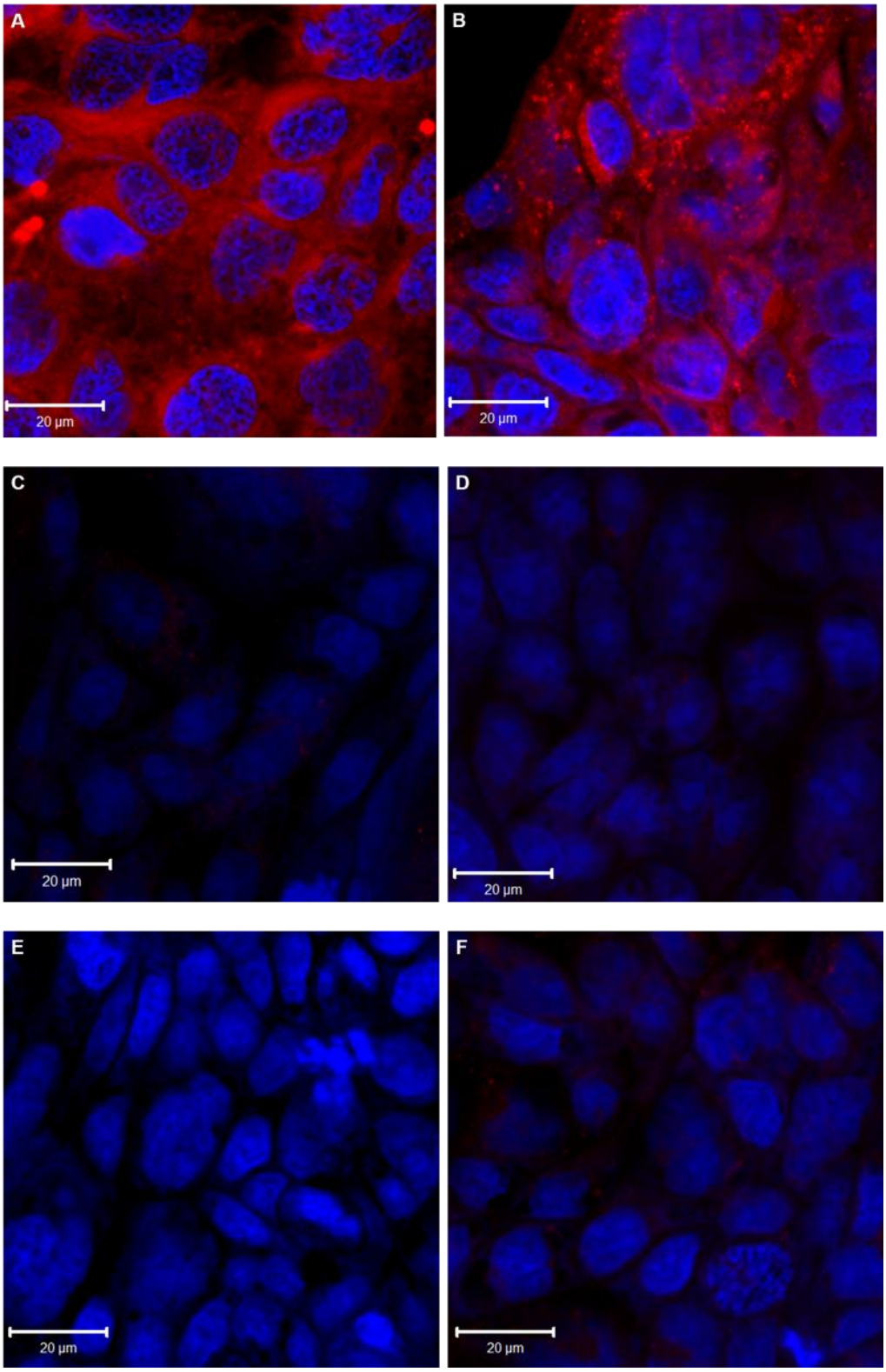


Figure 4-8: Confocal microscopy images of RBITC-labelled polymer coated IONPs incubated with Calu-3 cells for 4 hours, where (A and B) cells incubated with (25 and 50 µg/ml) NPs of size 22 nm, (C and D) cells incubated with (25 and 50 µg/ml) NPs of size 50 nm and (E and F) cell incubated with (25 and 50 µg/ml) NPs of size 80 nm (Scale bar 20 µm). A slice of 1 µm thickness was imaged from the middle of the sample by an individual confocal optical section.

Samples of the same previous experiment were processed for observation of the particle distribution within the depth of the polarised cell layers by confocal microscopy. Figure 4-9 (A, B and C) shows z-stack analysis of the confocal images of the Calu-3 cells incubated with polymer coated IONPs of all sizes for 2 hours. The presence of fluorescent signals inside the cells clearly demonstrates the actual internalisation of nanoparticles into cell layers as shown in the gallery series. The galleries showed that the fluorescence could be seen in the middle of Calu-3 cells with increasing diffusion distance of IONPs into different cell layer incubation time for 2 hours. Differences in intracellular fluorescence intensity can be observed between different cell layers, the fluorescence intensity is more concentrated in the centre of cells more in the margin, especially with polymer coated IONPs of size 22 nm as shown in Figure 4-9A. Looking at a cross section through the cells, xz and yz, at position marked by the arrow, it is possible to see these particles (22 nm) are indeed present in the nucleus. In contrast, only a few nanoparticles of size 50 or 80 nm could be observed in the nucleus.

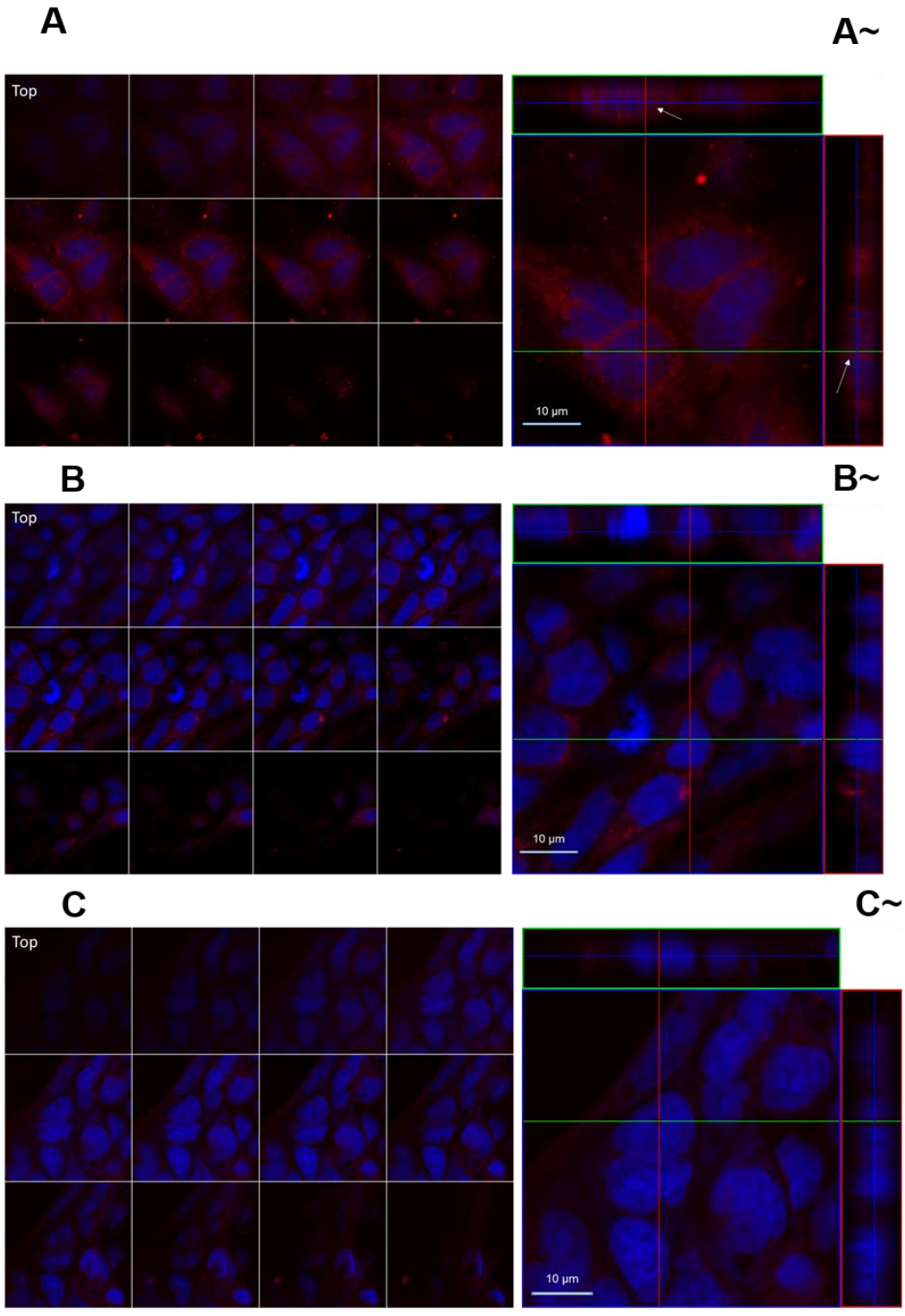


Figure 4-9: Serial confocal images was obtained by multiple optical sectioning of 1 µm thickness of each section (12 slices) showing an in vitro model of Calu-3 cells after 2 h incubation with RBITC-polymer coated IONPs (25 µg/ml, red). (A, B and C) showing Gallery series of images (slices), of polymer coated IONPs of sizes (22, 50 and 80 nm), starting from the top of the cell layers. (A~, B~ and C~) Orthogonal slice view. Cell nuclei (blue) were labelled with Draq-5.

4.3.6.2 Intracellular Localisation of RBITC Labelled Polymer Coated IONPs in Calu-3 Cells

The intracellular localisation of polymer coated IONPs following incubation with Calu-3 cells was investigated using confocal microscopy to assess whether these particles have different terminal destination according to their size or whether they could accumulate in the lysosomal compartments. Each different size of polymer coated IONPs was incubated with the Calu-3 cells for 2 hours. The conditions of the experiment was kept equal to previous experiments performed in 8-chambered well cover plates. After incubation, cells were treated with LysoTracker Green to stain the lysosomal compartment and finally visualised by bright field and confocal microscopy.

Figure 4-10 clearly shows an extensive red fluorescent nanoparticle of small size (22 nm) in cells stained for nuclei blue with somewhat prominent distribution of green fluorescence dots. Although the intensity of green stain of the LysoTracker® is weak, there is no appearance of yellow regions in the image, which would indicate co-localization of red (nanoparticles) with green (lysosome marker).

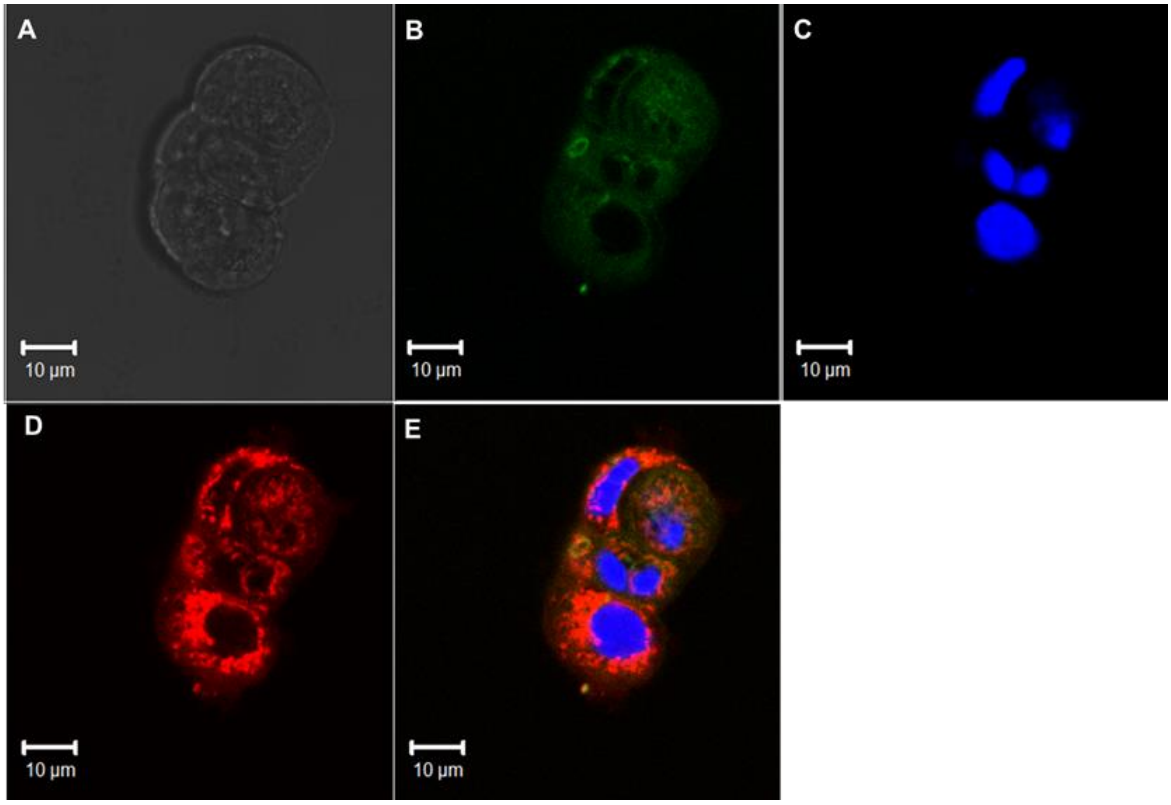


Figure 4-10: Confocal microscopy images demonstrating the intracellular distribution of 22 nm RBITC labelled polymer coated IONPs (50 µg) incubated with Calu-3 cells for 2 hours. (A) Bright field showing the outline of the cells. (B) Cells stained with LysoTracker Green (C) Draq 5 (nuclear stain), (D) Uptake of red fluorescent labelled polymer coated IONPs (E) Overlay of (B) and (D) showing location of nanoparticles compared to lysosomes. Scale bar 10 µm.

Merged images of nanoparticles size 50 nm in Figure 4-11 displayed a substantial large fraction of green fluorescence from LysoTacker, which indicate most of the nanoparticles were not localised in endosome, whereas there are a few yellow punctate areas in the overlay image, which could indicate to the co-localization of these nanoparticles (50 nm) with lysosomes.

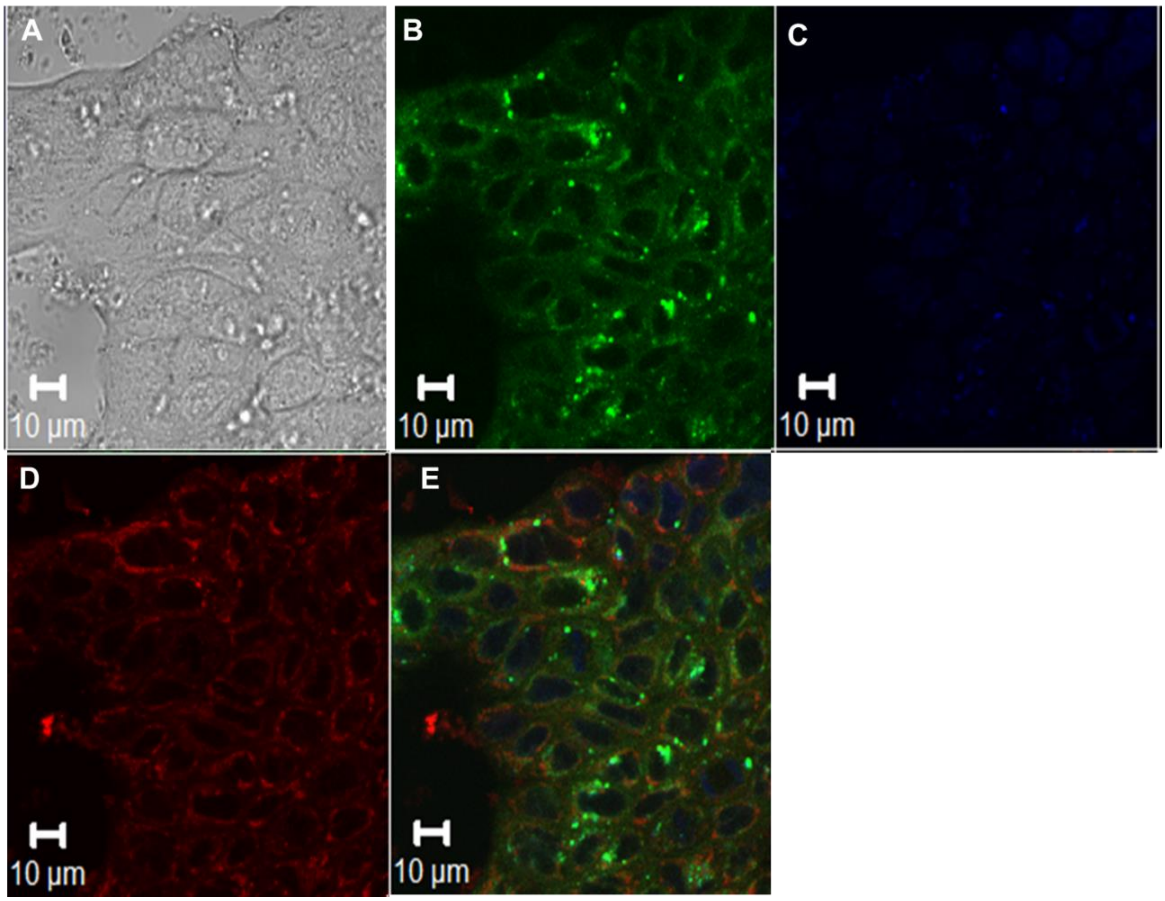


Figure 4-11: Confocal microscopy images demonstrating the intracellular distribution of 50 nm RBITC labelled polymer coated IONPs (50 µg) incubated with Calu-3 cells for 2 hours. (A) Bright field showing the outline of the cells. (B) Cells stained with LysoTracker Green (C) Draq 5 (nuclear stain), (D) Uptake of red fluorescent polymer coated IONPs (E) Overlay of (B) and (D) showing the relative localisation of nanoparticles and lysosomes. Scale bar 10 µm.

Cells incubated with polymer coated IONPs of size (80 nm) revealed appearance of some yellow regions in the merged image 4-12 which indicate the co-localization of nanoparticles with lysosomes to some extent with some fraction of green fluorescence from LysoTacker and red fraction from nanoparticles of size 80 nm (Figure 4-12).

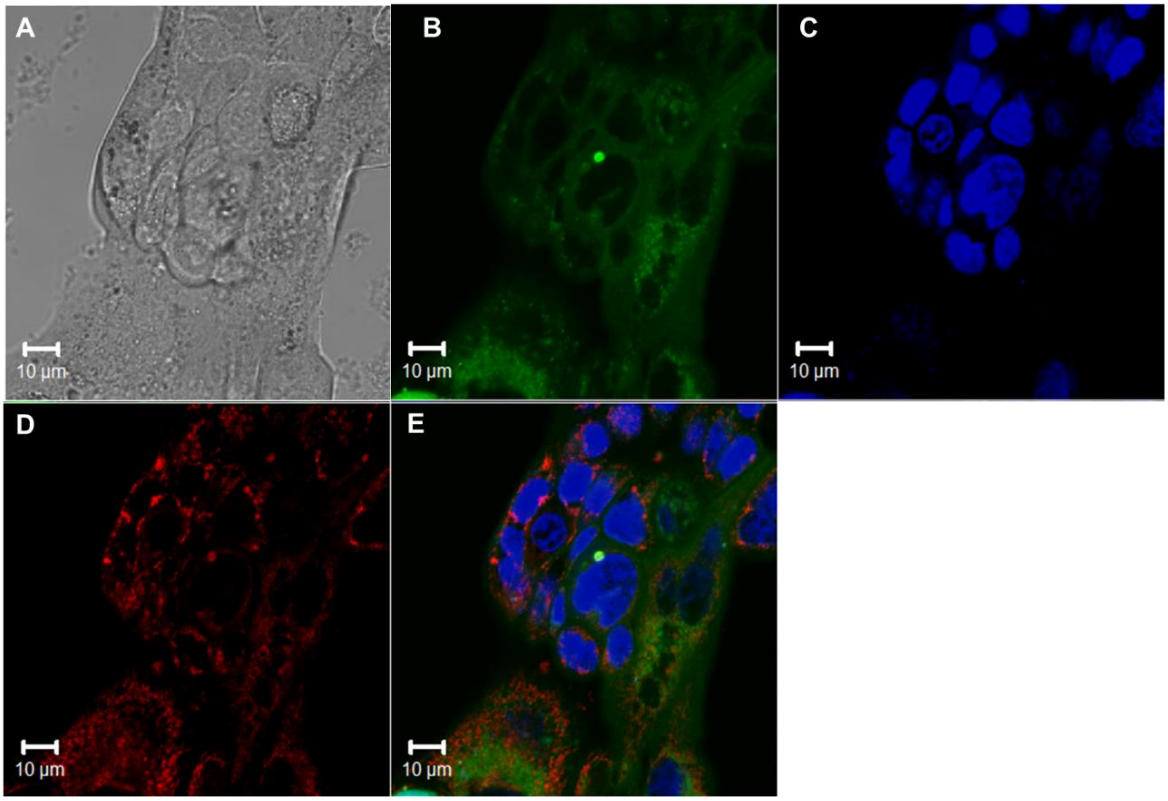


Figure 4-12: Confocal microscopy images demonstrating the intracellular distribution of 80 nm RBITC labelled polymer coated IONPs (50 µg) incubated with Calu-3 cells for 2hours. (A) Bright field showing the outline of the cells. (B) Cells stained with LysoTracker Green (C) Draq 5 (nuclear stain), (D) Uptake of red fluorescent labelled polymer coated IONPs (E) Overlay of (B) and (D) showing the relative localisation of nanoparticles and lysosomes. Scale bar 10 µm.

4.3.6.3 Time Dependent Intracellular Localisation of Polymer Coated IONPs Using Transmission Electron Microscopy (TEM)

TEM analysis of Calu-3 cells grown on transwells showed polarized cell layer with cilia, demonstrating the ability of Calu-3 cells to form functional epithelial layers under in vitro conditions. To find out the relationship between the size of particles and internalisation pathway, Calu-3 cells were incubated with polymer coated IONPs (50 µg/ml) for varying times (10 minutes, 2 and 4 hours) and various stages of intracellular translocation was documented using TEM. Due to the high electron density of IONPs, their clear identification was possible.

It was obvious that the smallest nanoparticle sizes (22 nm) were present even after 10 minutes of incubation with Calu-3 cells throughout the cells, in the cytoplasm, mitochondria and around the nuclear envelope with no surface binding to plasma membrane (Figure 4-13A). A similar nanoparticle (22 nm) distribution and intensity were seen at all the time points (Figure 4-13B and C). In addition, numerous particles were detected near the endoplasmic reticulum, the nuclear membrane and adsorbed inside the nucleolus. Furthermore, there was no evidence that the particles were clustered in endosomes as most of the particles were seen as individual particles. No obvious dense particles were detected in the control image as seen in Figure 4-13D.

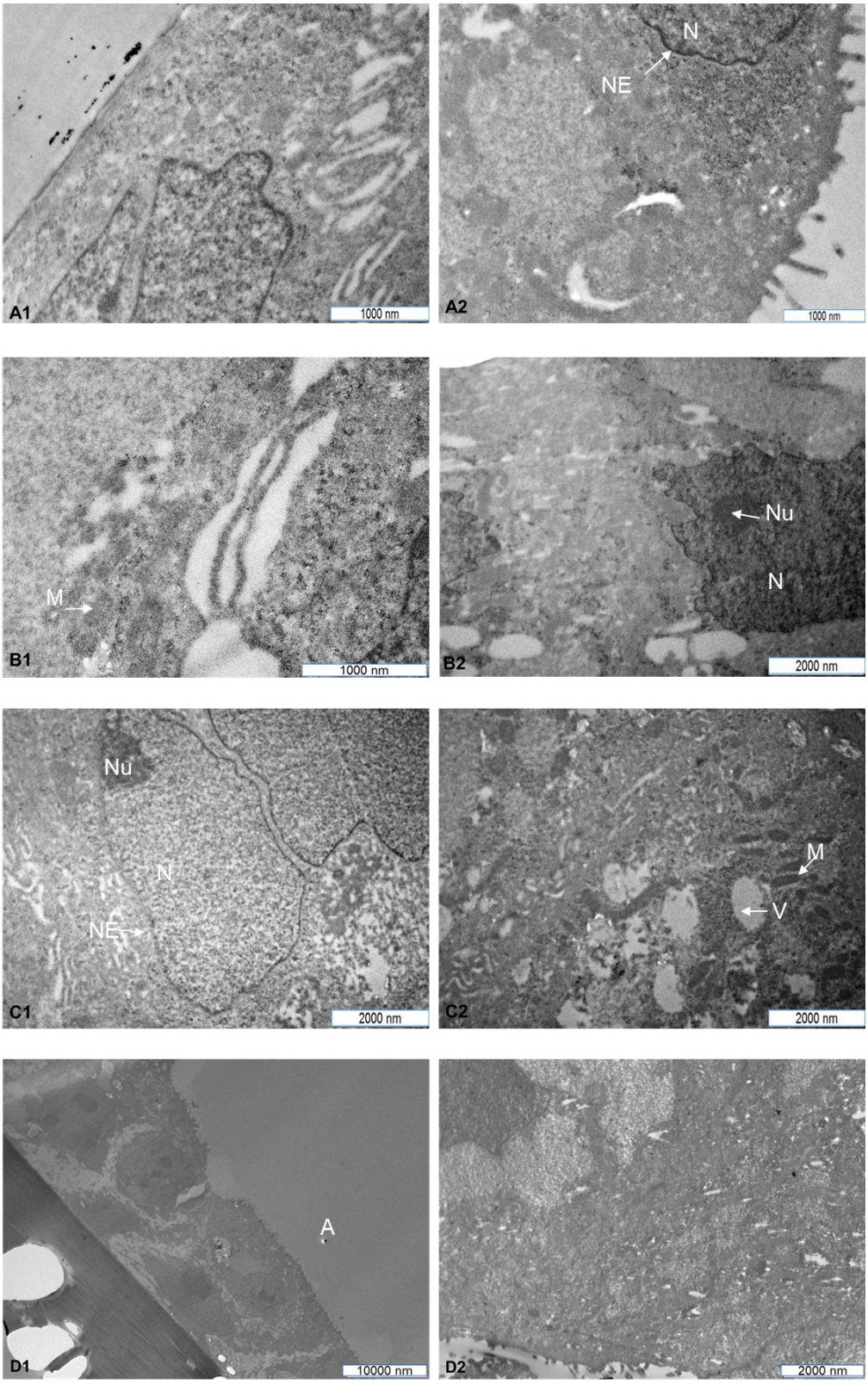


Figure 4-13: TEM image of Calu-3 cells grown on transwells incubated with polymer coated IONPs of size 22 nm (50 µg/ml) for different time where (A1 &2) 10 minutes, (B1&2) 2 hours, (C1&2) 4 hours and (D1&2) untreated cell control. Images shows nucleus (N), nuclear envelope (NE), nucleolus (Nu), mitochondria (M), vesicles (V) and apical side (A).

Polymer coated IONPs (50 nm) were seen in the cell membranes after 10 minutes of incubation with Calu-3 (Figure 4-14A). After 2 hours of incubation, the uptake of these particles was very high inside the cells around the nuclei and in the mitochondria. The particles were taken up as individual particle or in small groups. After prolonged time of incubation (4 hours), polymer coated IONPs were more widespread inside the cells, in cytoplasm, however, some of these particles can be detected around the vesicular boundary with small numbers present inside vacuoles (Figure 4-14C).

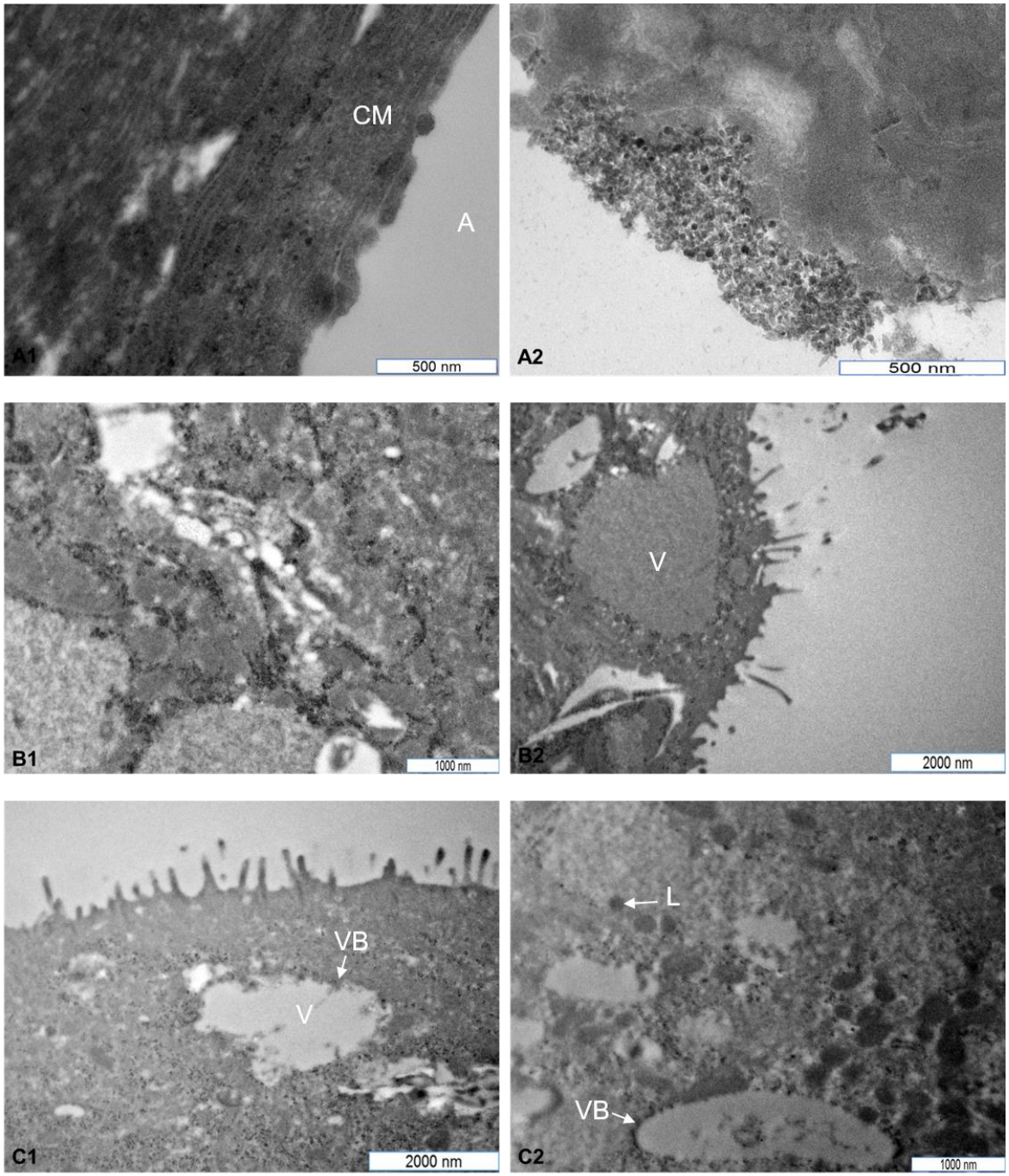


Figure 4-14: TEM image of Calu-3 cells grown on transwells incubated with polymer coated IONPs of size 50 nm (50 µg/ml) for different time where (A1 &2)) 10 minutes, (B1 &2) 2 hours and (C1 &2) 4 hours. Images shows cell membrane (CM), nucleus (N), vesicles (V), lipid (L) and vesicular boundary (VB).

Larger polymer coated IONPs size (80 nm) were found entrapped inside vesicles near the epithelial layer after 10 minutes of incubation (Figure 4-15A), however after 2 hours of incubation time, a notable increase in the number of cells with vacuolization was seen. The particles were seen inside the cells, in the cytoplasm, near membrane and some of nanoparticles in nuclei in very tiny groups (Figure 4-15B). In addition, the vacuole membrane seems to be densely covered with particles (80 nm). At a later incubation stage (4 hours), multi vesicular bodies containing polymer coated IONP (80 nm) clusters close to the plasma membrane were seen (Figure 4-15C), with a lower particle cellular uptake (80nm) at 4 hours.

Finally, from the TEM images it was obvious different polymer coated IONP sizes (22, 50 and 80 nm) showed mostly a high cellular uptake after an early time of incubation. Particle distributions were more widespread at later time both as individual particles and as groups of particles with no obvious collection of nanoparticles in endosomal compartments (22, 50 nm), however larger particles (80 nm) were seen as dense collections in vacuoles.

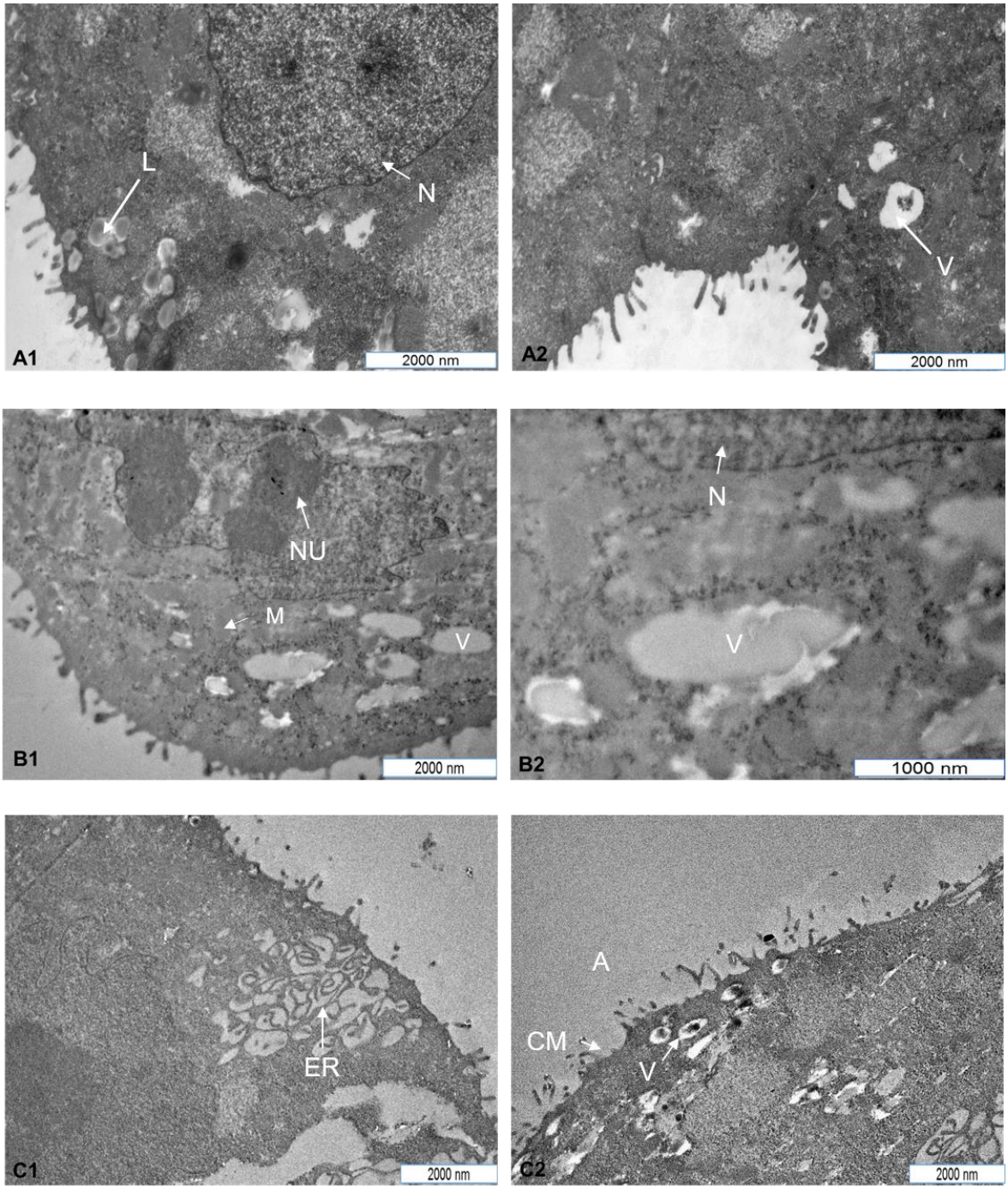


Figure 4-15: TEM image of Calu-3 cells grown on transwells incubated with polymer coated IONPs of size 80 nm (50 µg/ml) for different time where (A1 &2) 10 minutes, (B1 &2) 2 hours and (C1 &2) 4 hours. Images shows nucleus (N), nuclear envelope (NE), nucleolus (Nu), mitochondria (M), vesicles (V), cell membrane (CM), apical side (A) and endoplasmic reticulum (ER).

4.3.7 In Vitro Assessment of Polymer Coated IONPs Permeability across Calu-3 Epithelial Line

In order to assess differences in particle size of coated IONPs, the particle transport was analysed based on quantification of IONPS that were transported through the airway epithelial monolayer. Apical to basolateral movement of polymer coated IONPs was conducted using an epithelial cell monolayer model of Calu-3 cells grown on Transwell® inserts using air interfaced culture (AIC) and seeding density 2 x 10^5 cells/cm^2. The changes of the tight junction were monitored by measuring the TEER values. If the tight junctions open in the presence of nanoparticles, this will reduce the TEER values. High TEER value > 800 Ω.cm^2 was obtained around 21 days in culture with cell confluence of 100 %. Another study showed that the movement of nanoparticles through the paracellular route is considerably restricted and the permeability of nanoparticles predominantly occurred by transcellularly route compared to small molecules which could cross the membrane either paracellularly or transcellularly [250]. This indicate the effectiveness of epithelial tight junctions in limiting passive permeation. The experiment was designed to compare the cumulative amount of polymer coated IONPs of varied sizes crossing the Calu-3 cell layers as a function of time. Apical to basolateral movement of polymer coated IONPs (50 µg) of various sized 22, 50 and 80 nm for 3 hours is depicted in Figure 4-16. The data shows a higher rate of nanoparticle accumulation at the basolateral site for 22 nm nanoparticles compared to those for particles of size 50 and 80 nm. Interestingly, the rate of transport of 22 nm polymer coated nanoparticles was highest during the first 60 minutes experimental period while, from

the 90 to180 minutes time points the rate of accumulation was slower but constant over this second time period. However, the rate of accumulation of the 50 and 80 nm NPs did not change significantly at any of the assay time points (Figure 4-16A), and the amount of iron detected in the medium was similar to that of the control samples where no NP were applied. This means that the polymer coated IONPs did not pass through the cells of the Calu-3 model. NPs of size 22 nm accumulated in basolateral side of cell layer quite efficiently. After exposure of Calu-3 cells to 50 µg nanoparticles, TEER values were measured to assess change in resistance compared to initial reading, which showed no significant effect suggesting that the epithelium layer remained intact.

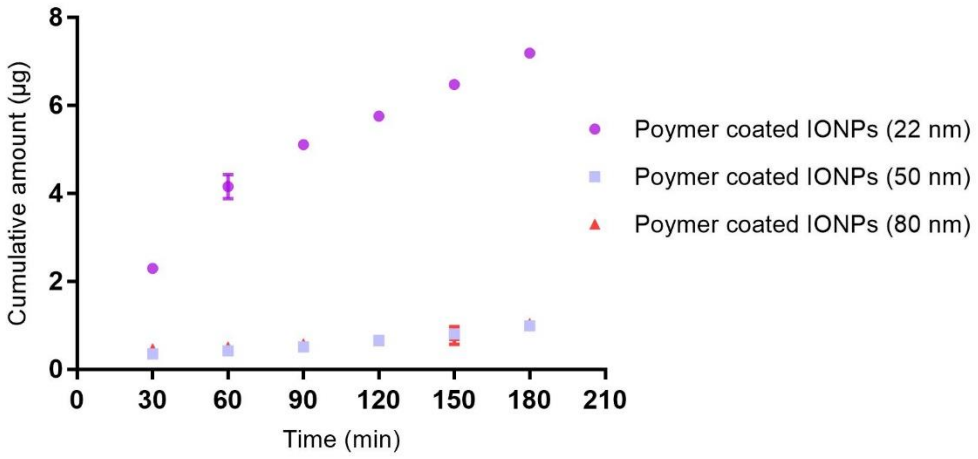


Figure 4-16: Cumulative amount for three sizes of polymer coated IONPs (22, 50 and 80 nm) that cross epithelial cell models of Calu-3 cultured on 12 well Transwell® inserts. The amount of NPs were tested at 50 µg in all groups in 3 hours cultures. NP cumulative amount was measured by applying the samples on the apical chamber and sampling the basolateral solution every 30 minutes for 3 hours and quantification of samples by ferrozine assay (through calibration curves) in all cases. Data are means ±SD of three different cell monolayer. One-way analysis of variance (ANOVA) was used for statistical analysis (A Sidak's multiple comparison test). **** indicates significant differences in the accumulation amount with ($p < 0.0001$) of NPs of size 22 nm with those of the 50 or 80 nm.

4.4 Discussion

Fluorescently labelling polymer coated IONPs with a size 22, 50 and 80 nm, and a range of charges between -31mV and -38 mV were characterised revealing that they continue to be one population with insignificant change in the size and surrounding charge, which indicated the stability of these nanoparticles.

4.4.1 Cytotoxicity of Polymer Coated IONPs

According to many studies, IONPs show low or no toxicity to cells, since they can be degraded and utilized by cells via physical iron metabolism pathway [60]. However, other groups have reported that Exposure to IONPs has been associated with significant toxic effects due to the generation of ROS or high Fe load, which lead to cell death [251-254]. The toxicity of IONPs is affected by many factors including size, charge, dose and agglomeration state of IONPs [255]. In vitro studies have been conducted to assess whether size or dose of polymer coated IONP resulted in cytotoxicity in Calu-3 cell line. MTT assay showed that cell viability was not significantly affected by the presence of polymer coated IONPs in size range 22 to 80 nm at 24 hours, however particles of size 22 nm showed 25 % decrease in the number of viable cells at concentration (200 µg/ml), which suggested the cells loaded with high Fe resulted in cell death (Figure 4-2). Trypan blue assay (Figure 4-3) confirmed the biocompatibility of these NPs for concentration up to (100 µg/ml). In summary, the results presented here indicate that polymer coated IONPs are safe and efficient nanoparticles in low concentrations for possible biomedical application. The cytotoxicity studies is a crucial

fact, that required to confirm the absence of toxicity induced by functionalized NPs even after accumulation in tumour cells to allow a high level of intracellular accumulation. The cytotoxicity studies show that at the doses used for cellular uptake studies in the present work, no adverse effects on physiological cell function would be expected.

4.4.2 Polymer Coated IONPs Uptake in Cultured Cells

The behaviour of NPs in biological solution such as cell culture medium or body fluid can affect cellular interaction and their responses [256-258]. Cellular uptake of nanoparticles depend mainly on whether the particles remain dispersed in suspension or become aggregated as the stability of nanoparticles is a key issue to achieve an efficient and controllable cell labelling. In addition, the properties of the surface layer of nanoparticles is important to avoid unwanted changes that result from dynamic adsorption of the proteins and macromolecules presented in biological medium. For this reason, PEGylated PGA 40%C_{18} layer was added to stabilise the IONPs and prevent their aggregation, as outer PEG layer resist protein adsorption by providing hydrophilic surface that play a powerful tool to enhance the dispersion state of IONPs under harsh conditions.

Generally, the normal pathway of drug absorption is by partition and diffusion, however nanoparticles and macromolecules are usually taken up into cells through various endocytic processes, which can determine their intracellular localisation. Once those particles attach on the plasma membrane, the lipid bilayer of cell membrane invaginates forming free

cytoplasmic vesicles around the particles, then these vesicles are accumulated in endo-lysosomal compartments. The cellular uptake study of different polymer coated IONPs sizes is very important in order to assess the efficiency of the nanoparticle uptake, the effect of time and dose on the accumulation, in addition to address the biological mechanisms involved in the process of nanoparticle translocation across the Calu-3 epithelial layers.

The physicochemical characteristics of nanoparticles are likely to play a very important role in their uptake and their wide distribution within the cells. NP size may affect the uptake efficiency, kinetics, the internalisation mechanism and subcellular localisation. For example, van der Waals between a particle and plasma membrane is proportional to the diameter of the particles, so nanoparticles with a small particle size exhibited lower Van der Waals adhesion forces and less accumulation at plasma membrane [31, 259].

Nanoparticle size and cell type are important parameters in determining internalisation of nanoparticles into cells [260, 261]. A previous study found polyvinylamine-coated IONPs and oleic acid coated IONPs were not transported across an endothelial cell culture model of the BBB [262]. However, another study reported a size dependent cellular response to polyethylene glycol gold nanoparticles using a rat brain microvessel endothelial cell culture model [263]. Hökstra et al. [260] used fluorescent latex beads of size ranges (50-1000 nm) to consider the effect of NP size on the uptake pathway by phagocytic B16 cells. They found NPs <200

nm were observed to involve clathrin-coated pits, however Caveolae mediated endocytosis having a size generally reported in the lower end of the 50–80 nm range [144, 264]. Another study showed that polystyrene (Ps) particles in ranges of about 250 nm to 3 μm have an optimal in vitro phagocytosis rate, and the uptake by phagocytosis increasing with the particle size, whereas nanoparticles smaller than 250 nm were less efficiently taken up by this route [265]. The present study exhibited a strong correlation between polymer coated IONPs and the level of accumulation into cells with a notably different behaviour in term of their cellular internalisation rates and transport across the epithelial Calu-3 cell monolayers.

It was important to find a simple, accurate and low cost method for determination IONP iron content. Ferrozine based assay was acknowledged as the most reliable method for iron quantification [266-268]. This assay is based on reduction of Fe^{3+} and formation of a coloured complex of Fe^{2+} that exhibit characteristic UV-Vis absorption at 562 nm. Quantification of uptake is an important aspect of understanding the amount of material taken up by cells, and this information is not so easily determined by microscopy. In microscopy based methods, it is only the label which is followed not the particles. By using a measurement of the iron we have a direct method for measuring the accumulated amount of particles, and this can be related to nanoparticle number by calculation. Using a particular weight of nanoparticles the number of nanoparticles is calculated from the volume of the particles multiplied by their density.

This method showed clearly that the kinetics of the accumulation as well as the saturation concentration varied with the different sized nanoparticles (22, 50 and 80 nm). As shown by ferrozine assay (Figure 4-4), 50 and 80 nm and the accumulation of 22 nm polymer coated IONPs in the cells reached a maximum by 25µg per well. Accumulation of 50nm IONP reached a similar maximum accumulation, but at 50µg per well whereas for 80 nm IONP accumulation reached a similar level to 22nm and 50 nm particles at 50µg per well but continued to increase even up to the maximum dose tested at 75 µg per well. So calculating the number of nanoparticles accumulated at 50 µg per well, this would be highest for 22 nm IONP and lowest for 80 nm IONP in inverse relationship to the IONP volume. From Figure 4-5, where 1 µg iron per well was accumulated in Calu-3 cells at 4 hours, the number of 22nm IONP per cell estimated to be present was about 1million. As the rates of the cellular accumulation were different, this may suggest different mechanisms by which the nanoparticles are accumulated inside the cells, although this will need further investigation.

More detailed information of the intracellular accumulation after different incubation time under the same previous condition was investigated. Results showed that the cellular accumulation of IONP was also dependent on the incubation time. The accumulation of the large NPs (80 nm) were higher than 22 and 50 nm for the first two hours, however, at 4 hours of incubation, the amount of 80 nm NP in cells decreased, which could be due to exocytosis, whereas, NPs of size 22 nm continued to be accumulated in Calu-3 cells up to 24 hours. Accumulation of NPs

with size 50 nm had no significant increase inside the cells beyond 2 hours incubation period (Figure 4-5). The differences in the amount of accumulated of polymer coated IONPs could be due to different of particle diameters. These results suggest that IONPs of small size persisted inside the cells 24 hours post incubation. Results obtained from analysing the culture medium (EMEM) using ferrozine assay after incubating different particle sizes with Calu-3 cells for 2 and 4 hours (Figure 4-6) showed an extremely significant decrease in the extracellular amount of size 22 nm NP within 4 hours of incubation compared with those of 50 and 80 nm which support the higher cellular accumulation of size 22 nm NP. An increase in the amount of nanoparticles (50 and 80 nm) in the medium after prolonging the incubation time to four hours suggests particles accumulate in the cells and then some are subsequently released back into the medium. These results are supported by the steady decrease of amount of nanoparticles of size 50 and 80 nm with the cells. The reason of these different results could indicate different internalisation mechanisms for the different particle sizes, although this will need further investigation.

To accurately show the intracellular localisation of uptake, confocal microscopy was used. Confocal microscopy permits to localize NPs, while ferrozine assay gives statistical quantification iron content of the treated cells. The results indicated that the red fluorescence intensity from the nanoparticles was within the cells not on the cell surface. This would otherwise have clearly been observed by a strong red line bordering the cells, but this feature was absent. After 2 hours of Calu-3

cells incubation with different concentrations RBITC-labelled polymer coated IONPs, the red fluorescence intensity was high particularly at high concentrations, which indicated the NPs have been taken up by the cells. It was clearly shown that the nanoparticles of size 22 nm were internalised into the cells to a much higher extent than those of 50 and 80 nm. This was in agreement with the results obtained using the ferrozine assay which showed the high interaction of the smallest particles with the cells. Within 4 hours of incubation, the fluorescence signals with 50 and 80 nm particles decreased, however there was an increase in fluorescence intensity of particle size (22 nm). The decreases of the fluorescent intensity signal could due to the dye degradation or some of big nanoparticles released out of the cells into the medium as showed previously by ferrozine assay (Figure 4-6).

Although it was difficult to observe the individual nanoparticles throughout the cells by the confocal microscope resolution, but distribution pattern of nanoparticle with size 50 and 80 nm appeared as a very fine granular distribution rather than the punctate distribution normally seen on uptake of nanoparticles into cells. Nanoparticles of 22 nm were smoothly distributed throughout the cells with some appearance of fluorescent in nucleus, which was observed by our groups in previous studies and it may indicate nanoparticle location throughout the cytoplasm and subcellular organelles. Serial z-sections of the cells (Figure 4-9) showed that the majority of the cells had different level of fluorescent intensity which could indicate the internalisation of the nanoparticles inside the cells. More importantly, estimates of the amount

of iron associated with the cells with the ferrozine-based assay are consistent with those observed by the confocal microscopy. Using these two different methods of determination of uptake (ferrozine and confocal analysis) led to obtain important information about IONPs uptake.

The more granular distribution patterns observed in places with the 50 and 80nm particles have previously been observed by studies by other groups and it suggests that some of the nanoparticles may be present within endosomes or lysosomes compartment [269, 270]. In the present work, the majority of nanoparticles were in the cytoplasm and the pattern of distribution was different which may suggest that, the mechanism of cellular uptake to these particles size 22nm, 50 nm or 80 nm are different. However, the intracellular localisation was still unclear as the confocal microscopy confirmed that nanoparticles were definitely taken up into the cells.

To get insight whether polymer coated IONPs were localized in endosomal/lysosomal or in other cell compartments, Calu-3 monolayer cells were incubated with NPs of all sizes (22, 50 and 80 nm) for 2 hours under the same condition of the previous experiment in the presence of LysoTracker green. Using LysoTracker® green, a pH sensitive dye that emits green fluorescence in acidic pH make it possible to determine the presence of nanoparticles in the acidic endo-lysosomal vesicles. The presence of red fluorescent nanoparticles in green fluorescent lysosomes shows up as yellow fluorescence in the overlay. The studies on smaller NPs (22 nm), showed very bright red fluorescent spots

throughout the cells was observed in the overlay image (Figure 4-10) which indicated NPs of size 22 nm were mainly not located in lysosomal compartments. However, NPs of size 50 nm and 80 nm demonstrated that a substantial fraction of green fluorescence from LysoTracker was also not colocalized with internalized NPs. Similarly there was also a large fraction of red fluorescence from NPs, which were not colocalised with green fluorescence from lysostracker. There were however, a few yellow fluorescent dots particularly in the 50 nm and 80 nm particle experiments (Figure 4-11 and Figure 4-12). These observations strongly suggested that at least not all polymer coated IONPs accumulated in endosomal/lysosomal compartments and that there were some endosomes/lysosomes, which did not contain any IONPs. There were differences in the cell confluences of the experimental Calu-3 cells between nanoparticle formulations. Fig 4-10 showed few cells with free spaces, but Fig 4-11 and Fig 4-12 are confluent monolayers (in contact with each other). However, fluorescence micrographs show a similar subcellular distribution of IONP in both non-confluent Calu-3 monolayers and polarized cells (data in appendix Figure III, IV and V). The data show clearly that not all the NPs were co-localised with lysosomal marker which suggest that 22nm IONP do not follow the endosomal-lysosomal pathway inside cells, but that there is some evidence that this occurs for the 50nm and 80nm IONP.

In order to determine whether IONPs uptake was dependent on the nanoparticle size, TEM was used. The TEM study supported the previous fluorescence and confocal microscopy results and the interesting

observation that the subcellular distribution of large amount of polymer coated IONPs throughout the cells even in the nucleus. Cellular uptake of iron oxide NPs has been readily identified for other cell types that have been prepared for TEM in a similar manner [271]. Since IONPs are a dense black metal they can be easily identified within the cellular compartments in the presence of stains which appear as light spots. The possibility of contamination as an artefact seems unlikely for a number of reasons. The cells were washed to remove external loosely bound IONP which may be present in the medium or on the external membrane. The fluorescence microscopy, suggests that the amount of surface bound material was not visually obvious, but that there was a massive number of IONP taken up by the cells, which has been calculated for 22nm nanoparticles to be about 1million IONP per cell. The overall widespread distribution of the nanoparticles within the cell, also suggests that this is the real picture of distribution consistent with the number of expected IONP from the ferrozine assay rather than a small number of particles introduced from the processing and cutting procedures. From the TEM as illustrated in Figure 4-13, after 10 minutes of incubation small IONPs (22 nm) with calu-3 cells, the particles were observed everywhere inside the cells even in the nucleus and more importantly no obvious binding of the nanoparticles at the outer surface of the plasma membrane. It is very likely because the increased internalisation of the smallest nanoparticles after short time of incubation (10 minutes), which could not only due to the decreased cellular energy required to internalise smaller particles as proposed in previous study [272], but also because the ability of small

particles to enter the cells via passive diffusion and endocytic pathways, however large nanoparticles enter largely via endocytosis alone. The TEM results here for nanoparticles of size 22 nm suggest that a non-endocytic route is likely to be in operation, but further investigations would need to be carried out to confirm this and exclude the possibility of some contribution by other routes.

These observations were confirmed also by confocal microscopy images (Figure 4-7C, D and E) showing that nanoparticles of the smallest size were distributed smoothly throughout the cells rather than in the punctate perinuclear intracellular distribution which is the hallmark of endocytic uptake. Internalisation of nanoparticles by a non-endocytic pathway has already been proposed and in other studies, nanoparticles have been observed in red blood cells (RBC) which do not carry out active endocytic uptake [122, 123]. This passive diffusion by RBC has been shown to include adsorption of nanoparticles on the cell surface that result in internalisation of nanoparticles [273]. In contrast to the clear picture showed by the 22nm IONP, polymer coated IONPs (50 nm) showed numerous nanoparticles distributed throughout the cytoplasm with a lesser extent in vesicles (Figure 4-14) suggesting these particles entered by both passive and active transport. However, larger particles (80 nm) showed accumulation of particles around the vesicular membrane with few particles distributed inside the cells (Figure 4-15) suggesting most of the particles of size 80 nm enter cells via an endocytic pathway. The TEM results is 2 D analysis, showed the absence of nanoparticles (22 nm) inside the vesicles along the endosomal network which could indicate a

non-endocytic pathway is in operation. In spite of this, it might be possible to perform further work using 3 D reconstruction electron tomography which then build a tilt series and give detailed of what was included in the depth of the cell compartments. Further investigation were carried out by confocal microscopy using lysosomal marker to observe the localization of the nanoparticles after 2 hours of incubation with the same NP exposure to the same conditions in this study. It was clearly showed no co-localisation of NPs (22 nm) with lysosomal marker which suggesting that transport of nanoparticles does not terminate inside the lysosomal compartment inside cells. It has been demonstrated caveolae dependent endocytosis could bypass lysosomes. The subcellular distribution of nanoparticles taken up by the caveolae typically show a punctate distribution throughout the cytoplasm due to the vesicular sub-cellular localisation [274, 275]. However in the present study, the widespread distribution of particles (22 nm) throughout the cells in TEM and confocal images rather than inside vesicles suggest these particles are not taken up by this route. For the larger particles, there was some association between the particles and the lysotracker which increased from the 50-80nm IONP (Figure 4-11 and Figure 4-12). The results suggest that particle size was a confounding factor in this study but is a similar conclusion to that of Thorley et al. [276] which show a size dependence for their studies indicating some non-endocytic uptake for polystyrene nanoparticles.

These qualitative results were also supported with quantification of intracellular iron content using ferrozine based assay (Figure 4-5), which

showed that the rate of accumulation of the smallest NPs (22 nm) was higher than nanoparticles of size 50 and 80 nm increased gradually with time and reached a maximum accumulation point at 24 hours of incubation. However, the amount of NPs of size 50 nm remained substantially unaltered inside the cells. Cellular content of IONPs (80 nm) beyond 2 hours incubation period was low with no noticeable change in cellular content of particle of size 50 nm after 2 hours. It was more likely because smaller nanoparticles enter the cell via passive diffusion and endocytic pathways whereas larger nanoparticles enter largely via endocytosis alone. The diffusion of the smaller NPs through the cell membrane depend on the surface properties of the particles. If the nanoparticles have inappropriate properties they would be unable to translocate and diffuse across lipid membranes. If particles enter invaginations and become endocytosed into cells, they will be retained in the vesicles if they are unable to translocate across the vesicles. However, if the particles can translocate across the membranes, they will escape to all parts of the cell. The rate of this membrane translocation process may depend on particle size.

Many studies reported that the IONPs taken up by endocytic mechanism are finally localized in intracellular vesicles. The distribution of the nanoparticles inside the cells could indicate the mechanism of entry. The cellular uptake pathway of NPs will have direct consequences on their final localisation. Usually distribution of NPs in specific compartment such as the lysosome/endosomes in which the nanoparticles appeared highly bright spots in perinuclear area of cells may provide some

suggestions for developing a future nanoparticle targeting [45, 277]. However, in this study some points of bright fluorescence were observed under confocal microscopy and different distribution patterns were seen for polymer coated IONPs of size 22 nm as the fluorescence was evenly distributed across the whole cell with no obvious bright spots were observed. This distribution pattern has not previously been observed in other studies and it suggests that NPs were dispersed throughout the cytoplasm and were not present within the intracellular compartments such as endosomes and lysosomes.

NP size can influence the subcellular distribution of the internalised particles. A study done by Lovrić et al. [283] established that CdTe QDs of size 5.2 were distributed throughout the cytoplasm of N9 cells but were not observed in the nucleus, while QDs of size 2.2 nm were localised mainly in the nuclear compartment. However, another study found that the different sizes of silica-coated QDs of size (8 and 16 nm) did not influence the intracellular distribution [284]. Another study reported that large size (170 nm) PGA polymer nanoparticles were taken up with a high extent into DAOY cell which showed a perinuclear distribution in the cells typical of lysosomal accumulation of particles [281].

Surface charge of nanoparticles has an effect on the uptake and transport pathway. Nanoparticles with positive surface charges are internalised into cells more efficiently than the nanoparticles with negative surface charges due to their electrostatic attraction to negatively

charged cellular membrane [37]. However, other studies showed an increase in the amount of nanoparticles uptake by cells when incubated with negatively charged particles, confirmed that, the particle with highly negative surface charge can enter the cells through nonspecific nanoparticle-cell interactions [285, 286].

Petri-Fink et al. (2008), investigated the effect of type of coating materials on the stability of IONPs in biological environment. They found that polyvinyl alcohol and a mixture of polyvinyl alcohol and vinyl alcohol/vinyl amine copolymer (PVA-SPION and A-PVA SPION) in cell culture medium and in presence of serum led to inhibition of the uptake of A-PVA-SPIONs into HeLa cells (cervical cancer cells) due to the adsorption of serum protein on the nanoparticle surface. However PVA-SPIONs were highly taken up by cells due to the very low serum adsorption which was attributed to the surface properties [89]. A study by Yamazaki et al. [287] found that the strong interaction between the PEGylated functionalized surface and the epithelial cell membrane was due to the capability of PEG to dissolve in both polar and non-polar solvents leading to higher diffusion in epithelial cell layer. The type of coating materials used in this study could indeed be directed towards a high cellular uptake.

On the size side, particles of hydrodynamic diameter of less than 100 nm are preferred over other sizes for cellular uptake by endocytic pathways [37]. The results here correlates with many studies in the literature that show the cellular uptake of small particle sizes is higher

than big particle sizes [288]. However, another study showed the opposite uptake behaviour indicating there may be a limit beyond it the size no longer plays an influencing key role in the extent of the uptake [289].

In the present work, polymer coated IONPs of different sizes showed different level of uptake and distribution. NPs were observed as single particles rather than in groups in all subcellular compartments, nucleus, cytoplasm, mitochondria and some of these particles were observed around vesicular membranes and inside the vesicles. This clearly demonstrated polymer coated IONPs seem to be taken up into the cells by different pathway according to their size. The uptake rate of NPs (22 nm) was very high even after 10 minutes of incubation with calu-3 cells (Figure 4-13 A1 and A2), which resulted in reduction of the association between the particles and the plasma membranes. Thus, the likelihood of the particles encapsulation on the cell membrane would be decreased. This could suggest that the uptake mechanism of polymer coated IONP particle of the smallest size is partly by non-endocytic mechanism, however some NPs of sizes 50 and 80 nm seemed to be incorporated via endocytosis, as indicated by the observation of particles in vesicles and around the membranes. A study by Thorley et al. [276] showed that small positively charged polystyrene nanoparticle are partly taken up into alveolar epithelial layer by non-endocytic mechanisms and found in the cytoplasm, however large particles enter the cells via endocytic pathway and found in endosomes. The hypothesised from this result that

this is more prominent for smaller than larger nanoparticles which support the finding of this study. .

The mechanism of the uptake determines the intracellular localisation of particles. These IONPs possibly interact with an area of the epithelial layer via Clathrin or caveloae mediated endocytosis and increase likelihood of their encapsulation to form intracellular vesicles ending up trapped in endosomal/lysosomal compartments via clathrin uptake pathway or could escape into endoplasmic reticulum through caveolae route [21, 131, 290]. Alternatively, as suggested in a literature report, that carboxymethyl-substituted dextran coated iron oxide nanoparticles may also enter the cells with nonspecific interaction between the particles and the cells [21]. Zhang et al. [291] described the uptake of IONPs by vesicular route after incubation at different time of incubation (30 min, 2 and 4 hours) and they did not behave as single particles, but were clustered into aggregates in the endosomal membrane and/or homogeneously dispersed in the endosome. Many studies found cellular internalisation of SPION was an active energy dependent transport [71, 292, 293]. Calero et al. [220] have reported that the incubation of dimercaptosuccinic acid SPION with a human breast adenocarcinoma for 24 hours, resulting in two different endocytic pathway depending on the size of particle aggregate as smaller size was internalised into cells using a clathrin dependent pathway, however larger aggregates were incorporated by micropinocytosis. In summary, it is rather difficult to compare our results with those reported in literatures previously, because NPs used in other studies have very different characteristics,

however it is well known that parameter such as NP size is crucial on nanoparticles cellular uptake.

4.4.3 Transcytosis of Polymer Coated IONPs

One of the important function of bronchial epithelium and supporting elements such as the epithelial layer is act as a physical barrier between the external and interior environment of the human body. In the present study, Calu-3 cells were cultured using AIC to produce a cell layer with good similarity to the airway epithelial morphology. This layer was used to quantify the translocation particles across the epithelial monolayer. In order to rule out paracellular transport, TEER was monitored during the experiment. Confluent monolayer of Calu-3 cells exhibited a TEER value > 800 $\Omega.cm^2$ which did not change after the experiment. This strategy of permeability through tight junction is limited to relatively small biomolecules such as small proteins or peptide, however transport of nanoparticles through this approach is shown to be negligible, since the paracellular spaces, sealed by tight junctions and pore diameter of these junctions was reported to be < 10 A° [250, 294]. Different relative cumulative amount transported in Calu-3 monolayers have been shown for different IONP sizes in this study (Figure 4-16). Measurements of cumulative amount usually focus on kinetics resulting from carefully characterizing the amount of solute only on one side of the membrane barrier. The fraction of polymer coated IONPs of size (22 nm) were accumulated in basolateral side after 30 minutes compared to those 50 or 80 nm where essentially no permeability through the cells was seen.

Nanoparticles of size 22 nm have a large capacity to enter and translocate through polarised Calu-3 cell layers.

Looking to the results of the ferrozine assay (Figure 4-5), it is clearly revealed the highest accumulation of polymer coated IONPs of size 22 nm gradually increase with time and reached a maximum accumulation point at the longest time period of 24 hours of incubation. In addition, the finding of microscopy study showed nanoparticles of small size (22 nm) were observed everywhere inside the cells not attached to the plasma membrane surface or encapsulated within the endocytic vesicles. TEM microscopy studies along with accumulation of polymer coated IONPs (22 nm) at the basolateral side support a transcellular process. The exact mechanisms of permeability of nanoparticles through the epithelial monolayer are still unknown, however as no IONPs have been imaged inside intracellular vesicles it seems unlikely that an endocytic mechanism could be involved in this translocation, however, this will need to be confirmed by other experiments. The characteristics of nanoparticles are more likely to play a very important rule in the uptake, particularly the size of nanoparticles. These findings, together with cellular uptake study suggest the small particle size of IONPs are more likely to favour the transcellular route by crossing cellular barrier depending in physicochemical properties of this size, and thus are more suitable for medical applications.

4.5 Conclusion:

Polymer coated IONPs were internalized differently depending on their size, Calu-3 cell uptake studies showed that the smaller particles size (22 nm) had a greater rate of uptake, however polymer coated IONPs of size 50 and 80 nm entered the cells to a more limited extent, with easier loss of IONP from the cells and with indications of some NP in endosomes. The subcellular localisation data imply that the nanoparticles were able to translocate across membranes however, this result needs to be confirmed by further physicochemical studies. Internalisation of nanoparticles were mostly observed throughout the cytoplasm surrounding the nucleus and some of them were found in the nucleus, especially in case of polymer coated IONPs of size 22 nm. The ferrozine assay used for IONP quantification showed cellular accumulation of polymer coated IONPs was dependent on the concentration and incubation time, which was in agreement with microscopy studies. The translocation mechanism explained the wide distribution of polymer coated IONPs observed in cells by TEM as there was no evidence of particle accumulation inside vesicles resulting from endocytic uptake pathways. TEM microscopy studies along with accumulation of polymer coated IONPs (22 nm) at the basolateral side is more likely that physicochemical mechanisms account for this but endocytic mechanisms may also play a role.

5 Polymer coated Iron oxide Nanoparticles as MRI contrast agents

5.1 Introduction

The tracking and monitoring of cells after delivery into the human body is very important for a comprehensive understanding of cellular proliferation and differentiation process. In addition, this may provide important information with respect to the therapeutic efficacy of the cells. Several imaging methodologies have been applied for this purpose including computed X-ray tomography (CT), ultrasound, bioluminescence imaging and magnetic resonance imaging (MRI). Among these, MRI has some definite advantages due to its high spatial resolution and rapid, multi-planar in vivo acquisition of images with no need for exposure to ionizing radiation [295, 296].

MRI images the hydrogen protons of water in the body or in a sample placed in a strong magnetic field. It does so by transmitting a pulse of electromagnetic radiation at a given frequency. This energy disturbs the resting equilibrium of the nuclei allowing a transition from a lower energy state to a higher one. Once the radiofrequency pulse transmission is switched off, the excited nucleus relaxes back to the equilibrium state, re-emitting energy in the form of electromagnetic radiation that can be detected with an aerial. When this process is carried out with additional, spatially varying magnetic field gradients then an MRI image of the object can be reconstructed. The process of re-emitting energy can be deconstructed in two distinct time constants termed T1 and T2. T1 is

known as the spin lattice relaxation or longitudinal relaxation time, and reflects the time constant of the dissipation of energy to the surrounding region (lattice). T2 is known as spin-spin relaxation or transverse relaxation time and depends, amongst other mechanisms, on the mobility of the protons and molecular exchanges. Tissues within the body have very different T1 and T2 values because of their different chemical constitutions and different physical states [297] which is where the richness of contrasts available in MRI comes from.

Specific compounds can affect dramatically the relaxation times and this ability has long been exploited to highlight specific tissues and/or abnormalities in the human body by changing artificially their contrast in the images. These are therefore called MRI contrast agents.

The MRI contrast agents are principally divided into two categories, T1 and T2 contrast agents, depending on the MRI time constant where they exert their desired relaxation effect. Most T1 contrast agents currently available are paramagnetic complexes, while those classed as T2 contrast agents are mostly superparamagnetic IONPs. IONPs are the most suitable materials as contrast agents for T2 weighted MRI for imaging of specific target tissues to enable the early detection of diseases and the cellular level with the engineered nanoparticles [298-300]. IONPs are characterized by their different behaviours and responses to an external applied magnetic field depending on their size [301]. Small particle sizes show an abrupt change in magnetic properties. For example, particles have superparamagnetic behaviour when their

size is between 3 and 50 nm [53, 302]. Superparamagnetic nanoparticles exhibit magnetic properties on application of an external magnetic field, and they no longer exhibit any residual magnetic interaction upon removal of magnetic field making them less likely to agglomerate due to their magnetic properties [210]. This superparamagnetism phenomenon is very important for their use for both diagnostic and therapeutic targeting. Additionally, small IONP in the range of size 10-100 nm have been shown to be optimal for avoiding rapid clearance from systemic circulation due to removal by the monoclear phagocytic systems (MPS) or by renal filtration, which lead to the accumulation of the contrast agents in the targeted area with sufficient amount for the imaging process [78]. These particles have been developed as contrast enhancement agents for MRI for the purpose of diagnosis, mostly of soft tissues, like cartilage pathologies and all other internal body structures. Contrast agents effectively alter the contrast provided by different tissues in specific MRI sequences and are therefore administered after non-contrast enhanced MRI scans are collected and prior to the planned contrast-enhanced MRI scanning. At the heart of this technique there is the ability of the contrast agents to alter the relaxation times of water protons in a given tissue environment which results in an increase in diagnostic sensitivity and specificity [303-305]. Such sensitivity is very important for detection of the diseases at early stages. Super paramagnetic IONPs allow researchers and clinicians to enhance the tissue contrast of an area of interest by increasing the relaxation rate of water.

Tracking of cells labelled with IONPs has emerged as a very effective method for the monitoring of cell based treatment strategies. IONPs are acting as contrast agents as they are widely used in tracking stem cells in both in vitro and in vivo. In addition, they are being used to detect an array of diseases. For example, in tuberculosis, IONPs are conjugated to anti-tuberculosis antibodies which bind to the bacteria through antibodies and the nanoparticles can be detected in an MRI scan and the affected area can be imaged [306]. In cancer diagnostics, IONPs are used as cell markers and they were used in studies of pancreatic cancer [307]. Labelling the cells with IONPs could be used for evaluation and development of stem cell based therapies for repair and regeneration of damaged or diseased tissue [308]. These applications require a high uptake efficiency of IONPs by the cells otherwise low tissue penetration may mostly limit this approach to preclinical analysis.

The important point in imaging is that tissues within the body have different T1 and T2 values because of their different chemical constitutions and different physical states. Thus nanoparticle properties have been engineered for magnetic or optical development in biomedicine due to their capability to track intracellular processes at a biomolecular level [309, 310]. The majority of research in this field concerns the effect of particle size, degree of aggregation and the chemical nature of the coating as well as the coating thickness on magnetic properties of IONPs [311-313]. The smallest particle sizes of up to 8–20 nm show a strong rise in magnetic properties at room temperature [82, 314].

It is known that changes in diameter and thickness can dramatically change the relaxivities, which in turn has an effect on the relaxivity of IONPs [315]. Indeed, it is desirable to make a thinner coating layer around each particle to keep the chemical properties of IONs and the coating materials constant [316-319]. Although, many studies showed the values of relaxivities increase linearly with increasing particle core size due to the higher magnetisation of larger particle core [320, 321], there is still a lack of knowledge about effects of hydrodynamic size of polymer coated IONPs on their relaxivities. The efficiency of relaxivities depend also on parameters such as the temperature, applied field and whether it was measured in aqueous solution or in vivo *[322, 323].* A range of relaxivity values have been reported for polymer coated IONPs. Some of the IONPs available commercially are shown in Table 5-1, which illustrates that these contrast agents can be markedly different, with considerable variability among T1 and T2 relaxivity values. This clearly shows that the transverse T2 relaxivity of IONPs is greater than their longitudinal relaxivity a desirable characteristic for their use as negative agents for T2. Several IONP formulations for either intravenous or oral administration have been approved for clinical use as MRI contrast agents by the U.S. Federal Drug Administration (FDA), however, most intravenous IONPs have, at present, been taken off the market due to their limited spectrum of applications[324]. Resovist is the only SPIO still being distributed for clinical liver imaging in Japan [325]. Therefore, extensive efforts have been made in the last decade in order to develop superparamagnetic IONPs that can be used for a wider spectrum of

imaging applications, which is also important for a rapid progress in the field of cell labelling.

Table 5-1: Some commercial MRI contrast agents **[78, 326]**

Brand name	Structure	T1 Relaxivity (L/mmol-s)	T2 Relaxivity (L/mmol-s)
Feridex (Endorem)	Dextran coated IONPs	23.9	98.3
Resovist®	Carboxydextran coated IONPs	25.4	151
Ferumoxsil®	Silicone coated IONPs	3.2	72
Feruglose NC100150	PEGylated-starch coated IONPs	20	35
Sinerem®(AMI-227)	Dextran coated IONPs	21.6	44

5.2 Aim

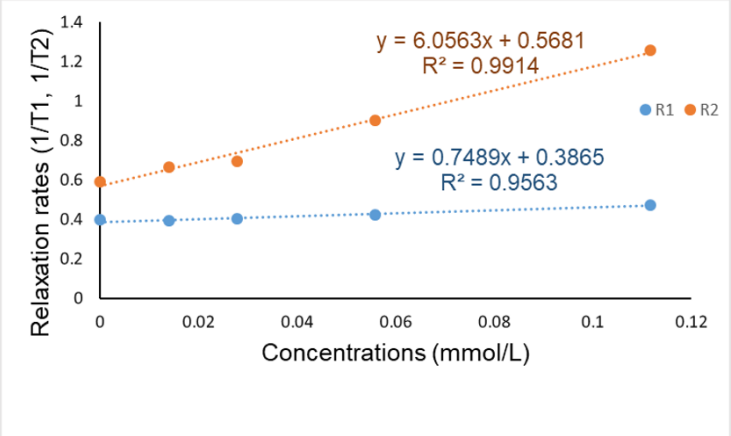
In this chapter, we will evaluate the effect of different PEGylated PGA 40%c_{18} sizes (22, 50 and 80 nm) on their relaxivities with a view to optimizing the design of magnetic nanoparticle probes for molecular imaging using MRI, also for the possible tracking of stem cells in vitro and in vivo.

5.3 Results

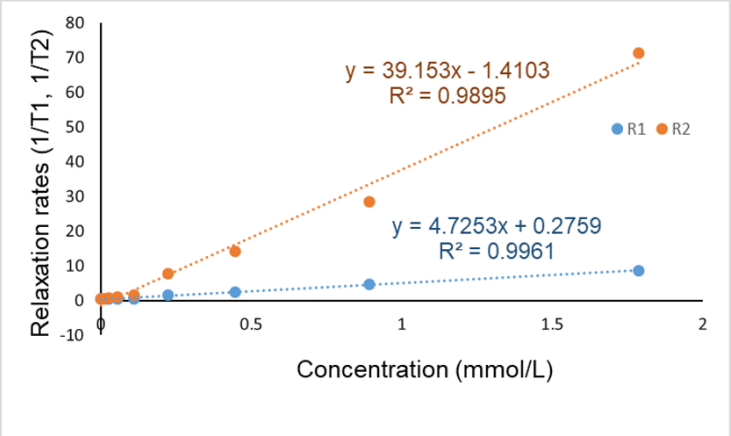
5.3.1 Size Dependent MRI Relaxivity

Relaxivity measurements of different size polymer coated IONPs were performed in order to assess the effect of the size and the coating thickness on the magnetic properties of IONPs. The trends of 1/T1 and 1/T2 of IONPs have been plotted as a function of the iron concentrations are represented in Figure 5-1. The slope of the linear fitting represents respectively the relaxivities r1 and r2. Looking at the plot of relaxation rate (r1 and r2) and concentrations of IONPs, a good fit was obtained as shown by the high R^2 values.

A



B



C

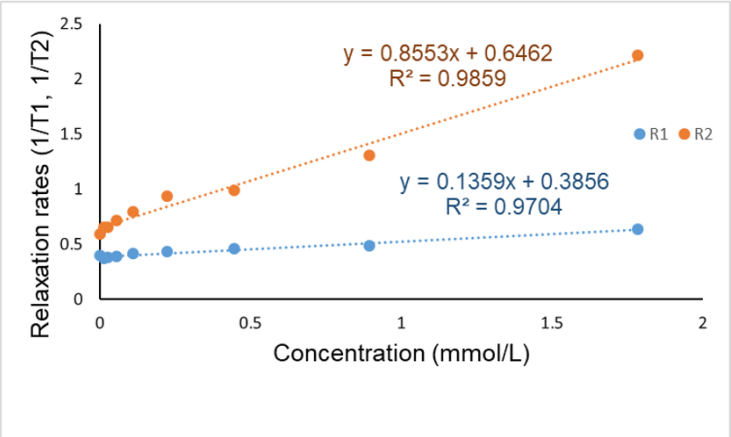


Figure 5-1: Plot of the proton relaxation rates (1/T1) and (1/T2) of water suspensions of polymer coated IONPs at various Iron concentrations versus the corresponding concentrations for samples A (22 nm), B (50 nm), and C (80 nm).

Table 5-2: r1 and r2 values of IONPs obtained at 1.5T

Polymer coated IONP sizes (nm)	r1[$mmol^{-1}sec^{-1}$]	r2 [$mmol^{-1}sec^{-1}$]
22	0.75	6.06
50	4.73	39.15
80	0.14	0.86

The longitudinal and transverse relaxivities (r1 and r2) were obtained by calculating the slope of the above graphs. Both 1/T1 and 1/T2 relaxation rates are linearly proportional to the iron concentration as shown in Figure 5-1. The results of these calculations are presented in Table 5-2. IONPs of size 50 nm give rise to higher molar relaxivity r2 than 22 and 80 nm. The r2 value is 39.15 mmol-1sec-1 for particle size 50 nm which is similar to the values reported for Feruglose NC100150 and Sinerem® (AMI-227) as showed in Table 5-1. A low r2 value was not expected for particle size 22 nm which may attributed to very low concentration of iron used compared to other formulations. The concentration could affect the MRI signal, but due to the unavailability of more sample of polymer coated IONPs of size 22 nm, it was not possible to investigate samples with a higher concentration of iron. Polymer coated IONPs of size 80 nm showed the lowest r2 value.

5.4 Discussion

IONPs have been recognized to hold a great potential in clinical diagnostic applications as the magnetic resonance (MR) imaging contrast agent that have the ability to change the proton relaxivity of water. T1 and T2 for different concentrations of each size group of polymer coated IONPs have been studied. The results of r1 and r2 (1/T1 and 1/T2, $mmol^{-1}s^{-1}$) as a function of polymer coated IONP sizes are shown in Figure 5-1. The changes of r1 and r2 could be due to either the particle size or the coating thickness or both. Ahmed et al. [320] considered the particle size dependence of the relaxivity of hydrogen protons in an aqueous suspension of silica coated IONPs and they found that the relaxivity r2 is much larger than r1 and it was increased linearly with increasing particle size. In their study, they showed that by increasing the size of IONPs with the magnitude of 17% the r1 and r2 increased with the magnitude of 13% and 22%, respectively. Here polymer coated IONPs of size 50 nm showed the highest value r2 as compared to particle sizes 22 and 80 nm.

Surface properties can also have effects on magnetic properties and MRI contrast efficiency, as the interaction between nanoparticles and water molecules in different environments occur primarily on the surface of the nanoparticles. The coating materials can affect the relaxation of water molecules in various forms, such as diffusion, hydration and hydrogen binding. Early investigations carried out by Duan et al suggested that hydrophilic surface coating contributes greatly to the resulting MRI contrast effect [321]. They investigated the relaxivities of IONPs coated

with different levels of hydrophilic polymers including poly (maleic acid) and octadecene (PMO), poly (ethylene glycol) grafted polyethylenimine (PEG-g-PEI), and hyperbranched polyethylenimine (PEI). They found IONPs coated with highly hydrophilic polymer showed the highest relaxivity (r2) and the largest signal drop inT2.

Thickness of the coating layer could also contribute to the relaxivity and contrast effect of nanoparticles. Tong et al modified the core size of IONPs (14 nm) and the thickness of polymer layer polyethylene glycol (PEG) for the maximal r2 relaxivity per particle [315]. They found at the optimal condition using 1000 Da of PEG coating 14 nm core iron oxide nanoparticles, the r2 relaxivity of PEG coated SPIO reached a value of 385 $s^{-1}mM^{-1}$ at 7 T, more than 2.5 fold higher than that coated with PEG 5000 Da. Another study indicated that change in the coating thickness influenced the relaxivity more than core size. An increase in 26% in the coating thickness of IONPs of size 8.78 nm resulted in a decrease of 13.64% in r1 and r2. In addition, IONPs coated with PEG 600 with the same core size (8.78 nm) and different coating thickness of 70 and 82 nm led to an increase in coating thickness by 17% which resulted in a decrease of r1 and r2 by factors of 26% and 12%, respectively [327]. The significance of a thinner coating thickness layer is considered to be the major factor of the improved relaxivity. In the present study, IONPs of size 22 and 50 nm were coated with a very thin coating layer. However, particle of size 50 nm showed the highest r2 relaxivity compared to the smallest particles, which have the thinnest coating layer. This may be attributed more to the particle core size rather than the coating thickness

as most of the research groups optimise the core size of IONP to improve relaxivities, however we have not optimise the particle core in this study. Thus, further optimisation of particle size by maintaining a very thin coating layer is required in order to enhance r2 values. IONPs of size 80 nm showed the lowest r2 value, which could be due to the thickness of polymer, as the increase of coating thickness leads to an increase in the distance between the particle core and the surrounding aqueous solution (water), resulted in decreasing the relaxivity.

The r2 values are important for medical applications, as higher contrast typically leads to a higher sensitivity and reduces the amount of contrast agent required for imaging. Coating thickness plays a significant role in the total contrast achieved as it may affect the proton relaxation times. A previous study by LaConte et al. have shown that the relaxivity of PEGylated monocrystalline IONPs was affected by the coating thickness. In their study, the r1 and r2 of IONPs were measured using a bench-top nuclear magnetic resonance (NMR) relaxometer. They found r2 and r2/r1 ratio of IONPs decreased when the coating thickness increased [316, 327]. This correlates well with the study presented here that showed the lower relaxivity ratio (r2/r1) of the NPs (80 nm) due to their highest coating thickness (80 nm) compared to NPs of size 22 and 50 nm.

5.5 Conclusion

Continued effort has taken place to improve the cell labelling properties for MRI development and cell tracking. Any improvement in MRI contrast agents will bring benefit to image contrast, diagnostics and monitoring of

therapies. In this chapter, the effect of the size of IONPs coated with PEGylated PGA 40%c18 on the relaxivity was examined. In summary, it has been demonstrated that the size of magnetite nanoparticles can significantly affect their relaxivity. The present work showed that polymer coated IONPs have a good performance in terms of r2 relaxivity and highlights the need for more optimisation of the core/shell structure of IONPs, which could enhance relaxivity effects in applications for targeted in vivo imaging of cells and tissues by MRI.

6 Conclusion and Future Progress

6.1 Conclusion

IONPs have been of great interest for use as MRI contrast enhancement, cell labelling and cell targeting, due to the ability to engineer the particle size and surface. However, questions remain regarding the effects of the physicochemical properties of IONPs, particularly the size on the cellular uptake. The work presented in this thesis aimed to investigate the endocytosis and transcytosis of PEGylated PGA 40%C_{18} coated IONPs of different sizes (22, 50 and 80 nm) into the Calu-3 lung cancer cell line.

A modified method of IONP preparations has been used, resulting in a uniform and a very narrow particle size distribution. The preparation of nanoparticles by the co-precipitation method was carried out under specific conditions such as the reaction pH, temperature, stirring rate and concentration of NaOH in order to produce different IONP sizes.

Both the appropriate structure and amount of polymer were important for successful coating of iron nanoparticles and producing small particle sizes not exceeding 100 nm and to provide stability in physiologically relevant media. PGA 40%C_{18}, PEG-PGA-SA and PEG-PGA 40%C_{18} have been used for coating IONPs using an Interfacial deposition method. PEG-PGA 40%C_{18} was selected in this study due to this polymer showing a good yield of particles with a thin polymer coating and narrow size distribution. Other polymers produced a large particle size, which may be attributed to small aggregates of particles coated with a layer of

polymer. Suitable surface coating for iron oxide particles was achieved with a very small amount of polymer resulting in a very thin polymer layer.

Based on TEM, DLS and zeta potential investigation, the size of PEG-PGA 40%C_{18} coated particles were small with good dispersity, arrangement, and morphology. The presence of free carboxyl groups hanging from the polymer chains on the surface of coated IONPs produced the negative charge around the particle surface. The change of charge from positive (on uncoated particles) to negative (on coated particles) due to the polymer, confirms the successful coating process of the iron nanoparticles. In addition, PEGylated PGA 40%C_{18} was shown to be an effective stabiliser at high concentrations of NaCl. The presence of polymer on the surface of nanoparticle core produced very stable particles, which were in agreement with zeta potential results. The thickness of the polymer was enough to act as a steric barrier against aggregation. The good stability of PEGylated PGA 40% C_{18} coated IONPs made them a useful candidate for cellular studies.

PEGylated PGA 40%C_{18} coated IONPs labelled with RBITC were used to assess cellular uptake and transport of nanoparticles across the epithelial layers of airway Calu-3 cultures. These coated particles can be conveniently labelled with fluorescent dye to produce a very stable incorporation of fluorophore. Cellular uptake, intracellular distribution, localisation and pathway of the uptake have been investigated over different incubation times and with different doses using ferrozine assay, confocal microscopy and TEM.

The present study showed a high cellular uptake rate even after a short incubation with coated particles. Intracellular uptake of coated nanoparticles was dependent on the incubation time and nanoparticle concentrations. The ferrozine assay used for IONP quantification showed the higher cellular association rate of the smallest particle sizes and cellular accumulation gradually increased with time and reached a maximum accumulation point at the maximum time point of 24 hours of incubation. However, for those bigger nanoparticles (50 and 80 nm) the cells tend to stop accumulating nanoparticles by 4 hours. Confocal microscopy study also showed similar differences in Calu-3 cellular uptake of coated IONPs as the ferrozine assay, which were dependent on the concentration and incubation time of nanoparticles. The confocal microscopy images showed a different distribution pattern of RBITC labelled nanoparticles as particles of size 50 and 80 nm appeared as a very fine granular distribution , however, nanoparticles of 22 nm were smoothly distributed inside the cells which may indicate nanoparticle location throughout the cytoplasm. Serial z-sections of the cells showed that the majority of the cells had different level of fluorescent intensity with no evidence for cell membrane binding which demonstrates the internalisation of the nanoparticles inside the cells.

The TEM images showed that the internalisation of coated IONPs inside the cells followed two different pathways depending on the size of particles. For the small NPs of size 22nm, the number of individual nanoparticles taken up was huge, and nanoparticles were found to be present in nuclei and in all subcellular compartments throughout the cell

which suggested the translocation by diffusion through cellular membranes, however a few of the larger 50 and 80nm particles were found surrounded by membranes, which localised in perinuclear area taken up into cells by vesicular pathway(s). This results were confirmed by LysoTracker experiment which showed NPs of size 22 nm were not associated with LysoTracker and mainly they are not located in lysosomal compartments. However, there was some association between the particles of size 50 nm and the LysoTracker and the fraction of association increased after the size increase to 80 nm which strongly suggested that at least not all polymer coated IONPs accumulated in endosomal/lysosomal compartments.

The permeability of coated nanoparticles through the epithelial layers of airway Calu-3 cultures was assessed. The study showed that the permeability of smaller nanoparticle sizes (22 nm) was higher compared to larger particle sizes (50 and 80 nm) which were not accumulated in the basolateral side. A high variability was observed in the measured IONP levels (22nm) in the basolateral compartments, however, the transport of large nanoparticles across the membrane appeared to almost be undetectable. This may be due to the slower penetration of the large particles through the membranes. These results have been confirmed previously by the confocal and TEM microscopy. All particles internalised by endocytic route are finally localised in intracellular vesicles which are appeared as bright spot in confocal images in a perinuclear distribution and surrounded by membrane in the TEM images. However, NPs (22 nm) were detected free in the cytoplasm,

subcellular organelles and nuclei in addition, many of the smaller particles seem to be associated with some of the internal membranes such as the endoplasmic reticulum and the nuclear membrane.

From the present study, it can be concluded that the small NPs have a higher probability to be internalised by physicochemical rather than a physiological uptake since there is no association between the nanoparticles and the subcellular compartment marked by lysotracker, and the punctate distribution which characterises uptake by caveolae is not seen in our studies. However, for the larger particles, there was some association between the particles and the lysostracker which increased from the 50-80nm IONP. Because the larger particles diffuse more slowly, there is more opportunity for them to be endocytosed, and less opportunity for them to diffuse out of the endosomal compartment.

This work contributes to science by providing more successful methods to produce IONPs with very low aggregation and very thin coating layer. Another important outcome that the nanoparticles display a defined size after synthesis which increase the accuracy of results. The study is also highlight the effect of particle size on cellular uptake and internalization cross the airway barrier through the epithelial cell model, Different route of uptake has various possibilities during drug delivery. The present work also showed polymer coated IONPs with a good performance in terms of r2 relaxivity. This could accelerate the development of general design for nanoparticles to meet the great challenge of providing improved imaging capabilities for lung diseases and disorders.

6.2 Limitations of current work

It is interesting to discuss some of the limitations of the present study for further developments. Although some progress has been made to produce polymer coated IONPs with different sizes, it was difficult to determine the exact coating thickness to particle core which could have an effect in the cell labelling as well as imaging by MRI. One of the most complete approach to study nanoparticle uptake is a combination of microscopy to determine the localisation of nanoparticles and Ferrozine assay for a quantification of uptake. Another difficulty in this work arose from the fact that the MRI experiment conditions were not set to better match the in vivo environment. This is because the measurements here were conducted in water rather than in plasma and at room temperature rather than at 37˚C.

6.3 Future Work

The future for the use of IONPs in stem cell labelling and tracking is hopeful. We have added evidence to the possibility of uptake of polymer coated IONPs through crossing epithelial layer as NPs enter cytoplasm and other cellular compartments, which could lead to deliver molecules that are enzymatically degraded in the lysosomes such as nucleic acids and proteins. The benefits of avoiding lysosomal degradation may be critical in delivering nucleic acids. The potential for crossing the lung epithelial barrier would be very useful for transferring a variety of chemical drugs, antibodies and genetic molecules such as siRNA and DNA to treat different lung diseases. Loading DNA in the shell of IONPs could be useful for cancer genetic therapy that could deliver to replace

the abnormal or absent genes with healthy ones that enable cell to produce useful proteins. The finding of a trace of IONPs in the mitochondria could lead to great hope among researchers in the field for the possibility of treatment of mitochondrial disorders and lung dysfunction in the near future by using drug-loaded IONPs.

In addition to drug delivery, using of IONPs is going to dramatically enhance the coincident diagnosis and local therapeutic applications. It is notable that most of current clinical approved nanotechnology products are involved in the passive targeting approach rather than active targeting [328]. Interestingly, the finding strongly support the future development of inhaled polymer coated IONPs-based drug delivery systems for modified local drug delivery to lung epithelia as well as trans pulmonary drug delivery. In this respect to confirm the passive tumour targeting and penetration, further experiment need to be done to complete this proof such as staining the cell membrane for observing NP uptake kinetic. This experiment will show whether NPs accumulate on the plasma membrane prior their internalisation by cells or directly internalise without prior accumulation. In addition, liposomes also can be used to investigate NP uptake route and may provide answers by incubation NPs with liposomes for different time and observe whether the nanoparticles crossing the plasma membrane or accumulated at it and the experiment will show also show also how fast they are translocated through the membrane. Further study could assess in further detail the depth of nanoparticle uptake in each cell compartment using 3 D reconstruction electron tomography. Additionally, to validate the

quantification method that used for cellular uptake study, imaging flow cytometer ImageStream^X could be used to distinguish between adsorbed and internalised fluorescent as well as non-fluorescent nanoparticles in living and fixed cells. In addition, using endocytosis inhibitors for further investigation the pathways of nanoparticle uptake route is required.

Further investigation on the physicochemical characteristics that affecting the mechanisms of uptake of particle is required, for example how physicochemical properties of nanoparticles could affect the diffusion of particles across membranes. Our results demonstrated that IONPs with appropriate size and surface coating could have a great potential for cell labelling as well as imaging using MRI. However, further research on the ability to accurately control the key parameters during production to optimise the relaxivity of these IONP. These include finding a method for the precise determination of the coating thickness and further optimisation of the particle core is required. Regarding the surface properties of IONPs, the polymer used in this study proved to be advantageous for the preparation of dispersed suspensions and can be greatly useful for particle coating. Coating IONPs with PEGylated PGA 40%C_{18} of MWT 2000 resulted in some effects on their magnetic property. However, does the molecular weight of polymer have an effect on cellular uptake efficiency as well as magnetic property? Does the polymeric nanoparticles of small sizes have the same cellular uptake extent of polymer coated IONPs? Further experiments to investigate in depth the potential of this polymer for use as a promising drug carrier system could help to obtain a deeper understanding of the

physicochemical phenomena involved during NP cellular uptake and tracking.

Further experiments could be carried out into MRI study to improve magnetic properties of these particles either by controlling the experiment condition or adjusting shell/core ratios, which were not controlled optimally. All these factors can be improved upon in future studies. There is also a need for in vivo stem cell labelling and imaging to monitor cellular uptake after incubation, and to follow the location as well as expansion of the stem cells for the future success of this field.

References

1. Chou, L.Y., K. Ming, and W.C. Chan, *Strategies for the intracellular delivery of nanoparticles.* Chemical Society Reviews, 2011. **40**(1): p. 233-245.

2. Wu, W., Q. He, and C. Jiang, *Magnetic iron oxide nanoparticles: synthesis and surface functionalization strategies.* Nanoscale research letters, 2008. **3**(11): p. 397.

3. Kolosnjaj-Tabi, J., et al., *Cell labeling with magnetic nanoparticles: Opportunity for magnetic cell imaging and cell manipulation.* Journal of nanobiotechnology, 2013. **11**(Suppl 1): p. S7.

4. Sun, C., J.S. Lee, and M. Zhang, *Magnetic nanoparticles in MR imaging and drug delivery.* Advanced drug delivery reviews, 2008. **60**(11): p. 1252-1265.

5. Kamaly, N., et al., *Targeted polymeric therapeutic nanoparticles: design, development and clinical translation.* Chemical Society Reviews, 2012. **41**(7): p. 2971-3010.

6. Unterweger, H., et al., *Development and characterization of magnetic iron oxide nanoparticles with a cisplatin-bearing polymer coating for targeted drug delivery.* International journal of nanomedicine, 2014. **9**: p. 3659.

7. Neuberger, T., et al., *Superparamagnetic nanoparticles for biomedical applications: possibilities and limitations of a new drug delivery system.* Journal of Magnetism and Magnetic Materials, 2005. **293**(1): p. 483-496.

8. Wu, W., Q. He, and C. Jiang, *Magnetic iron oxide nanoparticles: synthesis and surface functionalization strategies.* ChemInform, 2009. **40**(24): p. i.

9. Gupta, A.K. and M. Gupta, *Synthesis and surface engineering of iron oxide nanoparticles for biomedical applications.* Biomaterials, 2005. **26**(18): p. 3995-4021.

10. Yue-Jian, C., et al., *Synthesis, self-assembly, and characterization of PEG-coated iron oxide nanoparticles as potential MRI contrast agent.* Drug development and industrial pharmacy, 2010. **36**(10): p. 1235-1244.

11. Umut, E., *Surface Modification of Nanoparticles Used in Biomedical Applications.* Modern surface engineering treatment/Edited by M. Aliofkhazraei.–Croatia: InTech, 2013: p. 185-208.

12. Mahmoudi, M., et al., *Superparamagnetic iron oxide nanoparticles: promises for diagnosis and treatment of multiple sclerosis.* ACS chemical neuroscience, 2011. **2**(3): p. 118-140.

13. Prijic, S. and G. Sersa, *Magnetic nanoparticles as targeted delivery systems in oncology.* Radiology and oncology, 2011. **45**(1): p. 1-16.

14. Lübbe, A.S., et al., *Clinical experiences with magnetic drug targeting: a phase I study with 4'-epidoxorubicin in 14 patients with advanced solid tumors.* Cancer research, 1996. **56**(20): p. 4686-4693.

15. Wattendorf, U. and H.P. Merkle, *PEGylation as a tool for the biomedical engineering of surface modified microparticles.* Journal of pharmaceutical sciences, 2008. **97**(11): p. 4655-4669.

16. Mahmoudi, M., et al., *MRI tracking of stem cells in vivo using iron oxide nanoparticles as a tool for the advancement of clinical regenerative medicine.* Chem. Rev, 2011.

17. Mahmoudi, M., et al., *Interaction of stable colloidal nanoparticles with cellular membranes.* Biotechnology advances, 2014. **32**(4): p. 679-692.

18. Berry, C.C. and A.S. Curtis, *Functionalisation of magnetic nanoparticles for applications in biomedicine.* Journal of physics D: Applied physics, 2003. **36**(13): p. R198.

19. Laurent, S., et al., *Magnetic Iron Oxide Nanoparticles: Synthesis, Stabilization, Vectorization, Physicochemical Characterizations, and Biological Applications.* Chemical reviews, 2009. **110**(4): p. 2574-2574.

20. Modi, S., et al., *A DNA nanomachine that maps spatial and temporal pH changes inside living cells.* Nature nanotechnology, 2009. **4**(5): p. 325.

21. Ayala, V., et al., *Effect of surface charge on the colloidal stability and in vitro uptake of carboxymethyl dextran-*

coated iron oxide nanoparticles. Journal of nanoparticle research, 2013. **15**(8): p. 1874.

22. French, R.A., et al., *Influence of ionic strength, pH, and cation valence on aggregation kinetics of titanium dioxide nanoparticles.* Environmental science & technology, 2009. **43**(5): p. 1354-1359.

23. Yu, M., et al., *Dextran and polymer polyethylene glycol (PEG) coating reduce both 5 and 30 nm iron oxide nanoparticle cytotoxicity in 2D and 3D cell culture.* International journal of molecular sciences, 2012. **13**(5): p. 5554-5570.

24. Lee, S.-J., et al., *Nanoparticles of magnetic ferric oxides encapsulated with poly (D, L latide-co-glycolide) and their applications to magnetic resonance imaging contrast agent.* Journal of magnetism and magnetic materials, 2004. **272**: p. 2432-2433.

25. Mahmoudi, M., et al., *Templated growth of superparamagnetic iron oxide nanoparticles by temperature programming in the presence of poly (vinyl alcohol).* Thin Solid Films, 2010. **518**(15): p. 4281-4289.

26. Kanaras, A.G., et al., *Thioalkylated tetraethylene glycol: a new ligand for water soluble monolayer protected gold clusters.* Chemical Communications, 2002(20): p. 2294-2295.

27. Bartczak, D. and A.G. Kanaras, *Diacetylene-containing ligand as a new capping agent for the preparation of water-soluble colloidal nanoparticles of remarkable stability.* Langmuir, 2010. **26**(10): p. 7072-7077.

28. Pelaz, B., et al., *Interfacing engineered nanoparticles with biological systems: anticipating adverse nano–bio interactions.* Small, 2013. **9**(9-10): p. 1573-1584.

29. Doane, T.L., et al., *Electrophoretic mobilities of PEGylated gold NPs.* Journal of the American Chemical Society, 2010. **132**(44): p. 15624-15631.

30. Wilhelm, C., et al., *Intracellular uptake of anionic superparamagnetic nanoparticles as a function of their surface coating.* Biomaterials, 2003. **24**(6): p. 1001-1011.

31. Varela, J.A., et al., *Quantifying size-dependent interactions between fluorescently labeled polystyrene nanoparticles and mammalian cells.* Journal of nanobiotechnology, 2012. **10**(1): p. 39.

32. Bahmani, B., et al., *Effect of polyethylene glycol coatings on uptake of indocyanine green loaded nanocapsules by human spleen macrophages in vitro.* Journal of Biomedical Optics, 2011. **16**(5): p. 051303.

33. Alhareth, K., et al., *Conformation of surface-decorating dextran chains affects the pharmacokinetics and biodistribution of doxorubicin-loaded nanoparticles.* European Journal of Pharmaceutics and Biopharmaceutics, 2012. **81**(2): p. 453-457.

34. Hirn, S., et al., *Particle size-dependent and surface charge-dependent biodistribution of gold nanoparticles after intravenous administration.* European journal of pharmaceutics and biopharmaceutics, 2011. **77**(3): p. 407-416.

35. Win, K.Y. and S.-S. Feng, *Effects of particle size and surface coating on cellular uptake of polymeric nanoparticles for oral delivery of anticancer drugs.* Biomaterials, 2005. **26**(15): p. 2713-2722.

36. Hanada, S., et al., *Cell-based in vitro blood–brain barrier model can rapidly evaluate nanoparticles' brain permeability in association with particle size and surface modification.* International journal of molecular sciences, 2014. **15**(2): p. 1812-1825.

37. Jo, J.-i., I. Aoki, and Y. Tabata, *Design of iron oxide nanoparticles with different sizes and surface charges for simple and efficient labeling of mesenchymal stem cells.* Journal of Controlled Release, 2010. **142**(3): p. 465-473.

38. Zhang, S., H. Gao, and G. Bao, *Physical principles of nanoparticle cellular endocytosis.* ACS nano, 2015. **9**(9): p. 8655-8671.

39. Chaves, N.L., et al., *Exploring cellular uptake of iron oxide nanoparticles associated with rhodium citrate in breast cancer cells.* International journal of nanomedicine, 2017. **12**: p. 5511.

40. Taylor, A., et al., *Assessing the efficacy of nano-and micro-sized magnetic particles as contrast agents for MRI cell tracking.* PLoS One, 2014. **9**(6): p. e100259.

41. Chouly, C., et al., *Development of superparamagnetic nanoparticles for MRI: effect of particle size, charge and surface nature on biodistribution.* Journal of microencapsulation, 1996. **13**(3): p. 245-255.

42. Thomas, R., I.-K. Park, and Y.Y. Jeong, *Magnetic iron oxide nanoparticles for multimodal imaging and therapy of cancer.* International journal of molecular sciences, 2013. **14**(8): p. 15910-15930.

43. Stolnik, S., L. Illum, and S. Davis, *Long circulating microparticulate drug carriers.* Advanced drug delivery reviews, 1995. **16**(2-3): p. 195-214.

44. Treuel, L., X. Jiang, and G.U. Nienhaus, *New views on cellular uptake and trafficking of manufactured nanoparticles.* Journal of The Royal Society Interface, 2013. **10**(82): p. 20120939.

45. Kralj, S., et al., *Effect of surface charge on the cellular uptake of fluorescent magnetic nanoparticles.* Journal of Nanoparticle Research, 2012. **14**(10): p. 1-14.

46. Florez, L., et al., *How shape influences uptake: interactions of anisotropic polymer nanoparticles and human mesenchymal stem cells.* Small, 2012. **8**(14): p. 2222-2230.

47. Soppimath, K.S., et al., *Biodegradable polymeric nanoparticles as drug delivery devices.* Journal of controlled release, 2001. **70**(1): p. 1-20.

48. Hans, M. and A. Lowman, *Biodegradable nanoparticles for drug delivery and targeting.* Current Opinion in Solid State and Materials Science, 2002. **6**(4): p. 319-327.

49. des Rieux, A., et al., *Nanoparticles as potential oral delivery systems of proteins and vaccines: a mechanistic approach.* Journal of controlled release, 2006. **116**(1): p. 1-27.

50. Weinstein, J.S., et al., *Superparamagnetic iron oxide nanoparticles: diagnostic magnetic resonance imaging and potential therapeutic applications in neurooncology and central nervous system inflammatory pathologies, a*

review. Journal of Cerebral Blood Flow & Metabolism, 2010. **30**(1): p. 15-35.

51. Lee, H., et al., *Antibiofouling polymer-coated superparamagnetic iron oxide nanoparticles as potential magnetic resonance contrast agents for in vivo cancer imaging.* Journal of the American Chemical Society, 2006. **128**(22): p. 7383-7389.

52. Li, L., et al., *Superparamagnetic iron oxide nanoparticles as MRI contrast agents for non-invasive stem cell labeling and tracking.* Theranostics, 2013. **3**(8): p. 595.

53. Teja, A.S. and P.-Y. Koh, *Synthesis, properties, and applications of magnetic iron oxide nanoparticles.* Progress in crystal growth and characterization of materials, 2009. **55**(1-2): p. 22-45.

54. Li, Z., et al., *Ultrasmall water-soluble and biocompatible magnetic iron oxide nanoparticles as positive and negative dual contrast agents.* Advanced Functional Materials, 2012. **22**(11): p. 2387-2393.

55. Weinmann, H.-J., et al., *Characteristics of gadolinium-DTPA complex: a potential NMR contrast agent.* American Journal of Roentgenology, 1984. **142**(3): p. 619-624.

56. Aime, S., M. Botta, and E. Terreno, *Gd (III)-based contrast agents for MRI.* Adv. Inorg. Chem, 2005. **57**: p. 173-237.

57. Kuo, P.H., et al., *Gadolinium-based MR contrast agents and nephrogenic systemic fibrosis.* Radiology, 2007. **242**(3): p. 647-649.

58. Na, H.B. and T. Hyeon, *Nanostructured T1 MRI contrast agents.* Journal of Materials Chemistry, 2009. **19**(35): p. 6267-6273.

59. Seo, W.S., et al., *FeCo/graphitic-shell nanocrystals as advanced magnetic-resonance-imaging and near-infrared agents.* Nature materials, 2006. **5**(12): p. 971.

60. Bulte, J.W. and D.L. Kraitchman, *Iron oxide MR contrast agents for molecular and cellular imaging.* NMR in Biomedicine, 2004. **17**(7): p. 484-499.

61. Mahmoudi, M., et al., *Magnetic resonance imaging tracking of stem cells in vivo using iron oxide*

nanoparticles as a tool for the advancement of clinical regenerative medicine. Chemical Reviews, 2010. **111**(2): p. 253-280.

62. Gordon, R., J. Hines, and D. Gordon, *Intracellular hyperthermia a biophysical approach to cancer treatment via intracellular temperature and biophysical alterations.* Medical Hypotheses, 1979. **5**(1): p. 83-102.

63. Nellans, H.N., *(B) Mechanisms of peptide and protein absorption:(1) Paracellular intestinal transport: modulation of absorption.* Advanced drug delivery reviews, 1991. **7**(3): p. 339-364.

64. Chan, D.C., D.B. Kirpotin, and P.A. Bunn Jr, *Synthesis and evaluation of colloidal magnetic iron oxides for the site-specific radiofrequency-induced hyperthermia of cancer.* Journal of Magnetism and Magnetic Materials, 1993. **122**(1-3): p. 374-378.

65. Frank, J.A., et al., *Methods for magnetically labeling stem and other cells for detection by in vivo magnetic resonance imaging.* Cytotherapy, 2004. **6**(6): p. 621-625.

66. Horwitz, E.M., et al., *Clinical responses to bone marrow transplantation in children with severe osteogenesis imperfecta.* Blood, 2001. **97**(5): p. 1227-1231.

67. Callera, F. and C.M. de Melo, *Magnetic resonance tracking of magnetically labeled autologous bone marrow CD34+ cells transplanted into the spinal cord via lumbar puncture technique in patients with chronic spinal cord injury: CD34+ cells' migration into the injured site.* Stem Cells and Development, 2007. **16**(3): p. 461-466.

68. Guzman, R., et al., *Long-term monitoring of transplanted human neural stem cells in developmental and pathological contexts with MRI.* Proceedings of the National Academy of Sciences, 2007. **104**(24): p. 10211-10216.

69. Bull, E., et al., *Stem cell tracking using iron oxide nanoparticles.* International journal of nanomedicine, 2014. **9**: p. 1641.

70. Zhang, Y., N. Kohler, and M. Zhang, *Surface modification of superparamagnetic magnetite nanoparticles and their*

intracellular uptake. Biomaterials, 2002. **23**(7): p. 1553-1561.

71. Gratton, S.E., et al., *The effect of particle design on cellular internalization pathways.* Proceedings of the National Academy of Sciences, 2008. **105**(33): p. 11613-11618.

72. Brekke, C., et al., *The in vitro effects of a bimodal contrast agent on cellular functions and relaxometry.* NMR in Biomedicine, 2007. **20**(2): p. 77-89.

73. Van Buul, G., et al., *Ferumoxides–protamine sulfate is more effective than ferucarbotran for cell labeling: implications for clinically applicable cell tracking using MRI.* Contrast media & molecular imaging, 2009. **4**(5): p. 230-236.

74. Jasmin, et al., *Optimized labeling of bone marrow mesenchymal cells with superparamagnetic iron oxide nanoparticles and in vivo visualization by magnetic resonance imaging.* Journal of Nanobiotechnology, 2011. **9**(1): p. 4.

75. Chapon, C., et al., *An in vivo multimodal imaging study using MRI and PET of stem cell transplantation after myocardial infarction in rats.* Molecular Imaging and Biology, 2009. **11**(1): p. 31-38.

76. He, B., et al., *The transport mechanisms of polymer nanoparticles in Caco-2 epithelial cells.* Biomaterials, 2013. **34**(25): p. 6082-6098.

77. Kim, D., et al., *Synthesis and characterization of surfactant-coated superparamagnetic monodispersed iron oxide nanoparticles.* Journal of Magnetism and Magnetic Materials, 2001. **225**(1): p. 30-36.

78. Laurent, S., et al., *Magnetic iron oxide nanoparticles: synthesis, stabilization, vectorization, physicochemical characterizations, and biological applications.* Chemical reviews, 2008. **108**(6): p. 2064-2110.

79. Gribanov, N., et al., *Physico-chemical regularities of obtaining highly dispersed magnetite by the method of chemical condensation.* Journal of Magnetism and Magnetic Materials, 1990. **85**(1): p. 7-10.

80. Massart, R., *Preparation of aqueous magnetic liquids in alkaline and acidic media.* IEEE transactions on magnetics, 1981. **17**(2): p. 1247-1248.

81. Umer, A., et al., *Selection of a suitable method for the synthesis of copper nanoparticles.* Nano, 2012. **7**(05).

82. Teja, A.S. and P.-Y. Koh, *Synthesis, properties, and applications of magnetic iron oxide nanoparticles.* Progress in crystal growth and characterization of materials, 2009. **55**(1): p. 22-45.

83. Hassanjani-Roshan, A., et al., *Synthesis of iron oxide nanoparticles via sonochemical method and their characterization.* Particuology, 2011. **9**(1): p. 95-99.

84. Owens, D.E. and N.A. Peppas, *Opsonization, biodistribution, and pharmacokinetics of polymeric nanoparticles.* International journal of pharmaceutics, 2006. **307**(1): p. 93-102.

85. Kim, E.H., et al., *Synthesis of ferrofluid with magnetic nanoparticles by sonochemical method for MRI contrast agent.* Journal of Magnetism and Magnetic Materials, 2005. **289**: p. 328-330.

86. Unsoy, G., et al., *Synthesis optimization and characterization of chitosan-coated iron oxide nanoparticles produced for biomedical applications.* Journal of Nanoparticle Research, 2012. **14**(11): p. 964.

87. Kim, D.K., et al., *Protective coating of superparamagnetic iron oxide nanoparticles.* Chemistry of Materials, 2003. **15**(8): p. 1617-1627.

88. Huber, D.L., *Synthesis, properties, and applications of iron nanoparticles.* Small, 2005. **1**(5): p. 482-501.

89. Petri-Fink, A., et al., *Effect of cell media on polymer coated superparamagnetic iron oxide nanoparticles (SPIONs): colloidal stability, cytotoxicity, and cellular uptake studies.* European journal of pharmaceutics and biopharmaceutics, 2008. **68**(1): p. 129-137.

90. Amstad, E., M. Textor, and E. Reimhult, *Stabilization and functionalization of iron oxide nanoparticles for biomedical applications.* Nanoscale, 2011. **3**(7): p. 2819-2843.

91. Petcharoen, K. and A. Sirivat, *Synthesis and characterization of magnetite nanoparticles via the chemical co-precipitation method.* Materials Science and Engineering: B, 2012. **177**(5): p. 421-427.

92. Soenen, S.J., A.R. Brisson, and M. De Cuyper, *Addressing the problem of cationic lipid-mediated toxicity: the magnetoliposome model.* Biomaterials, 2009. **30**(22): p. 3691-3701.

93. Owens, D.E., 3rd and N.A. Peppas, *Opsonization, biodistribution, and pharmacokinetics of polymeric nanoparticles.* Int J Pharm, 2006. **307**(1): p. 93-102.

94. Gupta, A.K., et al., *Recent advances on surface engineering of magnetic iron oxide nanoparticles and their biomedical applications.* 2007.

95. Boyer, C., et al., *The design and utility of polymer-stabilized iron-oxide nanoparticles for nanomedicine applications.* NPG Asia Materials, 2010. **2**(1): p. 23-30.

96. Eamegdool, S.S., et al., *Ultrasmall superparamagnetic iron oxide nanoparticle prelabelling of human neural precursor cells.* Biomaterials, 2014. **35**(21): p. 5549-5564.

97. Hong, R., et al., *Synthesis, characterization and MRI application of dextran-coated Fe 3 O 4 magnetic nanoparticles.* Biochemical engineering journal, 2008. **42**(3): p. 290-300.

98. Josephson, L., et al., *High-efficiency intracellular magnetic labeling with novel superparamagnetic-Tat peptide conjugates.* Bioconjugate chemistry, 1999. **10**(2): p. 186-191.

99. Yan, H., M. Guo, and K. Liu, *Multifunctional magnetic hybrid nanoparticles as a nanomedical platform for cancer-targeted imaging and therapy*, in *Biomedical Science, Engineering and Technology*. 2012, InTech.

100. Strable, E., et al., *Synthesis and characterization of soluble iron oxide-dendrimer composites.* Chemistry of materials, 2001. **13**(6): p. 2201-2209.

101. Kallinteri, P., et al., *Novel functionalized biodegradable polymers for nanoparticle drug delivery systems.* Biomacromolecules, 2005. **6**(4): p. 1885-1894.

102. Gessner, A., et al., *Nanoparticles with decreasing surface hydrophobicities: influence on plasma protein adsorption.* International journal of pharmaceutics, 2000. **196**(2): p. 245-249.

103. Storm, G., et al., *Surface modification of nanoparticles to oppose uptake by the mononuclear phagocyte system.* Advanced Drug Delivery Reviews, 1995. **17**(1): p. 31-48.

104. Cho, K., et al., *Therapeutic nanoparticles for drug delivery in cancer.* Clinical cancer research, 2008. **14**(5): p. 1310-1316.

105. Gabizon, A. and D. Papahadjopoulos, *The role of surface charge and hydrophilic groups on liposome clearance in vivo.* Biochimica et Biophysica Acta (BBA)-Biomembranes, 1992. **1103**(1): p. 94-100.

106. Illum, L. and S.S. Davis, *Effect of the nonionic surfactant poloxamer 338 on the fate and deposition of polystyrene microspheres following intravenous administration.* Journal of pharmaceutical sciences, 1983. **72**(9): p. 1086-1089.

107. Artursson, P., *Epithelial transport of drugs in cell culture. I: A model for studying the passive diffusion of drugs over intestinal absorbtive (Caco-2) cells.* Journal of pharmaceutical sciences, 1990. **79**(6): p. 476-482.

108. Oh, N. and J.-H. Park, *Endocytosis and exocytosis of nanoparticles in mammalian cells.* International journal of nanomedicine, 2014. **9**(Suppl 1): p. 51.

109. Verma, A. and F. Stellacci, *Effect of surface properties on nanoparticle–cell interactions.* Small, 2010. **6**(1): p. 12-21.

110. Enochs, W., et al., *MR imaging of slow axonal transport in vivo.* Experimental neurology, 1993. **123**(2): p. 235-242.

111. Wu, Y.J., et al., *In vivo leukocyte labeling with intravenous ferumoxides/protamine sulfate complex and in vitro characterization for cellular magnetic resonance imaging.* American Journal of Physiology-Cell Physiology, 2007. **293**(5): p. C1698-C1708.

112. Singh, N., et al., *Potential toxicity of superparamagnetic iron oxide nanoparticles (SPION).* Nano reviews, 2010. **1**.

113. Komarova, Y. and A.B. Malik, *Regulation of endothelial permeability via paracellular and transcellular transport pathways.* Annual review of physiology, 2010. **72**: p. 463-493.

114. Rejman, J., et al., *Size-dependent internalization of particles via the pathways of clathrin-and caveolae-mediated endocytosis.* Biochemical journal, 2004. **377**(Pt 1): p. 159.

115. Foster, K.A., M. Yazdanian, and K.L. Audus, *Microparticulate uptake mechanisms of in-vitro cell culture models of the respiratory epithelium.* Journal of pharmacy and pharmacology, 2001. **53**(1): p. 57-66.

116. Gaumet, M., R. Gurny, and F. Delie, *Localization and quantification of biodegradable particles in an intestinal cell model: the influence of particle size.* European Journal of Pharmaceutical Sciences, 2009. **36**(4-5): p. 465-473.

117. Dausend, J., et al., *Uptake mechanism of oppositely charged fluorescent nanoparticles in HeLa cells.* Macromolecular bioscience, 2008. **8**(12): p. 1135-1143.

118. Labhasetwar, V., *Nanotechnology for drug and gene therapy: the importance of understanding molecular mechanisms of delivery.* Current opinion in biotechnology, 2005. **16**(6): p. 674-680.

119. Xiao, Y., et al., *Dynamics and mechanisms of quantum dot nanoparticle cellular uptake.* Journal of nanobiotechnology, 2010. **8**(1): p. 13.

120. Clift, M.J., et al., *The impact of different nanoparticle surface chemistry and size on uptake and toxicity in a murine macrophage cell line.* Toxicology and applied pharmacology, 2008. **232**(3): p. 418-427.

121. Xia, T., et al., *Cationic polystyrene nanosphere toxicity depends on cell-specific endocytic and mitochondrial injury pathways.* ACS nano, 2007. **2**(1): p. 85-96.

122. Geiser, M., et al., *Ultrafine particles cross cellular membranes by nonphagocytic mechanisms in lungs and in cultured cells.* Environmental health perspectives, 2005. **113**(11): p. 1555.

123. Rothen-Rutishauser, B.M., et al., *Interaction of fine particles and nanoparticles with red blood cells visualized*

with advanced microscopic techniques. Environmental science & technology, 2006. **40**(14): p. 4353-4359.

124. Mu, Q., et al., *Mechanism of cellular uptake of genotoxic silica nanoparticles.* Particle and fibre toxicology, 2012. **9**(1): p. 29.

125. Weissleder, R., *Molecular imaging in cancer.* Science, 2006. **312**(5777): p. 1168-1171.

126. Iversen, T.-G., T. Skotland, and K. Sandvig, *Endocytosis and intracellular transport of nanoparticles: present knowledge and need for future studies.* Nano Today, 2011. **6**(2): p. 176-185.

127. Mercer, J. and A. Helenius, *Virus entry by macropinocytosis.* Nature cell biology, 2009. **11**(5): p. 510.

128. Hirota, K. and H. Terada, *Endocytosis of particle formulations by macrophages and its application to clinical treatment*, in *Molecular Regulation of Endocytosis*. 2012, InTech.

129. Swanson, J.A. and C. Watts, *Macropinocytosis.* Trends in cell biology, 1995. **5**(11): p. 424-428.

130. Cell, B., *Enterocyte-like differentiation and polarization of the human colon carcinoma cell line Caco-2 in culture.* Biol. Cell, 1983. **47**: p. 323-330.

131. Cañete, M., et al., *The endocytic penetration mechanism of iron oxide magnetic nanoparticles with positively charged cover: a morphological approach.* International journal of molecular medicine, 2010. **26**(4): p. 533-539.

132. Canton, I. and G. Battaglia, *Endocytosis at the nanoscale.* Chemical Society Reviews, 2012. **41**(7): p. 2718-2739.

133. Doherty, G.J. and H.T. McMahon, *Mechanisms of endocytosis.* Annual review of biochemistry, 2009. **78**: p. 857-902.

134. Kaksonen, M., C.P. Toret, and D.G. Drubin, *Harnessing actin dynamics for clathrin-mediated endocytosis.* Nature reviews Molecular cell biology, 2006. **7**(6): p. 404.

135. Decuzzi, P. and M. Ferrari, *The role of specific and non-specific interactions in receptor-mediated endocytosis of*

nanoparticles. Biomaterials, 2007. **28**(18): p. 2915-2922.

136. Vácha, R., F.J. Martinez-Veracoechea, and D. Frenkel, *Receptor-mediated endocytosis of nanoparticles of various shapes.* Nano letters, 2011. **11**(12): p. 5391-5395.

137. Sahay, G., D.Y. Alakhova, and A.V. Kabanov, *Endocytosis of nanomedicines.* Journal of controlled release, 2010. **145**(3): p. 182-195.

138. Begum, G., et al., *Cellular permeation with nuclear infiltration capability of biomimetically synthesised fluorescent monodisperse mesoporous silica nanospheres in HeLa and human stem cells.* Journal of Materials Chemistry, 2010. **20**(39): p. 8563-8570.

139. Torgersen, M.L., et al., *Internalization of cholera toxin by different endocytic mechanisms.* Journal of cell science, 2001. **114**(20): p. 3737-3747.

140. Richter, T., et al., *High-Resolution 3D Quantitative Analysis of Caveolar Ultrastructure and Caveola–Cytoskeleton Interactions.* Traffic, 2008. **9**(6): p. 893-909.

141. Pelkmans, L., et al., *Caveolin-stabilized membrane domains as multifunctional transport and sorting devices in endocytic membrane traffic.* Cell, 2004. **118**(6): p. 767-780.

142. Kou, L., et al., *The endocytosis and intracellular fate of nanomedicines: Implication for rational design.* Asian Journal of Pharmaceutical Sciences, 2013. **8**(1): p. 1-10.

143. Ferreira, L., *Nanoparticles as tools to study and control stem cells.* Journal of cellular biochemistry, 2009. **108**(4): p. 746-752.

144. Bareford, L.M. and P.W. Swaan, *Endocytic mechanisms for targeted drug delivery.* Advanced drug delivery reviews, 2007. **59**(8): p. 748-758.

145. Verkman, A.S., *Solute and macromolecule diffusion in cellular aqueous compartments.* Trends in biochemical sciences, 2002. **27**(1): p. 27-33.

146. Karlsson, J. and P. Artursson, *A method for the determination of cellular permeability coefficients and aqueous boundary layer thickness in monolayers of intestinal epithelial (Caco-2) cells grown in permeable filter chambers.* International journal of pharmaceutics, 1991. **71**(1): p. 55-64.

147. Anderson, J.M. and C.M. Van Itallie, *Physiology and function of the tight junction.* Cold Spring Harbor perspectives in biology, 2009. **1**(2): p. a002584.

148. Fromter, E. and J. Diamond, *Route of passive ion permeation in epithelia.* Nat New Biol, 1972. **235**(53): p. 9-13.

149. Tang, V.W. and D.A. Goodenough, *Paracellular ion channel at the tight junction.* Biophysical journal, 2003. **84**(3): p. 1660-1673.

150. Artursson, P., K. Palm, and K. Luthman, *Caco-2 monolayers in experimental and theoretical predictions of drug transport.* Advanced drug delivery reviews, 2012. **64**: p. 280-289.

151. Patton, J.S., *Mechanisms of macromolecule absorption by the lungs.* Advanced Drug Delivery Reviews, 1996. **19**(1): p. 3-36.

152. Garnett, M., et al., *Drug delivery: epithelial cell models for drug transport and toxicology studies.* The Biochemist, 2014. **36**(3): p. 8.

153. Herce, H.D. and A.E. Garcia, *Molecular dynamics simulations suggest a mechanism for translocation of the HIV-1 TAT peptide across lipid membranes.* Proceedings of the National Academy of Sciences, 2007. **104**(52): p. 20805-20810.

154. Spiro, D., et al., *Wortmannin alters the transferrin receptor endocytic pathway in vivo and in vitro.* Molecular Biology of the Cell, 1996. **7**(3): p. 355-367.

155. Shang, L., K. Nienhaus, and G.U. Nienhaus, *Engineered nanoparticles interacting with cells: size matters.* J Nanobiotechnol, 2014. **12**(5): p. b26.

156. Chithrani, B.D., A.A. Ghazani, and W.C. Chan, *Determining the size and shape dependence of gold*

nanoparticle uptake into mammalian cells. Nano letters, 2006. **6**(4): p. 662-668.

157. Mu, Q., et al., *Mechanism of cellular uptake of genotoxic silica nanoparticles.* Part Fibre Toxicol, 2012. **9**(1): p. 29.

158. Baalousha, M., *Aggregation and disaggregation of iron oxide nanoparticles: influence of particle concentration, pH and natural organic matter.* Science of the total Environment, 2009. **407**(6): p. 2093-2101.

159. Thiele, L., et al., *Evaluation of particle uptake in human blood monocyte-derived cells in vitro. Does phagocytosis activity of dendritic cells measure up with macrophages?* Journal of Controlled Release, 2001. **76**(1): p. 59-71.

160. Zhu, Z.-J., et al., *Multiplexed screening of cellular uptake of gold nanoparticles using laser desorption/ionization mass spectrometry.* Journal of the American Chemical Society, 2008. **130**(43): p. 14139-14143.

161. Bannunah, A.M., et al., *Mechanisms of nanoparticle internalization and transport across an intestinal epithelial cell model: effect of size and surface charge.* Molecular pharmaceutics, 2014. **11**(12): p. 4363-4373.

162. Owens III, D.E. and N.A. Peppas, *Opsonization, biodistribution, and pharmacokinetics of polymeric nanoparticles.* International journal of pharmaceutics, 2006. **307**(1): p. 93-102.

163. Kobayashi, K., et al., *Surface engineering of nanoparticles for therapeutic applications.* Polymer Journal, 2014. **46**(8): p. 460-468.

164. Abo-zeid, Y., et al., *Synthesis of nucleoside-boronic esters hydrophobic pro-drugs: a possible route to improve hydrophilic nucleoside drug loading into polymer nanoparticles.* Journal of Drug Delivery Science and Technology, 2018. **46**: p. 354-364.

165. Meng, W., et al., *Penetration and intracellular uptake of poly (glycerol-adipate) nanoparticles into three-dimensional brain tumour cell culture models.* Experimental Biology and Medicine, 2016. **241**(5): p. 466-477.

166. Fowler, R., et al., *Uptake and transport of B12-conjugated nanoparticles in airway epithelium.* Journal of controlled release, 2013. **172**(1): p. 374-381.

167. Bhadriraju, K. and C.S. Chen, *Engineering cellular microenvironments to improve cell-based drug testing.* Drug discovery today, 2002. **7**(11): p. 612-620.

168. Fogh, J., J.M. Fogh, and T. Orfeo, *One hundred and twenty-seven cultured human tumor cell lines producing tumors in nude mice.* Journal of the National Cancer Institute, 1977. **59**(1): p. 221-226.

169. Zhu, Y., A. Chidekel, and T.H. Shaffer, *Cultured human airway epithelial cells (calu-3): a model of human respiratory function, structure, and inflammatory responses.* Critical care research and practice, 2010. **2010**.

170. Grainger, C.I., et al., *Culture of Calu-3 cells at the air interface provides a representative model of the airway epithelial barrier.* Pharmaceutical research, 2006. **23**(7): p. 1482-1490.

171. Geys, J., et al., *In vitro study of the pulmonary translocation of nanoparticles: a preliminary study.* Toxicology letters, 2006. **160**(3): p. 218-226.

172. de Jong, P.M., et al., *Serial culturing of human bronchial epithelial cells derived from biopsies.* In Vitro Cellular & Developmental Biology-Animal, 1993. **29**(5): p. 379-387.

173. Fiegel, J., et al., *Large porous particle impingement on lung epithelial cell monolayers—toward improved particle characterization in the lung.* Pharmaceutical Research, 2003. **20**(5): p. 788-796.

174. Crater, J.S. and R.L. Carrier, *Barrier properties of gastrointestinal mucus to nanoparticle transport.* Macromolecular bioscience, 2010. **10**(12): p. 1473-1483.

175. Cu, Y. and W.M. Saltzman, *Controlled surface modification with poly (ethylene) glycol enhances diffusion of PLGA nanoparticles in human cervical mucus.* Molecular pharmaceutics, 2008. **6**(1): p. 173-181.

176. Abushrida, A., *Formulation of novel polymer coated iron oxide nanoparticles*. 2012, University of Nottingham.

177. Kresse, M., et al., *Targeting of ultrasmall superparamagnetic iron oxide (USPIO) particles to tumor cells in vivo by using transferrin receptor pathways.* Magnetic Resonance in Medicine, 1998. **40**(2): p. 236-242.

178. Fessi, H., et al., *Nanocapsule formation by interfacial polymer deposition following solvent displacement.* International journal of pharmaceutics, 1989. **55**(1): p. R1-R4.

179. Sun, Z., et al., *Characterization of cellular uptake and toxicity of aminosilane-coated iron oxide nanoparticles with different charges in central nervous system-relevant cell culture models.* International journal of nanomedicine, 2013. **8**: p. 961.

180. Powell, D., *Barrier function of epithelia.* American Journal of Physiology-Gastrointestinal and Liver Physiology, 1981. **241**(4): p. G275-G288.

181. Wang, T., et al., *Cellular uptake of nanoparticles by membrane penetration: a study combining confocal microscopy with FTIR spectroelectrochemistry.* ACS nano, 2012. **6**(2): p. 1251-1259.

182. Zuo, H.D., et al., *The effect of superparamagnetic iron oxide with iRGD peptide on the labeling of pancreatic cancer cells in vitro: a preliminary study.* BioMed research international, 2014. **2014**.

183. Zeng, H. and S. Sun, *Syntheses, properties, and potential applications of multicomponent magnetic nanoparticles.* Advanced Functional Materials, 2008. **18**(3): p. 391.

184. Mahdavi, M., et al., *Synthesis, surface modification and characterisation of biocompatible magnetic iron oxide nanoparticles for biomedical applications.* Molecules, 2013. **18**(7): p. 7533-7548.

185. Sapsford, K.E., et al., *Functionalizing nanoparticles with biological molecules: developing chemistries that facilitate nanotechnology.* Chemical reviews, 2013. **113**(3): p. 1904-2074.

186. Ge, S., et al., *Facile hydrothermal synthesis of iron oxide nanoparticles with tunable magnetic properties.* The Journal of Physical Chemistry C, 2009. **113**(31): p. 13593-13599.

187. Sreeja, V. and P. Joy, *Microwave–hydrothermal synthesis of γ-Fe 2 O 3 nanoparticles and their magnetic properties.* Materials Research Bulletin, 2007. **42**(8): p. 1570-1576.

188. Chin, A.B. and I.I. Yaacob, *Synthesis and characterization of magnetic iron oxide nanoparticles via w/o microemulsion and Massart's procedure.* Journal of materials processing technology, 2007. **191**(1): p. 235-237.

189. Han, Y., et al., *Sonochemical synthesis of magnetic protein container for targeted delivery.* Macromolecular Rapid Communications, 2008. **29**(14): p. 1203-1207.

190. Herranz, F., et al., *A new method for the aqueous functionalization of superparamagnetic Fe2O3 nanoparticles.* Contrast media & molecular imaging, 2008. **3**(6): p. 215-222.

191. Khoshnevis, S., et al., *Water-based Double Layer Functionalized Iron Oxide Nanoparticles for Enhanced Gene Delivery Applications.* Biomacromolecular Journal, 2016. **2**(2): p. 152-161.

192. Thorek, D.L., et al., *Superparamagnetic iron oxide nanoparticle probes for molecular imaging.* Annals of biomedical engineering, 2006. **34**(1): p. 23-38.

193. Yan, H., K. Liu, and M. Guo, *Multifunctional magnetic hybrid nanoparticles as a nanomedical platform for cancer-targeted imaging and therapy*. 2012: INTECH Open Access Publisher.

194. Yu, C., et al., *A novel method to prepare water-dispersible magnetic nanoparticles and their biomedical applications: magnetic capture probe and specific cellular uptake.* Journal of Biomedical Materials Research Part A, 2008. **87**(2): p. 364-372.

195. Neoh, K.G. and E.T. Kang, *Surface modification of magnetic nanoparticles for stem cell labeling.* Soft Matter, 2012. **8**(7): p. 2057-2069.

196. Zhongming, Z., et al., *Preparation of aqueous magnetic liquids in alkaline and acidic media.* 1981.

197. Umut, E., *Surface modification of nanoparticles used in biomedical applications*, in *Modern Surface Engineering Treatments*. 2013, InTech.

198. Mirkin, C.A. and C.M. Niemeyer, *Nanobiotechnology II: more concepts and applications*. 2007: John Wiley & Sons.

199. Lodhia, J., et al., *Development and use of iron oxide nanoparticles (Part 1): Synthesis of iron oxide nanoparticles for MRI.* Biomedical imaging and intervention journal, 2010. **6**(2).

200. Tartaj, P., et al., *Synthesis, properties and biomedical applications of magnetic nanoparticles.* Handbook of magnetic materials, 2006. **16**(5): p. 403-482.

201. Peng, X., J. Wickham, and A. Alivisatos, *Kinetics of II-VI and III-V colloidal semiconductor nanocrystal growth:"focusing" of size distributions.* Journal of the American Chemical Society, 1998. **120**(21): p. 5343-5344.

202. Budhian, A., S.J. Siegel, and K.I. Winey, *Controlling the in vitro release profiles for a system of haloperidol-loaded PLGA nanoparticles.* International Journal of Pharmaceutics, 2008. **346**(1): p. 151-159.

203. Mahmoudi, M., et al., *Cell toxicity of superparamagnetic iron oxide nanoparticles.* Journal of colloid and interface science, 2009. **336**(2): p. 510-518.

204. Hradil, J., et al., *Dextran-modified iron oxide nanoparticles.* China Particuology, 2007. **5**(1): p. 162-168.

205. Amiri, H., M. Mahmoudi, and A. Lascialfari, *Superparamagnetic colloidal nanocrystal clusters coated with polyethylene glycol fumarate: a possible novel theranostic agent.* Nanoscale, 2011. **3**(3): p. 1022-1030.

206. Atta, A.M., H.A. Al-Lohedan, and S.A. Al-Hussain, *Synthesis of stabilized myrrh-capped hydrocolloidal magnetite nanoparticles.* Molecules, 2014. **19**(8): p. 11263-11278.

207. Hariani, P.L., M. Faizal, and D. Setiabudidaya, *Synthesis and properties of Fe3O4 nanoparticles by co-precipitation method to removal procion dye.* International Journal of Environmental Science and Development, 2013. **4**(3): p. 336.

208. Gnanaprakash, G., et al., *Effect of initial pH and temperature of iron salt solutions on formation of magnetite nanoparticles.* Materials chemistry and Physics, 2007. **103**(1): p. 168-175.

209. Wang, B., Q. Wei, and S. Qu, *Synthesis and characterization of uniform and crystalline magnetite nanoparticles via oxidation-precipitation and modified co-precipitation method.* Int J Electrochem Sci, 2013. **8**: p. 3786-3793.

210. Wahajuddin, S.A., *Superparamagnetic iron oxide nanoparticles: magnetic nanoplatforms as drug carriers.* International journal of nanomedicine, 2012. **7**: p. 3445.

211. Lucas, I.T., et al., *Surface Charge Density of Maghemite Nanoparticles: Role of Electrostatics in the Proton Exchange.* The Journal of Physical Chemistry C, 2007. **111**(50): p. 18568-18576.

212. Auffan, M., et al., *In vitro interactions between DMSA-coated maghemite nanoparticles and human fibroblasts: a physicochemical and cyto-genotoxical study.* Environmental science & technology, 2006. **40**(14): p. 4367-4373.

213. Zhang, Y., et al., *Stability of commercial metal oxide nanoparticles in water.* Water research, 2008. **42**(8): p. 2204-2212.

214. Labille, J. and J. Brant, *ChemInform Abstract: Stability of Nanoparticles in Water*. Vol. 42. 2011. no-no.

215. Namdeo, M., et al., *Magnetic nanoparticles for drug delivery applications.* Journal of Nanoscience and Nanotechnology, 2008. **8**(7): p. 3247-3271.

216. Yallapu, M.M., et al., *Multi-functional magnetic nanoparticles for magnetic resonance imaging and cancer therapy.* Biomaterials, 2011. **32**(7): p. 1890-1905.

217. Galindo-Rodriguez, S., et al., *Physicochemical parameters associated with nanoparticle formation in the salting-out, emulsification-diffusion, and nanoprecipitation methods.* Pharmaceutical research, 2004. **21**(8): p. 1428-1439.

218. Hu, Y., et al., *Effect of PEG conformation and particle size on the cellular uptake efficiency of nanoparticles with the*

HepG2 cells. Journal of Controlled Release, 2007. **118**(1): p. 7-17.

219. Garnett, M.C. and P. Kallinteri, *Nanomedicines and nanotoxicology: some physiological principles.* Occupational Medicine, 2006. **56**(5): p. 307-311.

220. Calero, M., et al., *Characterization of interaction of magnetic nanoparticles with breast cancer cells.* Journal of nanobiotechnology, 2015. **13**(1): p. 16.

221. Chithrani, B.D., A.A. Ghazani, and W.C. Chan, *Determining the size and shape dependence of gold nanoparticle uptake into mammalian cells.* Nano lett, 2006. **6**(4): p. 662-668.

222. ci Acar, H.Y., et al., *Superparamagnetic nanoparticles stabilized by polymerized PEGylated coatings.* Journal of magnetism and magnetic materials, 2005. **293**(1): p. 1-7.

223. Vonarbourg, A., et al., *Parameters influencing the stealthiness of colloidal drug delivery systems.* Biomaterials, 2006. **27**(24): p. 4356-4373.

224. *Leaf-nosed bat*, in *Encyclopædia Britannica*. 2009, Encyclopædia Britannica Online.

225. Galuppo, L.D., et al., *Gene expression in synovial membrane cells after intraarticular delivery of plasmid-linked superparamagnetic iron oxide particles—a preliminary study in sheep.* Journal of nanoscience and nanotechnology, 2006. **6**(9-1): p. 2841-2852.

226. Akinc, A. and G. Battaglia, *Exploiting endocytosis for nanomedicines.* Cold Spring Harbor perspectives in biology, 2013. **5**(11): p. a016980.

227. Johannes, L., et al., *Building endocytic pits without clathrin.* Nature Reviews Molecular Cell Biology, 2015. **16**(5): p. 311-321.

228. Li, Y., M. Kröger, and W.K. Liu, *Endocytosis of PEGylated nanoparticles accompanied by structural and free energy changes of the grafted polyethylene glycol.* Biomaterials, 2014. **35**(30): p. 8467-8478.

229. Osaki, F., et al., *A quantum dot conjugated sugar ball and its cellular uptake. On the size effects of endocytosis in*

the subviral region. Journal of the American Chemical Society, 2004. **126**(21): p. 6520-6521.

230. Wegner, K.D. and N. Hildebrandt, *Quantum dots: bright and versatile in vitro and in vivo fluorescence imaging biosensors.* Chemical Society Reviews, 2015. **44**(14): p. 4792-4834.

231. Le Bihan, O., et al., *Cryo-electron tomography of nanoparticle transmigration into liposome.* Journal of structural biology, 2009. **168**(3): p. 419-425.

232. Shilo, M., et al., *The effect of nanoparticle size on the probability to cross the blood-brain barrier: an in-vitro endothelial cell model.* Journal of nanobiotechnology, 2015. **13**(1): p. 19.

233. Schlorf, T., et al., *Biological properties of iron oxide nanoparticles for cellular and molecular magnetic resonance imaging.* International journal of molecular sciences, 2010. **12**(1): p. 12-23.

234. Jiang, W., et al., *Nanoparticle-mediated cellular response is size-dependent.* Nature nanotechnology, 2008. **3**(3): p. 145-150.

235. Brunner, T.J., et al., *In vitro cytotoxicity of oxide nanoparticles: comparison to asbestos, silica, and the effect of particle solubility.* Environmental science & technology, 2006. **40**(14): p. 4374-4381.

236. Foster, K.A., et al., *Characterization of the Calu-3 cell line as a tool to screen pulmonary drug delivery.* International Journal of Pharmaceutics, 2000. **208**(1-2): p. 1-11.

237. Ong, H.X., D. Traini, and P.M. Young, *Pharmaceutical applications of the Calu-3 lung epithelia cell line.* Expert opinion on drug delivery, 2013. **10**(9): p. 1287-1302.

238. Malugin, A. and H. Ghandehari, *Cellular uptake and toxicity of gold nanoparticles in prostate cancer cells: a comparative study of rods and spheres.* Journal of Applied Toxicology, 2010. **30**(3): p. 212-217.

239. Trono, J.D., et al., *Size, concentration and incubation time dependence of gold nanoparticle uptake into pancreas cancer cells and its future application to X-ray drug delivery system.* Journal of radiation research, 2010. **52**(1): p. 103-109.

240. Laurent, S. and M. Mahmoudi, *Superparamagnetic iron oxide nanoparticles: promises for diagnosis and treatment of cancer.* International journal of molecular epidemiology and genetics, 2011. **2**(4): p. 367.

241. Beija, M., C.A. Afonso, and J.M. Martinho, *Synthesis and applications of rhodamine derivatives as fluorescent probes.* Chemical Society Reviews, 2009. **38**(8): p. 2410-2433.

242. Ha, S.-W., et al., *New method to prepare very stable and biocompatible fluorescent silica nanoparticles.* Chemical Communications, 2009(20): p. 2881-2883.

243. Ram, R.N., P. Kumar, and A.K. Mukerjee, *A quick and simple conversion of carboxylic acids into their anilides of heating with phenyl isothiocyanate.* Journal of Chemical Education, 1983. **60**(6): p. 508.

244. Nguyen, D., et al., *Monodispersed polymer encapsulated superparamagnetic iron oxide nanoparticles for cell labeling.* Polymer, 2016. **106**: p. 238-248.

245. Diac, A., et al., *Covalent conjugation of carbon dots with Rhodamine B and assessment of their photophysical properties.* RSC Advances, 2015. **5**(95): p. 77662-77669.

246. Jeitner, T.M., *Optimized ferrozine-based assay for dissolved iron.* Analytical biochemistry, 2014. **454**: p. 36-37.

247. Sun, Z., et al., *Magnetic field enhanced convective diffusion of iron oxide nanoparticles in an osmotically disrupted cell culture model of the blood–brain barrier.* International journal of nanomedicine, 2014. **9**: p. 3013.

248. Riemer, J., et al., *Colorimetric ferrozine-based assay for the quantitation of iron in cultured cells.* Analytical biochemistry, 2004. **331**(2): p. 370-375.

249. Vercauteren, D., et al., *The use of inhibitors to study endocytic pathways of gene carriers: optimization and pitfalls.* Molecular Therapy, 2010. **18**(3): p. 561-569.

250. Vllasaliu, D., et al., *Barrier characteristics of epithelial cultures modelling the airway and intestinal mucosa: a comparison.* Biochemical and biophysical research communications, 2011. **415**(4): p. 579-585.

251. Dousset, V., et al., *How to trace stem cells for MRI evaluation?* Journal of the neurological sciences, 2008. **265**(1): p. 122-126.

252. Singh, N., et al., *Potential toxicity of superparamagnetic iron oxide nanoparticles (SPION).* Nano reviews, 2010. **1**(1): p. 5358.

253. Hanini, A., et al., *Evaluation of iron oxide nanoparticle biocompatibility.* International journal of nanomedicine, 2011. **6**: p. 787.

254. Chen, Y.-C., et al., *The inhibitory effect of superparamagnetic iron oxide nanoparticle (Ferucarbotran) on osteogenic differentiation and its signaling mechanism in human mesenchymal stem cells.* Toxicology and applied pharmacology, 2010. **245**(2): p. 272-279.

255. Lewinski, N., V. Colvin, and R. Drezek, *Cytotoxicity of nanoparticles.* small, 2008. **4**(1): p. 26-49.

256. Lynch, I., A. Salvati, and K.A. Dawson, *Protein-nanoparticle interactions: what does the cell see?* Nature nanotechnology, 2009. **4**(9): p. 546-547.

257. Lartigue, L.n., et al., *Nanomagnetic sensing of blood plasma protein interactions with iron oxide nanoparticles: impact on macrophage uptake.* Acs Nano, 2012. **6**(3): p. 2665-2678.

258. Moore, T.L., et al., *Nanoparticle colloidal stability in cell culture media and impact on cellular interactions.* Chemical Society Reviews, 2015. **44**(17): p. 6287-6305.

259. Israelachvili, J.N. and H. Wennerstroem, *Entropic forces between amphiphilic surfaces in liquids.* The Journal of Physical Chemistry, 1992. **96**(2): p. 520-531.

260. Rejman, J., et al., *Size-dependent internalization of particles via the pathways of clathrin-and caveolae-mediated endocytosis.* Biochemical Journal, 2004. **377**(1): p. 159-169.

261. Zhu, X.-M., et al., *Enhanced cellular uptake of aminosilane-coated superparamagnetic iron oxide nanoparticles in mammalian cell lines.* International journal of nanomedicine, 2012. **7**: p. 953.

262. Kenzaoui, B.H., et al., *Evaluation of uptake and transport of ultrasmall superparamagnetic iron oxide nanoparticles by human brain-derived endothelial cells.* Nanomedicine, 2012. **7**(1): p. 39-53.

263. Etame, A.B., et al., *Design and potential application of PEGylated gold nanoparticles with size-dependent permeation through brain microvasculature.* Nanomedicine: Nanotechnology, Biology and Medicine, 2011. **7**(6): p. 992-1000.

264. Conner, S.D. and S.L. Schmid, *Regulated portals of entry into the cell.* Nature, 2003. **422**(6927): p. 37.

265. Korn, E.D. and R.A. Weisman, *Phagocytosis of Latex Beads by Acanthamoeba: II. Electron Microscopic Study of the Initial Events.* The Journal of cell biology, 1967. **34**(1): p. 219-227.

266. Walczak, P., et al., *Magnetoelectroporation: improved labeling of neural stem cells and leukocytes for cellular magnetic resonance imaging using a single FDA-approved agent.* Nanomedicine: Nanotechnology, Biology and Medicine, 2006. **2**(2): p. 89-94.

267. Bulte, J.W., et al., *Magnetodendrimers allow endosomal magnetic labeling and in vivo tracking of stem cells.* Nature biotechnology, 2001. **19**(12): p. 1141-1147.

268. Wang, Z. and A. Cuschieri, *Tumour cell labelling by magnetic nanoparticles with determination of intracellular iron content and spatial distribution of the intracellular iron.* International journal of molecular sciences, 2013. **14**(5): p. 9111-9125.

269. Coupland, P.G., S.J. Briddon, and J.W. Aylott, *Using fluorescent pH-sensitive nanosensors to report their intracellular location after Tat-mediated delivery.* Integrative Biology, 2009. **1**(4): p. 318-323.

270. Coupland, P.G., et al., *Internalisation of polymeric nanosensors in mesenchymal stem cells: Analysis by flow cytometry and confocal microscopy.* Journal of controlled release, 2008. **130**(2): p. 115-120.

271. Singh, N., et al., *The role of iron redox state in the genotoxicity of ultrafine superparamagnetic iron oxide nanoparticles.* Biomaterials, 2012. **33**(1): p. 163-170.

272. Gao, H., W. Shi, and L.B. Freund, *Mechanics of receptor-mediated endocytosis.* Proceedings of the National Academy of Sciences, 2005. **102**(27): p. 9469-9474.

273. Zhao, Y., et al., *Interaction of mesoporous silica nanoparticles with human red blood cell membranes: size and surface effects.* ACS nano, 2011. **5**(2): p. 1366-1375.

274. Bohmer, N. and A. Jordan, *Caveolin-1 and CDC42 mediated endocytosis of silica-coated iron oxide nanoparticles in HeLa cells.* Beilstein journal of nanotechnology, 2015. **6**: p. 167.

275. Voigt, J., J. Christensen, and V.P. Shastri, *Differential uptake of nanoparticles by endothelial cells through polyelectrolytes with affinity for caveolae.* Proceedings of the National Academy of Sciences, 2014. **111**(8): p. 2942-2947.

276. Thorley, A.J., et al., *Critical determinants of uptake and translocation of nanoparticles by the human pulmonary alveolar epithelium.* ACS nano, 2014. **8**(11): p. 11778-11789.

277. Brown, W. and E. Bertke, *Textbook of cytology 2nd edition (Saint Louis: CV Mosby).* 1974.

278. Bramini, M., et al., *Imaging approach to mechanistic study of nanoparticle interactions with the blood–brain barrier.* ACS nano, 2014. **8**(5): p. 4304-4312.

279. Rimai, D., D. Quesnel, and A. Busnaina, *The adhesion of dry particles in the nanometer to micrometer-size range.* Colloids and surfaces A: Physicochemical and engineering aspects, 2000. **165**(1): p. 3-10.

280. Goodman, T.T., P.L. Olive, and S.H. Pun, *Increased nanoparticle penetration in collagenase-treated multicellular spheroids.* International journal of nanomedicine, 2007. **2**(2): p. 265.

281. Meng, W., et al., *Uptake and metabolism of novel biodegradable poly (glycerol-adipate) nanoparticles in DAOY monolayer.* Journal of controlled release, 2006. **116**(3): p. 314-321.

282. Mironava, T., et al., *Gold nanoparticles cellular toxicity and recovery: effect of size, concentration and exposure time.* Nanotoxicology, 2010. **4**(1): p. 120-137.

283. Lovrić, J., et al., *Differences in subcellular distribution and toxicity of green and red emitting CdTe quantum dots.* Journal of Molecular Medicine, 2005. **83**(5): p. 377-385.

284. Parak, W.J., et al., *Cell motility and metastatic potential studies based on quantum dot imaging of phagokinetic tracks.* Advanced Materials, 2002. **14**(12): p. 882-885.

285. Pradhan, P., et al., *Cellular interactions of lauric acid and dextran-coated magnetite nanoparticles.* Journal of Magnetism and Magnetic Materials, 2007. **311**(1): p. 282-287.

286. Ayala, V., et al., *Effect of surface charge on the colloidal stability and in vitro uptake of carboxymethyl dextran-coated iron oxide nanoparticles.* Journal of nanoparticle research, 2013. **15**(8): p. 1-14.

287. Yamazaki, M. and T. Ito, *Deformation and instability of membrane structure of phospholipid vesicles caused by osmophobic association: mechanical stress model for the mechanism of poly (ethylene glycol)-induced membrane fusion.* Biochemistry, 1990. **29**(5): p. 1309-1314.

288. Desai, M.P., et al., *The mechanism of uptake of biodegradable microparticles in Caco-2 cells is size dependent.* Pharmaceutical research, 1997. **14**(11): p. 1568-1573.

289. McClean, S., et al., *Binding and uptake of biodegradable poly-DL-lactide micro-and nanoparticles in intestinal epithelia.* European Journal of Pharmaceutical Sciences, 1998. **6**(2): p. 153-163.

290. Calero, M., et al., *Characterization of interaction of magnetic nanoparticles with breast cancer cells.* Journal of nanobiotechnology, 2015. **13**.

291. Zhang, Y., et al., *Zeta potential: a surface electrical characteristic to probe the interaction of nanoparticles with normal and cancer human breast epithelial cells.* Biomedical microdevices, 2008. **10**(2): p. 321-328.

292. Calero, M., et al., *Efficient and safe internalization of magnetic iron oxide nanoparticles: two fundamental requirements for biomedical applications.* Nanomedicine: Nanotechnology, Biology and Medicine, 2014. **10**(4): p. 733-743.

293. Gu, J., et al., *The internalization pathway, metabolic fate and biological effect of superparamagnetic iron oxide nanoparticles in the macrophage-like RAW264. 7 cell.* Science China Life Sciences, 2011. **54**(9): p. 793-805.

294. Jung, T., et al., *Biodegradable nanoparticles for oral delivery of peptides: is there a role for polymers to affect mucosal uptake?* European Journal of Pharmaceutics and Biopharmaceutics, 2000. **50**(1): p. 147-160.

295. Akbarzadeh, A., M. Samiei, and S. Davaran, *Magnetic nanoparticles: preparation, physical properties, and applications in biomedicine.* Nanoscale research letters, 2012. **7**(1): p. 144.

296. Cromer Berman, S.M., P. Walczak, and J.W. Bulte, *Tracking stem cells using magnetic nanoparticles.* Wiley Interdisciplinary Reviews: Nanomedicine and Nanobiotechnology, 2011. **3**(4): p. 343-355.

297. Corot, C., et al., *Recent advances in iron oxide nanocrystal technology for medical imaging.* Advanced drug delivery reviews, 2006. **58**(14): p. 1471-1504.

298. Xie, J., et al., *Iron oxide nanoparticle platform for biomedical applications.* Current medicinal chemistry, 2009. **16**(10): p. 1278-1294.

299. Xie, J., S. Lee, and X. Chen, *Nanoparticle-based theranostic agents.* Advanced drug delivery reviews, 2010. **62**(11): p. 1064-1079.

300. Laurent, S., et al., *Magnetic iron oxide nanoparticles for biomedical applications.* Future medicinal chemistry, 2010. **2**(3): p. 427-449.

301. Santoyo Salazar, J., et al., *Magnetic iron oxide nanoparticles in 10− 40 nm range: composition in terms of magnetite/maghemite ratio and effect on the magnetic properties.* Chemistry of materials, 2011. **23**(6): p. 1379-1386.

302. Lawaczeck, R., M. Menzel, and H. Pietsch, *Superparamagnetic iron oxide particles: contrast media for magnetic resonance imaging.* Applied organometallic chemistry, 2004. **18**(10): p. 506-513.

303. Koenig, S. and R. Brown 3rd, *Relaxometry of magnetic resonance imaging contrast agents.* Magnetic resonance annual, 1987: p. 263.

304. Patel, H., *Serum opsonins and liposomes: their interaction and opsonophagocytosis.* Critical reviews in therapeutic drug carrier systems, 1992. **9**(1): p. 39-90.

305. Sohn, B. and R. Cohen, *Processible optically transparent block copolymer films containing superparamagnetic iron oxide nanoclusters.* Chemistry of materials, 1997. **9**(1): p. 264-269.

306. Lee, C.-N., et al., *Super-paramagnetic iron oxide nanoparticles for use in extrapulmonary tuberculosis diagnosis.* Clinical Microbiology and Infection, 2012. **18**(6): p. E149-E157.

307. Yang, F., et al., *Emerging inorganic nanomaterials for pancreatic cancer diagnosis and treatment.* Cancer treatment reviews, 2012. **38**(6): p. 566-579.

308. Arbab, A.S., et al., *In vivo trafficking and targeted delivery of magnetically labeled stem cells.* Human gene therapy, 2004. **15**(4): p. 351-360.

309. Deb, K.D., et al., *Nanotechnology in stem cells research: advances and applications.* Front Biosci, 2012. **17**: p. 1747-1760.

310. Solanki, A., J.D. Kim, and K.-B. Lee, *Nanotechnology for regenerative medicine: nanomaterials for stem cell imaging.* 2008.

311. Lind, K., et al., *A novel formulation for superparamagnetic iron oxide (SPIO) particles enhancing MR lymphography: comparison of physicochemical properties and the in vivo behaviour.* Journal of drug targeting, 2002. **10**(3): p. 221-230.

312. Reimer, P., et al., *Dynamic signal intensity changes in liver with superparamagnetic MR contrast agents.* Journal of Magnetic Resonance Imaging, 1992. **2**(2): p. 177-181.

313. Huang, J., et al., *Improving the magnetic resonance imaging contrast and detection methods with engineered magnetic nanoparticles.* Theranostics, 2012. **2**(1): p. 86.

314. Zysler, R., D. Fiorani, and A. Testa, *Investigation of magnetic properties of interacting Fe 2 O 3 nanoparticles.* Journal of magnetism and magnetic materials, 2001. **224**(1): p. 5-11.

315. Tong, S., et al., *Coating optimization of superparamagnetic iron oxide nanoparticles for high T2 relaxivity.* Nano letters, 2010. **10**(11): p. 4607-4613.

316. LaConte, L.E., et al., *Coating thickness of magnetic iron oxide nanoparticles affects R2 relaxivity.* Journal of Magnetic Resonance Imaging, 2007. **26**(6): p. 1634-1641.

317. Morales, M., et al., *Spin canting due to structural disorder in maghemite.* Journal of Physics: Condensed Matter, 1997. **9**(25): p. 5461.

318. Spada, F., et al., *Studies of anisotropy mechanisms in polyphosphate-treated magnetic iron oxide particles.* Journal of magnetism and magnetic materials, 1993. **120**(1-3): p. 129-135.

319. Xie, J., et al., *PET/NIRF/MRI triple functional iron oxide nanoparticles.* Biomaterials, 2010. **31**(11): p. 3016-3022.

320. Ahmad, T., et al., *Particle size dependence of relaxivity for silica-coated iron oxide nanoparticles.* Current Applied Physics, 2012. **12**(3): p. 969-974.

321. Duan, H., et al., *Reexamining the effects of particle size and surface chemistry on the magnetic properties of iron oxide nanocrystals: new insights into spin disorder and proton relaxivity.* The Journal of Physical Chemistry C, 2008. **112**(22): p. 8127-8131.

322. Wang, Y.-X.J., S.M. Hussain, and G.P. Krestin, *Superparamagnetic iron oxide contrast agents: physicochemical characteristics and applications in MR imaging.* European radiology, 2001. **11**(11): p. 2319-2331.

323. Caravan, P., et al., *Influence of molecular parameters and increasing magnetic field strength on relaxivity of gadolinium-and manganese-based T1 contrast agents.* Contrast media & molecular imaging, 2009. **4**(2): p. 89-100.

324. Bulte, J.W., *In vivo MRI cell tracking: clinical studies.* American Journal of Roentgenology, 2009. **193**(2): p. 314-325.

325. Daldrup-Link, H.E., *Ten things you might not know about iron oxide nanoparticles.* Radiology, 2017. **284**(3): p. 616-629.

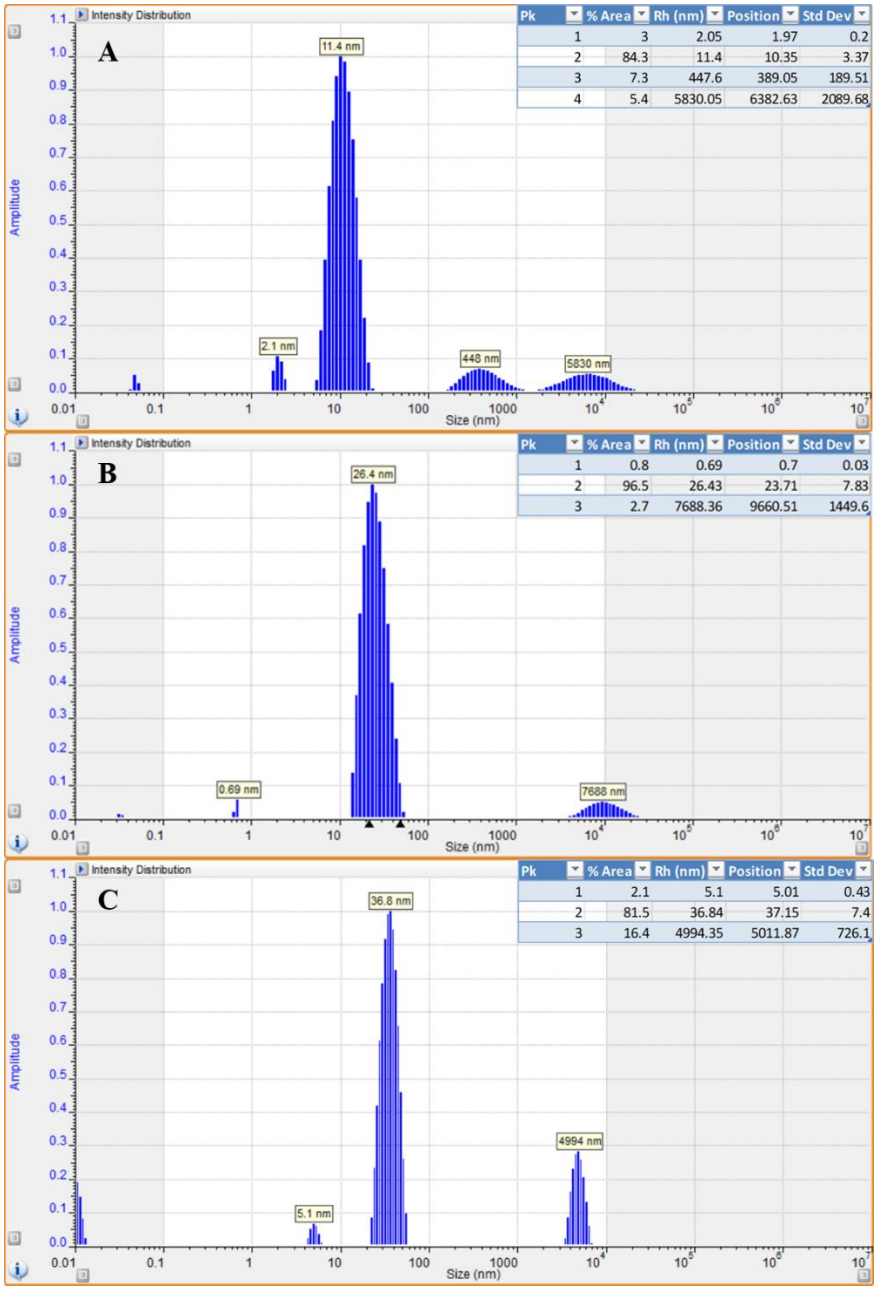
326. Liu, Y. and N. Zhang, *Gadolinium loaded nanoparticles in theranostic magnetic resonance imaging.* Biomaterials, 2012. **33**(21): p. 5363-5375.

327. Hajesmaeelzadeh, F., et al., *Effect of coating thickness of iron oxide nanoparticles on their relaxivity in the MRI.* Iranian journal of basic medical sciences, 2016. **19**(2): p. 166.

328. Farokhzad, O.C. and R. Langer, *Impact of nanotechnology on drug delivery.* ACS nano, 2009. **3**(1): p. 16-20.

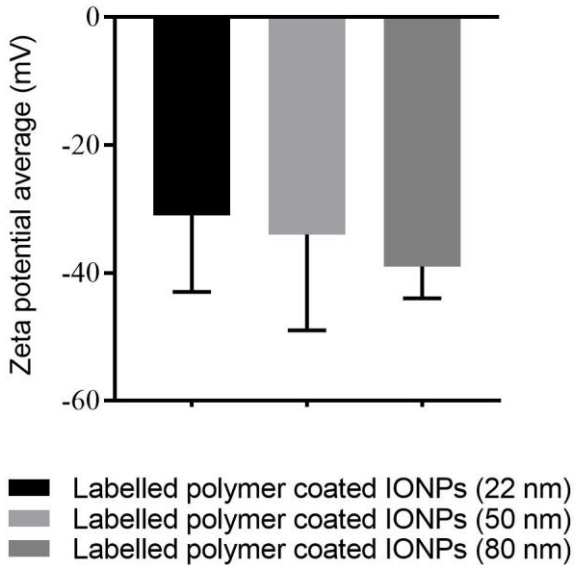
Appendix

Particle Size of RBITC Labelled Polymer Coated IONPs



Appendix I: Hydrodynamic radius distribution of RBITC labelled PEG-PGA 40%C_{18} coated IONPs: NP suspension was diluted with ultrapure water to an appropriate concentration to give 300-600 kcps. Particle size was the mean hydrodynamic radius and measured by Dynamic light scattering instrument where (A, B and C) are particle radii of average (11, 26, 37 nm) of RBITC labelled PEGylated PGA 40% C_{18} IONPs. The particle size of each sample is expressed as the mean particle hydrodynamic radius ± standard deviation of 10 readings.

Surface Charges of RBITC Labelled Polymer Coated IONPs



Appendix II: Surface charge of RBITC labelled PEGylated PGA 40% C_{18} coated IONPs of radii 11, 26 and 37 nm. Zeta potential measurements were performed in PBS (15 mM) at pH 7.4 using Zeta sizer (Mavern Instruments,Malvern,UK). Results are expressed as the mean ± standard deviation of 5 readings.

Dose Dependent and Intracellular Distribution of RBITC Labelled Polymer Coated IONPs in Calu-3 Cells Using Fluorescence Microscopy

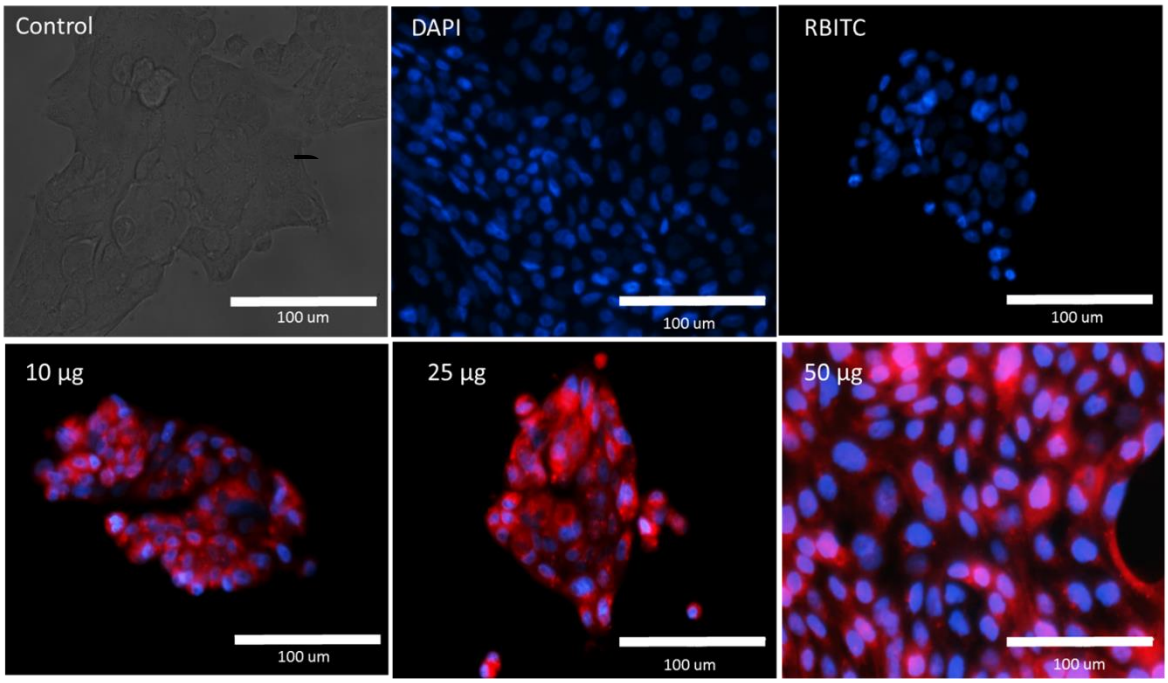


Figure III: Fluorescence microscopy images of RBITC-labelled polymer coated IONPs of size 22 nm incubated with Calu-3 cells for 2 hours showing Control untreated cells, cells incubated with 0.02 µg/ml free RBITC, cell incubated with 2.5 µg nanoparticles, cell incubated with 10 µg nanoparticles, cell incubated 25 µg nanoparticles and cell incubated 50 µg nanoparticles (Scale bar 100 µm).

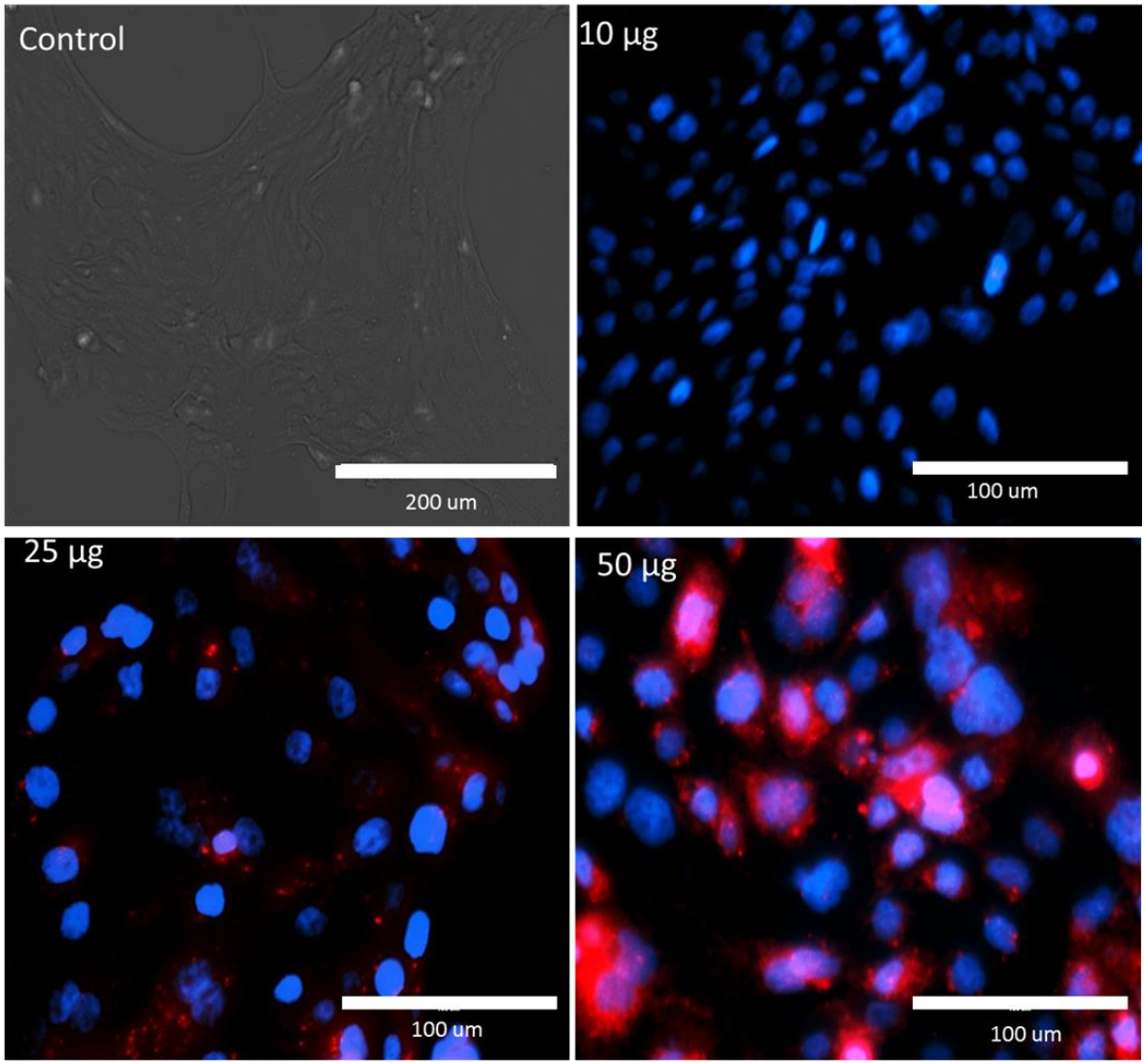


Figure IV: Fluorescence microscopy images of RBITC-labelled polymer coated IONPs of size 50 nm incubated with Calu-3 cells for 2 hours showing Control untreated cells, cell incubated with 10 µg nanoparticles, cell incubated 25 µg nanoparticles and cell incubated 50 µg nanoparticles (Scale bar 100 µm).

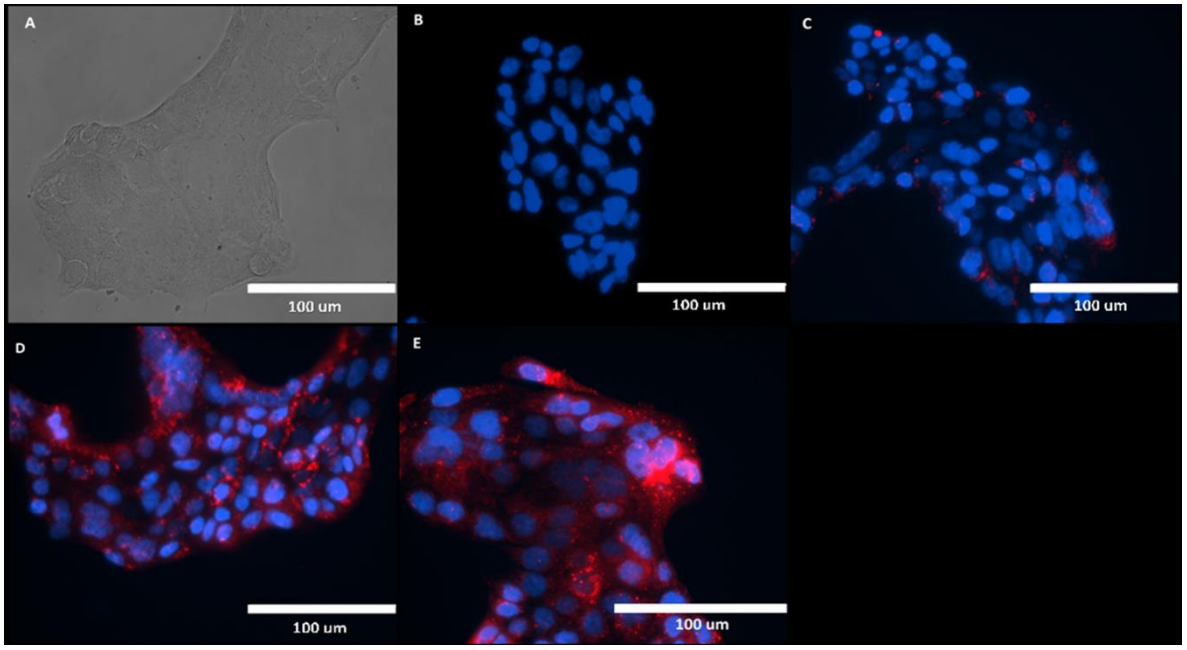


Figure V: Fluorescence microscopy images of RBITC-labelled polymer coated IONPs of size (80 nm), incubated with Calu-3 cells for 2 h. (A) control untreated cells, (B) cells incubated with 10 µg nanoparticles, (C) cells incubated with 25 µg nanoparticles, (D) cells incubated with 50 µg nanoparticles. However, (E) Cells incubated with 50 µg for 4 h.